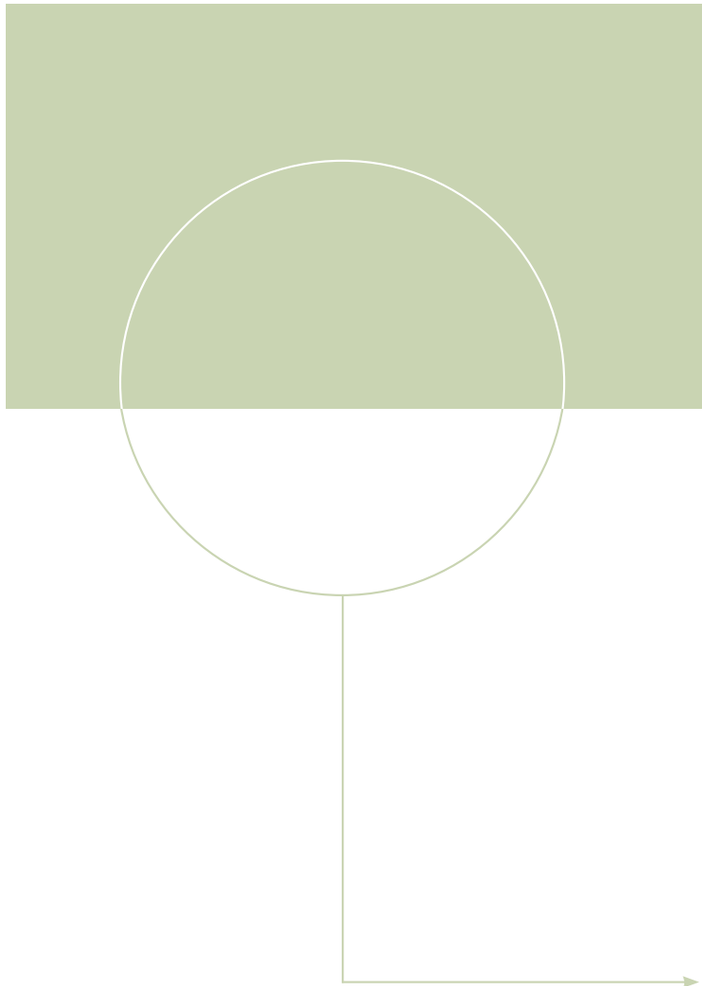

Master's thesis 2019 Live Forfang Bjørnstad, Maria Arild Solstad

NTNU
Norwegian University of
Science and Technology
Faculty of Engineering
Department of Marine Technology

Live Forfang Bjørnstad
Maria Arild Solstad

Investigation of light response and swimming behavior of salmon lice (*Lepeophtheirus salmonis*) using feature detection and object tracking

June 2019

NTNU
Norwegian University of
Science and Technology

NTNU
Norwegian University of
Science and Technology

NTNU
Norwegian University of
Science and Technology

Investigation of light response and swimming behavior of salmon lice (*Lepeophtheirus salmonis*) using feature detection and object tracking

Live Forfang Bjørnstad
Maria Arild Solstad

Master of Science in Engineering and ICT
Submission date: June 2019
Supervisor: Martin Ludvigsen
Co-supervisor: Øystein Sture

Norwegian University of Science and Technology
Department of Marine Technology

Problem description

NTNU Trondheim
Norwegian University of Science and Technology
Department of Marine Technology

MASTER THESIS IN MARINE CYBERNETICS

SPRING 2019

FOR

STUD. TECH. Bjørnstad Live Forfang

STUD.TECH. Solstad Maria Arild

Title: Investigation of light response and swimming behaviour of salmon lice (*Lepeophtheirus salmonis*) using feature detection and tracking

Work Description

Management of *Lepeophtheirus salmonis* (salmon lice) is a massive challenge in the fish farming industry today, both with regards to fish welfare, costs and decrease in the growth rate of fish. In the past years, one has seen an increasing resistance amongst the salmon lice against the medicinal treatments used to overcome the louse problem. Mechanical methods have been introduced to remove the lice as an alternative to chemical treatments. This has led to high costs and serious injuries on the fish.

Previous studies have found that salmon lice at the copopodite stage has a significant attraction towards light with wavelengths above 550 nm (Bron et al., 1993). New methods using updated technology based around this can be introduced to increase knowledge about salmon lice and get closer to managing the related problems in the fish farming industry.

The objective of this thesis is to quantify the phototactic swimming behavior of salmon lice, using image processing, object detection and tracking. The goal is to validate the attraction towards light, and which wavebands, intensities and pulsations of light the louse is the most attracted to.

Scope of work

1. Background study on salmon lice focusing on:
    a. Light sensitivity
    b. Behavioral patterns
2. Background study on the fish farming industry and problems caused by salmon lice, computer vision for detection and tracking of multiple objects, and light propagation in water.
3. Analysis of light sensitivity experiments:
    a. Initial detection of salmon lice in one video frame
    b. Identify a general movement pattern of salmon lice
    c. Identify the movement patterns of salmon lice with respect to different light stimuli
    d. Track individual lice over time to obtain information about swimming behavior

NTNU Trondheim
Norwegian University of Science and Technology
Department of Marine Technology

e. Identify which wavelengths, intensity and pulsation rates of light that has the most significant impact on the behavior of salmon lice

4. Analysis of light propagation under water with resulting light settings

The report shall be written in English and edited as a research report including literature survey, description of mathematical models, description of control algorithms, simulation results, model test results, discussion and a conclusion including a proposal for further work. Source code should be provided on a CD, memory stick or similar. It is supposed that the Department of Marine Technology, NTNU, can use the results freely in its research work, unless otherwise agreed upon, by referring to the student's work. The thesis should be submitted in two copies within June 2019.

Supervisor: Martin Ludvigsen
Co-supervisor: Øystein Sture

Summary

This thesis has been part of the multidisciplinary project Profylax, focusing on increasing the knowledge about salmon lice, which is an increasing problem in the fish farming industry. The possibility of using computer vision tools to quantify the phototactic swimming behavior of salmon lice (*Lepeophtheirus salmonis*) in the copepodid stage when exposed to different light settings, has been investigated. The aim was to find a method for quantifying how different types of light settings attract salmon lice with respect to wavebands, light irradiance and pulsation rates, and at what time this response happens. In further writing, the term salmon lice refers to salmon lice in the copepodid stage.

Salmon lice live and reproduce on salmonid fish [1]. They eat mucus, skin, and blood, resulting in injuries and poor salmon welfare, as well as an increased mortality rate in Norwegian aquaculture [2]. With increased resistance towards medicinal treatments, new methods have emerged [3]. Today, many mechanical treatments exist; however, these treatments have shown to harm the salmon due to the rough handling of the fish [4]. The result is significant economic losses for the breeders. The aim of this project was to exploit the light sensitivity in the development of new methods to overcome the problems regarding the salmon louse.

One pilot experiment and two main experiments have been completed. The results from the pilot experiments laid the basis for the chosen light settings in the main experiment. Wavebands corresponding to green, blue and white light were selected. Additionally, three different irradiance levels and four different pulsation rates were tested. The pulsation rates had an on/off ratio of 0.1/0.1 s, 2.0/3.0 s, and 5.0/5.0 s. Constant light without pulsation was also tested. The experiments were executed in a small tank, with the light source placed at one end, and infrared (IR) light was used to illuminate the lice from beneath the tank. To analyze the phototactic swimming behavior of the salmon louse, the experiments were recorded. Computer vision tools for feature detection and object tracking were used on the videos, including background subtraction, thresholding, blurring, and moment calculations. For each frame, the centroid locations of the detected lice were extracted and used for further analysis, including computation of tracks for each salmon louse over time. The response towards the different light settings was measured using distance and speed calculations, and by looking at the change in swimming behavior be-

fore and after turning on the light. Lastly, the light attenuation for six of the light settings used in the experiments was calculated using coefficients from oceanic water at Hosenøyan in Norway to investigate the potential effects of artificial light in the ocean with regards to the attraction of salmon lice.

The developed method was able to distinguish between salmon lice behavior when exposed to different light stimuli. The detection algorithm showed an overall attractive response towards light stimuli. When tracking each salmon louse, it was seen that the swimming behavior differed with different pulsation rates and irradiance levels. From a total of nine experiments with three different light settings, the median maximum swimming velocities were in the range 23.01-36.56 mm/s, where the maximum velocity registered was 115.64 mm/s. These swimming velocities coincide with previous findings in the literature. How determined the swimming behavior was before and after light stimuli was measured. It was seen that the salmon lice had more directed swimming patterns after light stimuli than in the dark periods for all light settings. With the given attenuation coefficients, green light shows to propagate furthest (58 m) before the irradiance is reduced to a level where the attraction of salmon lice is at a minimum. The same reduction is seen after 47 m and 42 m for white and blue light, respectively.

When considering the color of the light source, attraction of salmon lice was seen for blue, green, and white light. The white light gave the highest response when considering median displacement; however, these results were more dispersed than the results for green and blue light. Green light gave the second highest displacement, with the lowest dispersion. High pulsation frequencies gave less response than lower frequencies. Increased swimming velocities were seen during the periods of light for the lower pulsation frequencies.

The algorithm performed sufficiently for the detection of a group of lice in the experimental videos. The algorithm worked well for the videos without pulsating light. When pulsation was present, the algorithm worked better for light settings having high irradiance values than for lower irradiance values. The salmon lice positions were mapped over time for the whole experiment, giving insight into when the lice started to respond, and whether they swam towards or away from the light sources. The performance of the tracking algorithm was dependent on the detection algorithm, as the tracking algorithm was an extension of the algorithm developed for detecting salmon lice. The tracking algorithm was able to map the quick jumps of the salmon lice and the velocities and tracks over time. Hence, it can be concluded that it is possible to differentiate between the light responses and track the swimming behavior of salmon lice for different light settings with the use of computer vision for feature detection and object tracking.

Sammendrag

Denne masteroppgaven har vært en del av det tverrfaglige prosjektet Profylax, som har hatt fokus på å øke kunnskapen om lakselus som er et økende problemet i oppdrettsnæringen. Muligheten for å bruke datasynverktøy til å kvantifisere den fototaktiske oppførselen til lakselus (*Lepeophtheirus salmonis*) når den blir utsatt for lystimuli har blitt undersøkt. Målet har vært å finne en metode for å kvantifisere hvordan ulike typer lysinnstillinger, som bølgebånd, lysintensitet og pulseringsrate, tiltrekker lakselus, og på hvilket tidspunkt denne responsen oppstår.

Lakselus lever og reproduserer seg på laks [1]. De spiser slim, hud og blod, noe som resulterer i skader og dårlig laksvelferd, samt økt laksedødelighet i norsk akvakultur [2]. Grunnet en økende resistens mot medisinske behandlinger av laksen, har nye metoder blitt utviklet [3]. I dag finnes det mange mekaniske behandlinger. Disse behandlingene har imidlertid vist seg å ha en negativ innvirkning på laksevelferden på grunn av hard håndtering av laksen [4]. Dette resulterer også i store økonomiske tap for oppdretterne. Målet med dette prosjektet har vært å utforske hvordan lysfølsomhet kan brukes i utviklingen av nye metoder for å forhindre oppblomstring av lakselus i oppdrettsnæringen.

Ett eksperimentelt pilotforsøk og to eksperimentelle hovedforsøk ble gjennomført. Basert på resultatene fra pilotforsøket ble nye lysinnstillinger valgt i hovedeksperimentene. Det ble brukt bølgebånd som tilsvarer grønt, blått og hvitt lys, og tre nivåer av lysintensitet ble brukt. Fire forskjellige pulseringsrater ble testet, der pulseringsratene hadde et på/av-forhold på 0.1/0.1 s, 2.0/3.0 s og 5.0/5.0 s. I tillegg ble konstant lys uten pulsering testet. Forsøkene ble utført i en liten tank, med en lyskilde plassert i den ene enden. Infrarødt (IR) lys ble brukt til å belyse lusene fra undersiden av tanken. For å analysere det fototaktiske svømmemønsteret til lakselusen ble forsøkene filmet. Datasynverktøy for deteksjon og sporing ble brukt på videoene, inkludert bakgrunnsubtraksjon, filtre og egenskapsuttrekking. For hvert bilde ble koordinatene for de detekterte lusene hentet ut for videre analyse. Disse koordinatene ble også brukt til å spore hver lus over tid. Responsen på de ulike lysinnstillingene ble målt ved hjelp av avstands- og hastighetsberegninger, og ved å se på endringen i svømmeadferden før og etter at lyset ble slått på. Til slutt ble lysforplantningen av de seks ulike lyskildene brukt i forsøkene beregnet i havvann ved Hosenøyan i Norge. Disse ble beregnet for videre å kunne undersøke de potensielle

effektene av kunstig lys i havet med hensyn til tiltrekning av lakselus.

Ved den utviklede metoden var det mulig å måle forskjeller i lakselusas oppførsel ved ulike lysstimuli. Deteksjonsalgoritmen viste at lusa hadde en overordnet respons mot lysstimuli. Ved sporing av hver enkelt lus ble det observert at svømmemønsteret var forskjellig med varierende pulseringsrater og bestrålingsnivåer. Av totalt ni eksperimenter med tre forskjellige lysinnstillinger var medianen i maksimal svømmehastighet for lus i samme forsøk i intervallet 23.01-36.56 mm/s, hvor den absolutt maksimale hastighet som ble målt var 115.64 mm/s. Disse svømmehastighetene sammenfaller med tidligere funn i litteraturen. Hvor målbevisst lusa var da den ble utsatt for lysstimuli har også blitt målt. Det ble observert at lakselusen hadde et mer rettet svømmemønster etter lysstimuli enn før lyset ble slått på i alle lysinnstillingene.

Med de gitte dempningskoeffisientene fra Hosenøyan viste det grønne lyset å forplante seg lengst (58 m) før lysintensiteten ble redusert til et nivå hvor tiltrekningen av lakselus ble var på et minimum. For hvitt og blått lys skjedde tilsvarende reduksjon etter henholdsvis 47 og 42 meter.

Tiltrekning av lakselus mot lyskilden ble observert for de fleste lysinnstillingene, men det var stor variasjon i observasjonene. Siden lakselus er levende organismer med individuell adferd, var variasjonen til en viss grad forventet. De ulike replikatene brukte ulike populasjoner av lus, noe som kan underbygge den høye variasjonen i resultatene.

Deteksjonsalgoritmen fungerte godt for deteksjon av lus i eksperimentelle videoer. Den fungerte best for videoene uten pulserende lys. Ved pulsering fungerte algoritmen best for lysinstillinger hvor lysintensiteten var høy. Lakselusen ble sporet over tid, noe som ga innsikt i når lusene responderte, og om de svømte mot eller fra lyskilden.

Sporingsalgoritmens utførelse var avhengig av deteksjonsalgoritmen, ettersom den bygget videre på denne. Sporingsalgoritmen var i stand til å fange opp raske hopp og bevegelser, og å kartlegge hastighetsprofiler over tid.

Så konklusjonen er at det er mulig å skille mellom lysresponsen hos lakselusa for ulike lysinstillinger ved hjelp av maskinsyn for deteksjon og sporing, samt at lys har en påvirkning på lakselusens oppførsel.

Preface

This is a master thesis reflecting work conducted throughout the fall of 2018 and the spring of 2019. The thesis constitutes 100 % of the final grade in the subject TMR4930 *Marine Technology, Master's Thesis* at the Norwegian University of Science and Technology.

The topic of this thesis was chosen due to the common interest among the authors within the intersection between cybernetics and marine biology applied to aquaculture. We both believe that the utilization of aquaculture can be significantly improved by applying technological tools such as computer vision, to this industry.

This master thesis was a part of the multidisciplinary project Profylax, initiated by Jørgen Ås Vatn, master student at The Norwegian University of Life Science (NMBU). The other contributors to this project are Anna Solvang Båtnes and Cecilie Miljeteig, both employed as researchers at NTNU, Elisabeth Børset from the Department of Mathematical Sciences at NTNU, and Mads Francis from the Department of Marine Technology at NTNU. The overall goal for the project was to increase the knowledge about salmon lice and what attraction it has towards different light settings, concerning waveband, pulsation rate, and light irradiance levels.

Margrét Alsvik, master student at the Department of Biology and part of Taskforce salmon lice, has, together with Anna Båtnes, provided the data needed for calculations regarding light propagation in water.

In the work reflected in this thesis, much time was spent on gaining knowledge about computer vision. This was done through online research and by talking to researchers at NTNU, among them Edmund Brekke and Annette Stahl. A background study was performed to gain knowledge about what has previously been done within the area of multiple object detection. Then, the methodology was developed, and the implementation of code took place. To obtain knowledge about tracking, several people were contacted. Among them were Marco Leonardi and Simen Haugo, both research fellows at the Department of Engineering Cybernetics, NTNU. Lastly, studying the behavior of light in water, was in focus.

The results presented in this thesis are just an excerpt of the available results, where the rest can be found attached to the delivery of the thesis. Due to troubles related to big amounts of data

leading to time-consuming processes, the work will continue after the delivery of this thesis, as part of the research towards the publication of an article.

This thesis, and the work reflected in it, is a result of teamwork between both the authors, Live and Maria. We have contributed equally, and worked efficiently, by having a continuous dialogue and changing between writing the thesis and the code for video analysis. When writing the code, both have come up with ideas based on research for what to implement. Both have contributed to every part of the thesis. After four years of studying together at NTNU, we have learned that the collaboration and teamwork have worked very well between us. Working together in a pair increased motivation, as well as it left us with a broader spectrum of knowledge.

Trondheim, June 11, 2019

Live Forfang Bjørnstad

Maria Arild Solstad

Acknowledgment

We want to thank our supervisor Professor Martin Ludvigsen for the motivation and assistance during this thesis. His ability to always give concise and professional feedback has been appreciated. Additionally, Ph.D. Candidate and co-supervisor Øystein Sture deserves a big thanks for his support and for always being available to answer questions. Technical support provided by Senior Engineer Bjørn Tore Bach has been greatly appreciated. Thanks should also be directed towards Professor Asgeir Sørensen for motivation and feedback. The work would not have been possible without their help.

We would also like to thank the rest of the Profylax team. The interdisciplinary cooperation has been an educating process, and the project would not have been possible without them. A special thanks should be directed towards Anna Båtnes for her continuous feedback and valuable input throughout the project period.

A big thanks should also be directed towards fellow students at the office C1.058 for their contributions and inspirational input throughout the semester.

In the end, we would like to thank each other. It has been an educating and motivating process, and the teamwork and collaboration has been extraordinary.

Contents

List of figures

List of tables

Nomenclature

CV	Computer vision
Fps	Frames per second
IQR	Interquartile range
IR	Infrared
MCMC	Markov Chain Monte Carlo sampling
MRF	Markov random field
OD	Optical density
OD1	Optical density level 1, corresponding to high light intensity
OD2	Optical density level 2, corresponding to medium light intensity
OD3	Optical density level 3, corresponding to low light intensity
P1	Pulsation rate 1
P2	Pulsation rate 2
P3	Pulsation rate 3
R1	Replicate 1
R2	Replicate 2
R3	Replicate 3
RGB	Red Green Blue
SD	Standard deviation

Chapter 1

Introduction

This chapter includes background and motivation for this thesis and an explanation about the connection to the multidisciplinary project Profylax. The objectives for the thesis, as well as research questions, the scope of work, and contributions, are also included.

1.1 Background and motivation

Fish farming is a leading industry in Norway. In 2017, the export of Norwegian salmon was estimated to 1 million tons resulting in a first-hand value of 61.6 billion NOK [5]. Despite an increase in Norwegian salmon export value over the past years, the mortality rate in Norwegian salmon farms was close to 20 % in 2016, according to the Norwegian Veterinary Institute [6]. This was an increase from 2012-2013, where the mortality rate was estimated to about 13-14 %. The increase can be linked to the five-fold increase in mechanical treatments for sea lice during this period [7]. The salmon lice are copepod ectoparasites found on salmonids in seawater, which live and reproduce on fish in this family [1]. They injure salmonid fish by eating mucus, skin, and blood, which leads to poor salmon welfare and opens up for other infections such as bacteria and fungus [2]. It is estimated that 9–23 % of the total production cost per kg salmon is related to salmon lice. Thus, development of new methods should be emphasized.

Laboratory experiments have shown that the salmon louse copepodid reacts positively to light stimuli. Bron et al. [8] showed that salmon lice were attracted towards light in the visible spectrum, with the highest response towards light with wavelength 550 nm. The results from this study were obtained by the use of manual counting and detection [9].

Studies show that the salmon lice are attracted to flickering daylight, simulating a group of fish swimming above the lice and that the attraction is strongly dependent on the brightness

of the light. Fields et al. [10] tested attraction towards light with different on/off ratios. The study showed a significant attraction towards a pulsating light with an on/off ratio of 3.5/5.5 s. However, the study was done with only one type of light source; white LED light. This means that there might be other light settings and other pulsation rates giving higher attraction.

It can be investigated whether light can be used in order to create new and efficient methods to prevent salmon lice from causing injuries to the salmon, by taking advantage of the positive phototaxis of the salmon louse larvae. Thus, achieving specific information about the most attractive light sources is essential.

1.2 Profylax

This master thesis was a part of the multidisciplinary project Profylax. The overall goal for the project was to increase the knowledge about salmon lice and attraction towards different light settings, concerning wavebands, pulsation rate, and light irradiance. With this knowledge, the aim was to get closer to finding a solution to the problem of salmon lice in the fish farming industry. The project was initiated by Jørgen Ås Vatn, master student at The Norwegian University of Life Science (NMBU). The project consisted of five students and two researchers. In addition to J. Å. Vatn, the other students in the project were Elisabeth Børset (Mathematical Sciences, NTNU), Mads Francis Vale Kjeldsberg (Marine Technology, NTNU) and the authors of this thesis; Live Forfang Bjørnstad (Engineering and ICT, NTNU) and Maria Arild Solstad (Marine Technology, NTNU). The researchers were Anna Solvang Båtnes and Cecilie Miljeteig, both employed at NTNU. All the contributors have focused on different fields of the project. The authors' focus have been on the analyses of videos provided by Båtnes, Vatn, and Miljeteig, who were responsible for the execution of experiments. Some requirements for the dimensions of the experimental tanks, and the quality of the videos recorded was provided, were provided by the authors of this thesis. Båtnes, Vatn and Miljeteig took care of the whole process from lice hatching to uploading of experimental videos. Børset has been responsible for the statistical planning of the experiments and associated statistical analysis of the data provided by the authors.

The project has resulted in four master theses, whereas three of these were based on the same problem description. In addition to this thesis, Vatn has written a thesis with focus on the development of the experimental method, and Børset has written a thesis with focus on statistical planning of the experiments and analyses of the data extracted from the experimental videos, provided by the authors.

Båtnes will publish the results from the studies conducted in this project for the Aquacultute

Europe 2019 conference, and Miljeteig will publish a scientific paper on the same topic.

1.3 Objective and research questions

The objective of this thesis is to gain knowledge about the phototactic response of the salmon lice in the copepodid stage. By developing a method for analysis of the swimming behavior, velocity, and swimming direction of the salmon louse can be quantified. The hypothesis in this project is that the quantification procedure and the analysis of the lice behavior can be done extensively with custom made methods, using computer vision for object detection and tracking. The information gained about the behavior of the salmon louse copepodid is necessary to understand how the louse finds its host. Further, this knowledge can be used to prevent and control salmon lice infestation in the fish farming industry.

The need for more knowledge about salmon lice to prevent infection of the salmonid population raises the following research questions:

- Can the phototactic behavior of salmon lice be quantified and analyzed by algorithms based on computer vision for feature detection and tracking?
- Can this algorithm be used to evaluate the salmon lice responses to different light settings with respect to wavebands, light intensities, and pulsation rates?
- How will the light settings that give the highest response among the salmon lice in an experimental environment propagate in the ocean?

1.4 Scope

The scope of this project is to create a method for analyzing videos of salmon lice copepodids, hereby referred to as salmon lice, in an experimental tank with the use of computer vision for feature detection and tracking. This involves analyses of experimental videos, where data should be extracted and visualized. The propagation of light in the ocean should be investigated with the use of results from the salmon lice behavior analyses. The following list concretizes the scope of this thesis.

1. Perform a background study on problems in the fish farming industry related to salmon lice, the impact of external stimuli on salmon lice, feature detection and multiple object tracking using computer vision, and light propagation in water.

2. Develop a method for analysis of the phototactic swimming behavior of salmon lice using feature detection and tracking and use this for measuring velocity and swimming direction of the salmon lice.
3. Extract and analyze data from experimental videos.
4. Identify differences between light settings in terms of attraction of the salmon lice concerning wavebands, light intensities, and pulsation rates.
5. Investigate potential effects of artificial light in the ocean based on the results from the light response analyses.

1.5 Contributions

The main contributions of this thesis include the development of a method for detection and tracking of multiple moving salmon lice in experimental videos. Analyses of 128 experimental videos, including 36 different light settings and three replicates for both detection and tracking, are completed.

The objects were detected using image processing operations such as background subtraction, noise filtering, binarization, and contour detection. The experimental method tested for wavebands within the visible part of the spectrum (400-700 nm) with four different pulsation rates. On/off ratios of 0.1/0.1 s (P1), 2.0/3.0 s (P2) and 5.0/5.0 s (P3) were tested, as well as no pulsation (P0). With the implemented algorithms, exact behavior of the salmon lice when exposed to 36 different light settings was quantified in terms of overall movement within a group of lice, as well as individual velocity and swimming patterns. The methods developed using feature detection and identification tools showed that light has an impact on the swimming behavior of the salmon lice. Light settings using white light gave the highest overall attraction of the salmon lice. The swimming velocities of the salmon lice oscillated with the light pulsation, having increased velocity during the periods when the light was turned on. P0, P2, and P3 gave a higher response than P1. In addition, the propagation of the investigated light in the ocean was investigated theoretically and discussed.

Recommendations for further work on the topic are outlined. The algorithms developed as part of this thesis are, with some parameter tuning, applicable to related multiple object detection and tracking cases.

1.6 Structure of the thesis

The outline of the thesis can be seen below. Figure 1.1 is a visual description with the aim of tying together the different parts of the thesis.

Chapter 2 provides a background study done on the biology of the salmon lice focusing on external stimuli. Additionally, a background study on how computer vision tools are used for detection and tracking of multiple objects is provided.
Chapter 3 presents background theory on computer vision for feature detection and object tracking, as well as theory on the behavior of light with focus on how it propagates in water.
Chapter 4 presents the experimental setup and execution, the approach used for the implementation of the detection and tracking algorithms, and the measurements used for quantification of salmon louse behavior. This chapter also presents the approach taken in calculating the light propagation range for different light settings.
Chapter 5 shows the results from detection and tracking analyses, as well as results from light propagation calculations.
Chapter 6 provides a discussion about project limitations, interpretation of the results, and validations of the methods used.
Chapter 7 presents conclusions and further work.

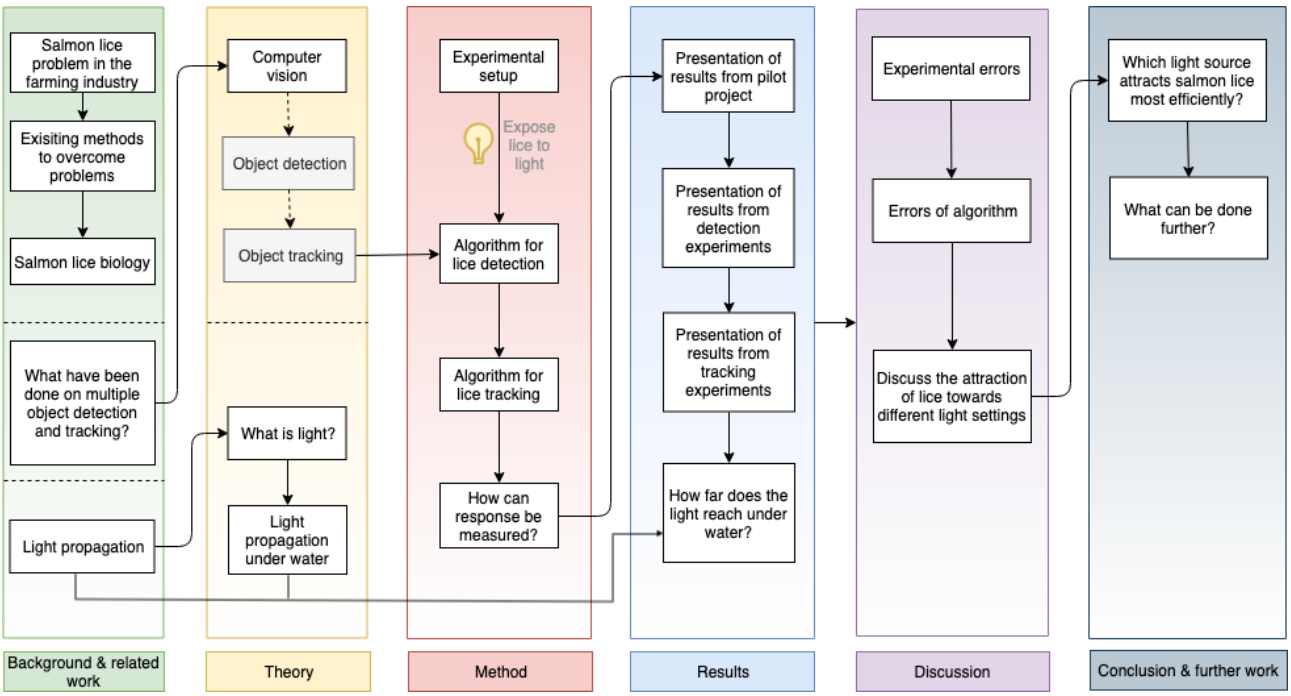

Figure 1.1: Thesis outline.

Chapter 2

Background and related work

In order to develop new methods for handling of salmon lice in the fish farming industry, it is important to understand the biology of the salmon lice. Thus, the biology of salmon lice and external stimuli is highlighted. Further, light as a source of attraction is presented. Computer vision for feature detection and object tracking can be used to analyze whether the light affects the salmon lice, and related work on this topic is therefore presented. Lastly, to understand the effect of light in water, a short review of literature about light propagation in water is presented.

2.1 Biology of *Lepeophtheirus salmonis*

Salmon lice is a copepod species in the genus Lepeophtheirus. It has a life cycle of 8 stages (Figure 2.1), where nauplii and copepodid are found in the upper layer of the water column and travels with the ocean currents [11], [12]. The length of the copepodid is around 0.7 mm [13]. According to the sea lice research center at the Univerity of Bergen, the copepodid stage has a life span of about 12 days, depending on temperature, to locate and attach to a host. During this time, it feeds on internal yolk proteins and fat [14].

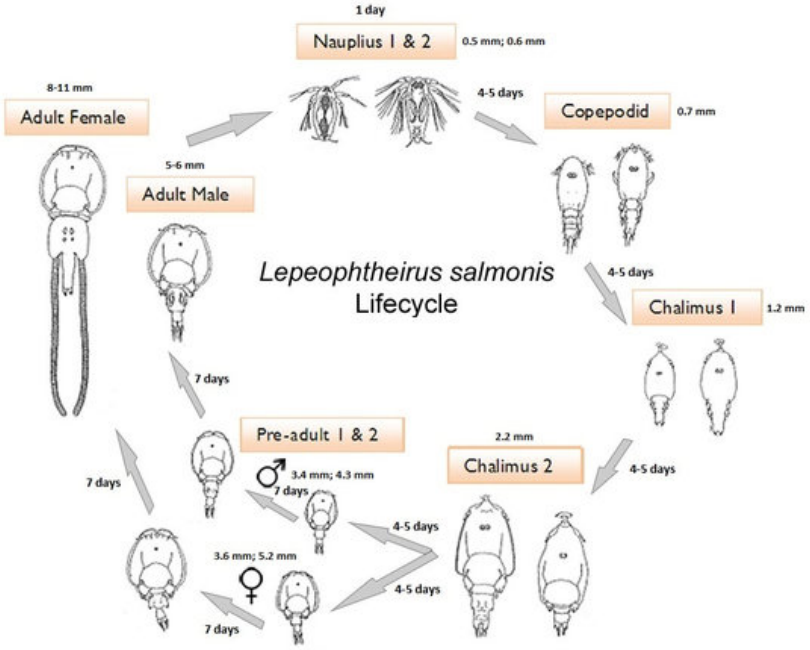

Figure 2.1: The life cycle of *L. salmonis*, retrieved from [15].

The salmon louse copepodid is equipped with a range of sensory structures [8], where some of them are explained below.

2.1.1 Mechanical and olfactory cues

The salmon lice have chemoreceptors making them able to detect chemical signals from the salmon [16]. In addition, they have antennules that are important for the detection of water flow or vibration stimuli. Earlier studies show that salmon lice can detect several external stimuli both related to the host and the environment. These stimuli include pressure from moving water, water temperature, chemicals, and light [17].

The salmon lice copepodids can detect near-field water accelerations produced by the host, and the swimming behavior changes according to these stimuli [18]. To detect this acceleration, the copepodids need to be within centimeters of the host as it passes. The attraction is also shown to be dependent on the swimming speed of the fish. Slow speed gives a thicker boundary layer around the fish; therefore, the landing conditions for the lice become better [19].

Several studies have been conducted on mapping the response to chemical stimuli of salmon lice. It is shown that olfactory cues (smell) can stimulate directional swimming of the copepodids over some centimeters [20].

2.1.2 Light response

The eye of the salmon louse is relatively big compared to the body length and has the capability of forming images. Additionally, the eyes have pigments and photoreceptors that can be sensitive to light of different wavelengths and have the ability to locate the light or a shadow source [21], [8]. Laboratory experiments have shown that copepodids have a positive and directed response to light stimuli, where the light can be related to the reflection in the skin of the host fish, and shadows caused by groups of fish swimming above the lice. Bron et al. [8] stated that this reaction was strongly related to the intensity and wavelength of the light, with the most significant response at wavelengths of 550 nm. In their study, the light sensory organs of the salmon lice were investigated, and a behavioral pattern was proposed from experiments. Wavelengths in the range of 400 to 700 nm were tested, and highest response was achieved at 550 nm. Aarseth and Schram [21] showed that the phototactic response was negative when exposed to ultraviolet light, with a peak at 313 nm. Arseth and Schram further concluded that the copepodids could differ between ultraviolet light and visible light and that their biology gives them the potential of sensing different wavelengths of light. Gravil [22] conducted experiments on salmon lice with light of wavelengths 400 - 700 nm. These experiments showed that the highest responses were reached for wavelengths in the range 500 - 560 nm. Gravil did also show that the salmon lice copepodid had a positive response to light intensities between 3 and 850 lux.

Fields et al. [10] conducted a laboratory experiment in order to define the host-related sensory cues of the salmon lice. In this experiment, the emphasis was on categorizing the responses to visual and olfactory signals. The behavioral response of the salmon lice copepodids to light pulsations was examined. The light pulsations simulated the flickery reflections of light from the salmon skin or shadows caused by groups of fish swimming above the lice. It was shown that the effect of light intensity was significant, giving increased swimming speeds towards the light at bright and medium bright intensity. In this study, four different pulsation rates were tested. The on/off periods were 1.8/0.9 s, 3.7/0.9 s, 3.7/5.5 s, and 3.7/16.5 s. The highest attraction was reached for 3.7/5.5 s.

Fields et al. [10] state that in order to estimate the distance for which the salmon lice can react to light stimuli, the depth range where the lice can differ between light and shadow has to be estimated. This is highly dependent on the clarity of the water. Fields et al. estimate that the copepodids of salmon lice can detect light/shadows from a depth of 31-37 m, at the western coast of Norway. They further estimate that the copepodids can swim with an average speed of 5.5 mm/s, and sustain this speed for one hour. This means that the salmon lice can move towards a group of fish (or flickery light) at a rate of 20 m/hr.

2.1.3 Geographical dispersion of salmon lice

Skarohamar et al. [12] state that the appearance of salmon lice is dependent on the ocean currents. These currents can transfer salmon lice between farms, making the lice infestation in one farm dependent on infestation in another farm connected by the same current. This means that the salmon lice can be spread to fish farms tenths of kilometers away from the origin. Since the currents tend to be strong and variable in certain areas, such as e.g., in the Norwegian fjords, the salmon lice can rapidly be spread over large areas and cause high infestation numbers. As stated by Fields et al. [10], the swimming speeds of salmon lice are significantly lower than the measured speeds of the ocean currents, and their natural swimming direction is mainly vertical. Hence, Skarohamar et al. [12] do not include the swimming speed of the salmon lice in the modeling of the infestation pattern. The swimming speeds of the salmon lice are more significant when it comes to the investigation of infestation at local levels, only meters away or in the fish farm [10], [22].

When considering the localization of salmon lice in the ocean, it is natural to take into account the natural position of the salmon. Juell et al. [23] state that there are seasonal variations among the salmon in sea cages, which is dependent on environmental conditions. Swimming depth is related to light conditions, feed availability, and hunger level. Huse and Holm [24] show that salmon tend to display a deeper vertical distribution during summer when there are high light intensities than during winter when the light intensity is lower. It was shown that salmon in a 20-m-deep cage had lower levels of lice infection during spring than lice in a 6-m-deep cage. When given a choice, the salmon tend to swim deeper and thus develop a lower lice infection. Hevrøy et al. [25] confirm that the depth positioning of salmon can be important in lice infestation, by counting the number of lice per salmon at different water depths. According to Heuch et al. [26], the copepodids in large enclosures in the sea tend to congregate near the surface during the day and disperse into deeper layers at night. Kadri et al. [27] state that the infestation of lice on salmon occurs mostly during the day when lice congregate near the surface, and the salmon swims at the highest speeds.

2.2 Multiple object detection

Bron et al. [28] showed that copepodites were attracted towards the light in the visible spectrum, with the highest response towards light with wavelength 550 nm. In their study, a tank of $15\times3\times3$ cm was used and divided into five equal sized areas separated by thin partitions. To determine phototactic response, ten salmon lice were placed in the center section. Immediately after placement in the tank, the partitions were raised, and the animals were stimulated with a

collimated horizontal light beam for 30 s before the partitions were lowered. The distribution of animals was then recorded in each section by manual counting. Positive phototactic response was defined for the animals ending up in the section nearest the light source [28]. The results from this study were obtained by the use of manual counting and detection.

Computer vision for detection and quantification of objects in the ocean has been in use for several years, making the process more efficient than manual detection. Kocak et al. [29] show that the results from the use of computer vision are just as good as human expert performance would be. In [29], contour models were used for image-segmenting, labeling, tracking, and mapping of plankton filmed with an underwater video camera. The object detection method used active contour models called snakes, defined by Kass et al. [30]. Snakes can be used to track, group, and differentiate organisms from noise and the background. A snake consists of nodes, and uses an energy-minimization method, to reach a local minimum or maximum area of intensity, also called a contour, in an image. Through iterations, the snakes follow the intensity gradients, defined by the pixel values, in order to settle along the contour of an object. This can be a favorable method when tracking of the objects is also part of the intention, and when the changes in the position of the objects from image to image are small. When segmenting the objects of interest from other noise and the background, Kocak et al. [29] used the following basic image processing techniques. First, the image was cropped to the desired size. Then, the morphological operations dilation and erosion were applied, followed by subtraction of the eroded image from the dilated image, leaving only the edges of the objects of interest. After the subtraction of the eroded image, it was inverted, and snakelets (groups of snakes) were dropped in the image to find the contours of the desired objects. When the snakelets had converged, the positions were stored for further analysis. With the use of snakes, tracking of the plankton was possible, assuming small movements from frame to frame. This method gives the opportunity to automatically identify and extract features of the plankton species [29].

When it comes to the detection of multiple small objects in an image or a video frame, the study of cell biology is relevant. Multiple algorithms are proposed for counting and categorizing cells in a microscopic image, to reduce time-consuming manual work. Common problems in object detection for this purpose are images of low contrast, low resolutions, and low frame rates. Additionally, cells can be grouped, making it hard to separate them [31]. Lizanes et al. [31] looked at methods for detecting cells on a chip, using image processing and computer vision. They divided cell detection in the image into two stages; the refinement stage yielding a conversion from the red, green, and blue (RGB) color space to grayscale before the detection stage could take place. And a detection stage, where the first proposed step was a thresholding algorithm, changing the image from grayscale to a binary scale. The thresholding algorithm changes all the pixels above a specific brightness value, a threshold, to 1 (white), and all the

pixels below to 0 (black). This method is useful when the objects of interest have a high contrast towards a uniform background. Without a uniform background, other algorithms such as edge detection, multiple thresholds, and background elimination can be used. When the objects were sufficiently marked in white, a contour search algorithm was applied. Parameters for each detected contour were calculated, including area, size, convex hull, the center of mass, and fitting ellipse. These characteristics could further be used to categorize the cells. Lizanes et al. [31] used C++11 programming language and OpenCV 3.0 programming library to implement the method described above.

In the research done by Fields et al. [10], a custom-designed image analysis software, provided by JASCO Scientific, was used. This software was used to monitor a field of view with a height of 15 cm and kept track of the number of salmon lice that traveled past the field in the vertical direction. The cameras used in this experiment were positioned in three different levels of the tank; bottom, middle, and top. The cameras were configured to produce sharp images of the salmon lice so that they could be counted by the object detection software, JASCO Scientific. In this experiment, the researchers extracted images from the three cameras every second for counting. The number of lice detected in each camera was plotted and used to quantify the swimming behavior of the lice.

Båtnes et al. [32] and Miljeteig et al. [33], characterized the movement of the calanoid copepods *Calanus* spp. using the conventional image analyzing software ImageJ. The analysis was based on one image per minute from a video stream of the experiment. The ImageJ software provides image processing in several steps and was used to detect the organisms in each frame. The first step in this study, included cropping of the image to get the desired area of the image for analysis, followed by a contrast adjustment in order to increase the contrast between background and objects of interest. A median subtraction was applied to remove unwanted static objects in the image before the image was converted to binary scale by thresholding. With a binary image, ImageJ can detect the objects of interest.

2.3 Tracking and mapping of swimming behavior

The salmon lice show directed swimming behavior when exposed to external stimuli such as water pressure, chemicals and light [10], [8], [18], [21], [22]. The behavior and swimming pattern of the salmon louse copepodid should be investigated further with a focus on mapping swimming patterns and swimming velocities, in order to gain more knowledge for further development of solutions to remove salmon lice from fish farms.

Gravil [22] showed that the salmon lice copepodids could obtain a swimming speed of maxi-

mum 10.23 cm/s when the salmon lice were mechanically stimulated by tapping the top of the test chamber. The average maximum natural swimming velocity was calculated to be 2.14 cm/s ($\pm$ 0.24). This study was done with a camera obtaining a frame rate of 25 frames per second (fps), and the swimming velocities were calculated manually by looking at the difference in positions from frame to frame, with a marked grid on the test chamber.

Planktonic copepods have a vast repertoire of different motions. Since these animals are of small dimensions, up to a few millimeters, the characterization of the swimming behavior can be tricky and require complex software systems. Bianco et al. [34] used a telecentric 3D computer vision system to characterize the swimming behavior of the copepod, *Clausocalanus furcatus*. The experiments were conducted using 30-37 individual copepods in a one-liter aquarium and filmed for one hour. The study showed an unexpected regularity in the swimming behavior when exposed to food, as opposed to previous studies showing that the swimming behaviour of this copepod was random. Salmon lice and textitClausocalanus furcatus are both in the subclass called Copepoda; hence, the findings from Bianco et al. [34] can be used for comparison when investigating the swimming pattern of the salmon lice. *Clausocalanus furcatus* repeatedly swims in a triangular or circular pattern in the horizontal plane. The experiments showed that the copepods move faster and sinks less when the concentration of food is higher.

In [34], a complex and advanced 3D observation system that allowed accurate mapping of the swimming speeds and directions of the copepods was used. This was done with the use of two digital cameras, telecentric lenses and infrared light sources in combination with the image processing software ImageJ and the tracking software MTrack2. The cameras used in this study had a frame rate of 15 fps. The videos were processed and transformed into binary videos by manually choosing the threshold to separate the foreground from the background. The 3D trajectories were obtained by combining the 2D images from each of the cameras. For each trajectory that was obtained, a custom Java software was used to calculate the velocities of the copepods by the use of the central finite difference formula with Δt being the time between two frames. The high-speed swimming results show a triangular swimming pattern and that the maximum speed of the copepod *Clausocalanus furcatus* is approximately 10 mm/s with a short duration (Figure 2.2).

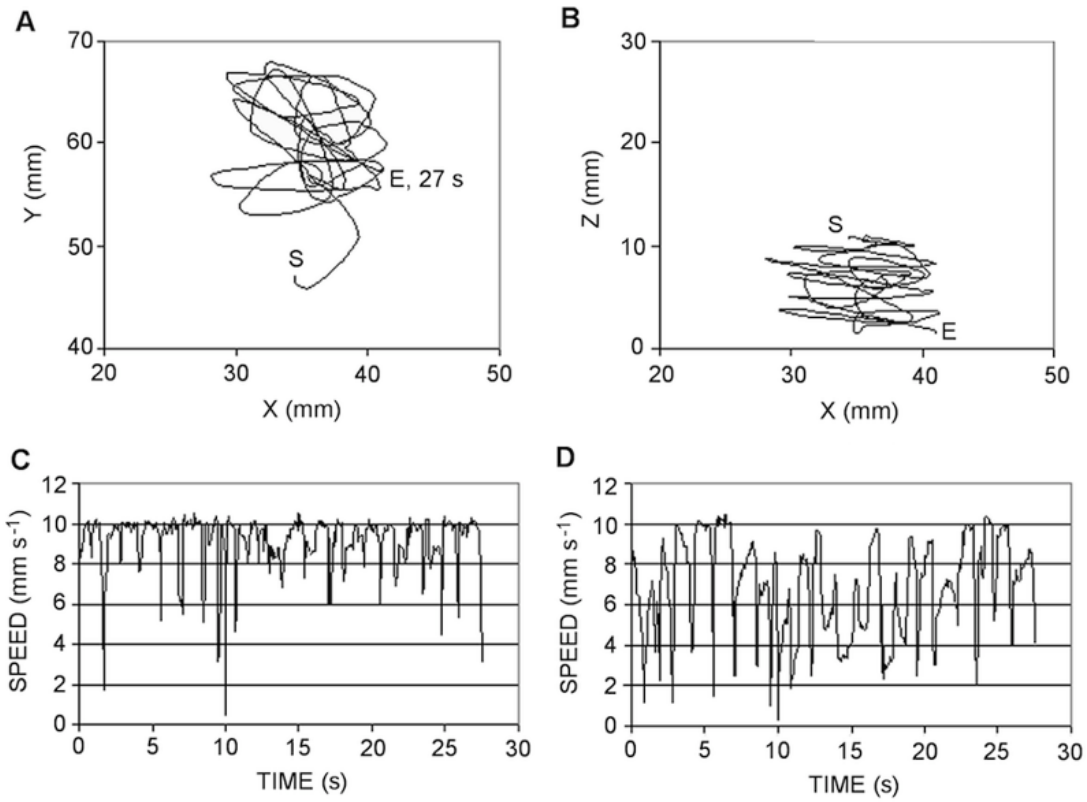

Figure 2.2: Swimming patterns and swimming velocities of *C. furucatus* in the horizontal and vertical plane, retrieved from [34].

Walter et al. [35] published the conference paper *Detection and tracking of objects in underwater video*, where a separate linear Kalman filters was used to estimate the x and y coordinates of the detected objects in the videos, and track their centroids over the image plane. The use of Kalman filter has become a popular method when analyzing the movement of objects such as persons, cars, animals, and insects. When investigating the swimming behavior of salmon lice, similar problems as in the analysis of insect behavior can be found. Straw et al. [36] used a standard extended Kalman filter (EKF) for detailed tracking of insects. The experiments in this study were conducted with the use of 11 cameras with a frame rate of 60 fps. In total, this setup was able to simultaneously track three flies, where the obtained tracks can be seen in Figure 2.3.

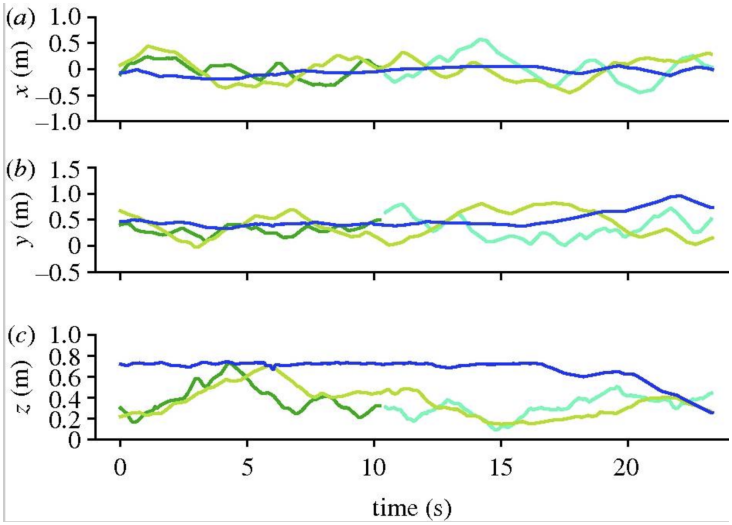

Figure 2.3: Illustration of trajectories of three flies in x, y and z direction, retrieved from [36].

When tracking multiple objects, the problem of interacting targets is common, especially when analyzing the movement of several small organisms in an enclosed area. Khan et al. [37] used a particle filter in order to solve the problem of interaction between targets. Their aim was not to create an accurate behavioral model but to gain knowledge that can help improve tracking performance. The particle filter can give robustness to unpredictable motion. Additionally, it can handle complicated nonlinear measurement models. In animal tracking, this is relevant, since the motion tends to be unpredictable. In [37] a solution using Markov random field (MRF) was proposed, which shows how to solve the problem with mixing up tracks when objects intersect. Secondly, they show how the exponential complexity given by the MRF, can be handled with the use of Markov chain Monte Carlo (MCMC) sampling and how this solution can be expanded into handling the case where the number of targets changes over time.

Snakelets, which was described in Section 2.2, can also be used for tracking of fast-moving objects, but with some modifications of the method used in [29]. The problem with the conventional method is that it does not take into account prior knowledge about color and motion. Hence, Seo and Lee [38] showed how the conventional snake model can be adapted for tracking of fast moving objects with the use of optical flow and condensation algorithms for motion estimation, and stochastic matching of the degree of color. This model is called *adaptive color snake model* (ACSM).

Another method that is commonly used for obtaining tracks and velocity of a moving object is the knowledge of where the object is in each frame, and Euclidean distance measures. By knowing the position of the object in each frame, the distance traveled can be used to calculate the velocity of the object. Sirisha et al. [39] showed how to track and obtain velocity of a circular moving object in a sequence of frames with the use of feature detection and Euclidean

distance. The same method was used by Tharanidevi et al. [40] for tracking of a moving person in a video sequence.

2.4 Light propagation

It is important to understand the behavior of light in water when looking at the attraction of salmon lice towards different light settings. Thus, the reduction in irradiance with increased distance from a light source, also referred to as how fast the light is attenuated, is of relevance.

Alsvik [41] performed an experiment intending to calculate the attenuation coefficient for different wavelengths of light at the SINTEF ACE full-scale laboratory facility at Hosenøyan, using Equation (2.1) [42].

$$K_d(z_2 \leftrightarrow z_1) = \frac{1}{z_2 - z_1} ln\Big(\frac{E_d(z_1)}{E_d(z_2)}\Big) \tag{2.1}$$

K_d is the vertical diffuse attenuation coefficient, z is the water depth, and E_d is irradiance, meaning the radiant flux (power) received by a surface per unit area. In Alsvik's calculations, E_d was measured with five different samples, where the mean of these samples was used in the calculations of K_d. For flat surfaces, such as the sea surface, it is common to distinguish between down-welling irradiance from above (E_d) and up-welling irradiance from below (E_u) [42].

The light intensity at the sea surface should be measured at the same time as the calculation of the attenuation coefficient at different depths. This should be done in order to account for variations in intensity that occur if, for instance, clouds are present. A weakness of Alsviks measurements is the absence of measurements at the sea surface.

In order to look at the propagation of light in water, the light irradiance also needs to be taken into consideration. In Båtnes et al. [32], experiments with different wavebands of light were conducted. The irradiance (E) was measured for each waveband and optical density (OD) to ensure experimental quality. An OD filter controls the percentage of light to be let through the filter, and an increase of 1 OD level means a decrease in the percentage of light irradiance by $10^{-1} \times 100 = 10\%$. OD1 means that $10^{-1} \times 100 = 10\%$ of the light is let through the filter, while OD2 means that $10^{-2} \times 100 = 1\%$ light is let through. The irradiance values achieved for OD5 in [32] can be found in Table 2.1.

Table 2.1: Irradiance E (400–700 nm) for the different wavebands with OD5 used in Båtnes et al. [32] experiments. Values are in μ mol photons $m^{-2}s^{-1}$.

	White	**Blue**	**Green**	**Red**
OD5	$7.9412E^{-05}$	$7.8064E^{-05}$	$3.923E^{-05}$	$31.142E^{-05}$

2.5 Profylax pilot project

Preliminary studies were done by the authors of this report and the rest of the Profylax project in the fall of 2018 as part of the preparation for the main experiments of this thesis. These preliminary experiments are referred to as the pilot project. The purpose of the pilot project was to get an understanding of the effects of color and irradiance levels, measured in μ mol photons m^{-2} s^{-1}, on the salmon lice response, and thus be able to eliminate some light settings before going further with new experiments.

In addition to different irradiance levels, light with wavebands within the range of green, blue, white, and red light were tested,in addition to different light irradiances. The irradiance levels were controlled by an optical density (OD) filter. Each experiment was conducted with three different replicates; R1, R2, and R3. The authors of this thesis extracted the salmon lice response data in November 2018, and statistical data analyses were performed by Børset. In this section, all figures are retrieved from Børset's thesis [43].

From the analysis based on the color of light, it was seen that the light response was positive for blue, green and white light, while the response for red light was small (Figure 2.4).

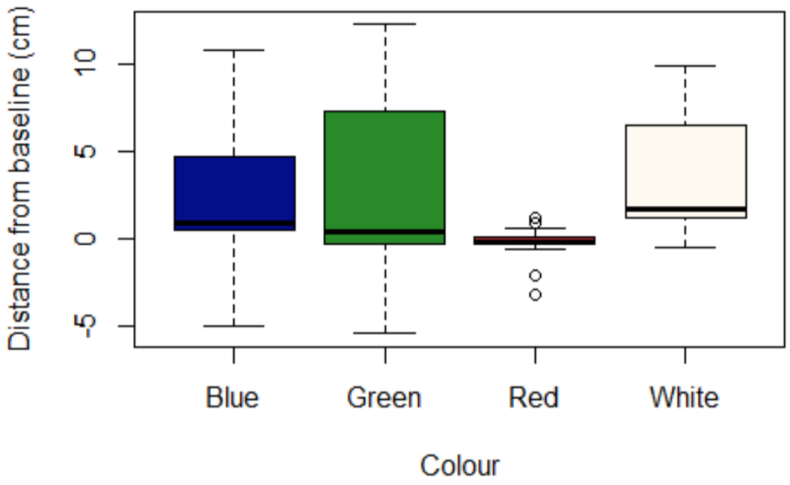

Figure 2.4: Box-plot of the response as the function of color, retrieved from [43]. The mean position of lice before light was turned on was used as a baseline. The distance from the mean position of lice to the baseline was used as the response variable, where positive values correspond to the lice moving towards the light source. The distance from the baseline within each colored light in experiments with different light sources is presented. All replicates and OD levels are included in each box.

When looking into each OD level, it was seen that an increased response occurred with decreasing OD level (Figure 2.5). It should be kept in mind that the response for OD2 was measured the last minute of this OD level, meaning the light had been on for a long time, starting with OD7. This means that the later OD levels could have been helped by the earlier OD levels. Thus, the results (Figure 2.5) do not entirely show the effect of each OD level.

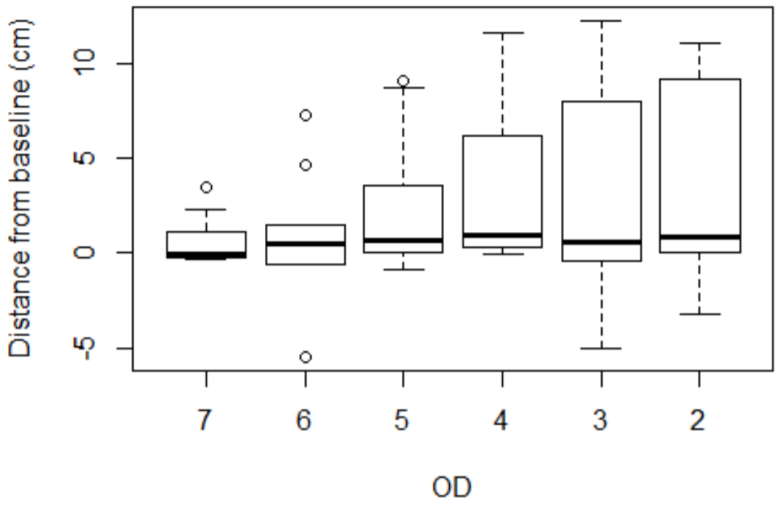

Figure 2.5: Box-plot of the response as the function of OD levels, retrieved from [43]. The mean position of lice before a certain light irradiance was turned on was used as a baseline. The distance from the mean position of lice to the baseline was used as the response variable, where positive values correspond to the lice moving towards the light source. The distance from baseline within each OD level is presented. This means that all colors and all replicates are included in each box, where the only distinguishing factor is the OD level. For each OD level, only data from the last minute within this OD level was used to calculate the mean position.

The response was also measured with respect to the each replicate. The distance from baseline was bigger for R2, meaning R2 had a more significant response towards the light (Figure 2.6). The big difference in response among the three replicates may be linked to the reuse of lice in experiments, where lice in R1 and R3 already had been through extensive light stimuli.

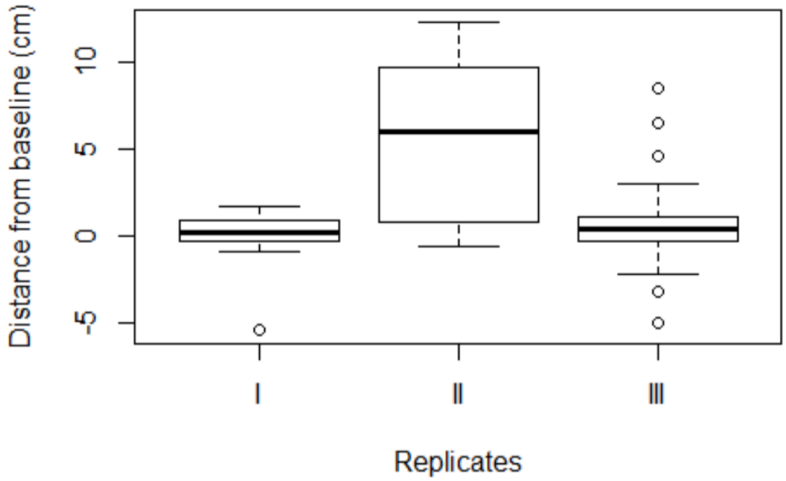

Figure 2.6: Box-plot of the response as the function of replicates, retrieved from [43]. The mean position of lice before a certain light irradiance was turned on was used as a baseline. The distance from the mean position of lice to the baseline was used as the response variable, where positive values correspond to the lice moving towards the light source.

As R2 showed to have a better response, a profile plot of the response as a function of OD levels for this replicate was plotted. Red light gave a generally low response, whereas green, blue, and white light had an increased response for decreasing OD levels (Figure 2.7).

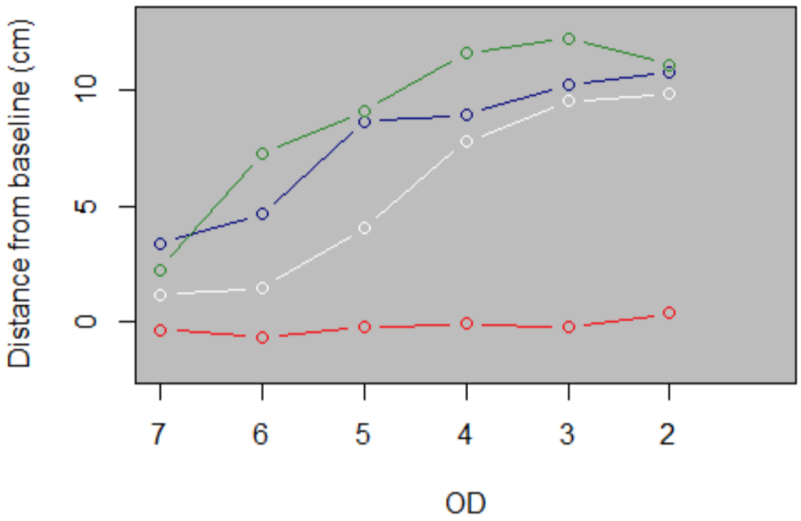

Figure 2.7: Profile plot of the response as a function of OD in replicate 2 (R2), retrieved from [43]. Green, blue, white and red refers to the color of the light source.

Combining all results, a significant response was seen for white light with OD5. For green and blue light, the response occurred already for OD7. Red light showed little response for all OD levels.

Chapter 3

Theory

The theory used in this thesis can be divided into two main categories; computer vision and the propagation of light.

3.1 Computer vision

By the use of computer vision, it is possible to achieve an objective quantification of the image frames extracted from a video, that can be used in further studies of the video content, such as detecting and achieving swimming velocity and swimming patterns of salmon lice [44]. To achieve a computer vision system, image processing is used in preliminary stages [45].

In this thesis, methods within computer vision for video analysis are further explored. This chapter explains the basic concepts of some image processing techniques, that lay the basis for computer vision and the method developed for salmon lice detection and tracking in this thesis. The book *Computer vision: algorithms and applications* by R. Szeliski [46] has been used in large part throughout this chapter. The image processing steps used before object detection can take place are summarized in Figure 3.1.

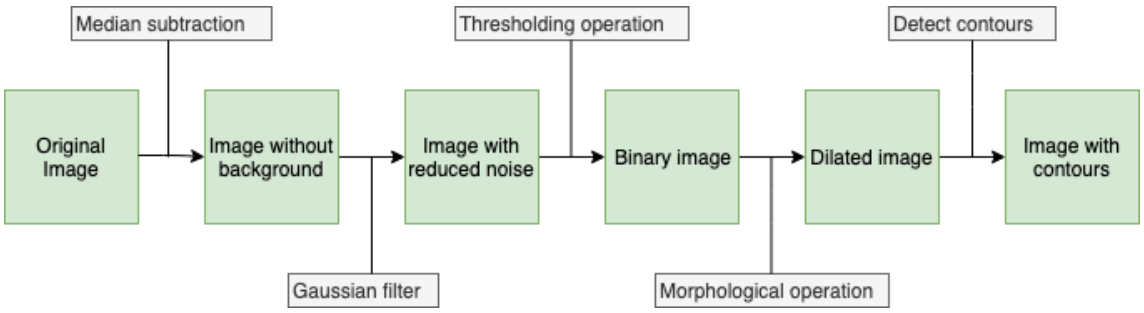

Figure 3.1: Typical steps of image processing for multiple object detection.

3.1.1 Color spaces

The color space is an essential factor to take into consideration when processing an image frame. The red, green, and blue (RGB) color space is the most used color space for the representation of colors in, e.g., monitors, scanners, and video cameras. If a pixel is represented in the RGB scale, it has a combination of different portions of red, green, and blue. For 8-bit color graphics, the portion is represented with a number between 0 and 255. If all the color portions are 0, the color is black, and if they are 255, the color is white. The RGB color space can be visualized as a color cube (Figure 3.2), with the primary and secondary colors as corners, the origin is black, and the opposite of the origin is white. The diagonal between black and white is the grayscale [46].

When converting an image to grayscale, Equation (3.1) is often used [47].

$$Y = 0.299R + 0.587G + 0.114B \tag{3.1}$$

R is the amount of red color, G is the amount of green color, and B is the amount of blue color in one pixel. This equation is a useful conversion for further image analysis, as it converts the three-dimensional RGB vector to a one-dimensional scalar Y, showing the light intensity in the pixels. By converting the image to grayscale, operations such as thresholding can be done as a step in object detection and recognition [46].

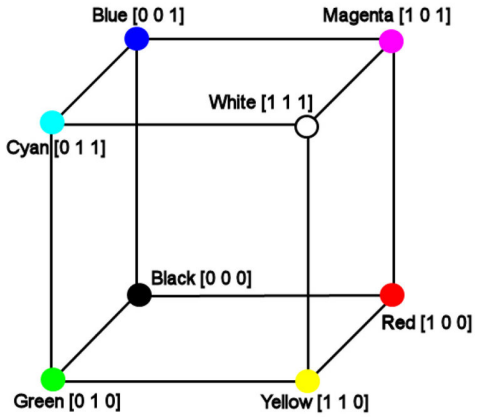

Figure 3.2: Red, Gren, Blue (RGB) color cube, retrieved from [48].

3.1.2 Image filtering

Image filtering is used for modifying and enhancing an image. This technique can be used when there is a need for emphasizing an object of interest, for instance a salmon louse, or remove irrelevant features in an image such as dust particles. Filtering can include adding blur to an image, sharpen edges and other details, and reducing noise [46]. The filters used can be both linear and nonlinear. Both types are explained below.

Linear filters

Linear filtering uses local or neighborhood operations and convolution, meaning that it uses pixels in the neighborhood of the relevant pixel to determine the output. It outputs a pixel value as a weighted sum of the values of the input pixels (Figure 3.3).

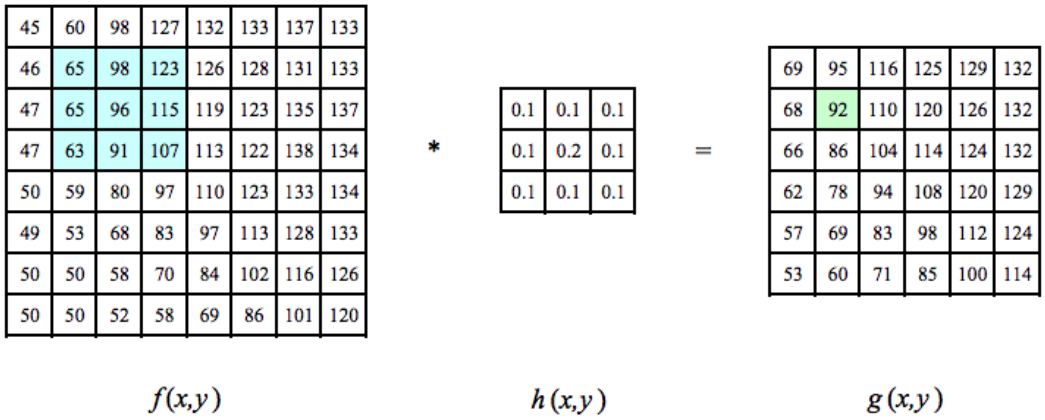

Figure 3.3: Convolution (neighborhood filtering): $f(x, y)$ is convolved by the use of the kernel/mask $h(x, y)$, often called filter coefficients, and outputs $g(x, y)$. The blue pixels is the neighborhood that gives the basis for the destination pixel illustrated as a green pixel in $g(x, y)$. Figure is retrieved from [46].

The linear filter is described by Equation (3.2), where $g(i, j)$ is the output pixel after the original pixel neighborhood $f(i, j)$ is convolved with the kernel $h(k, l)$.

$$g(i,j) = \sum_{k,l} f(i+k, j+l)h(k,l) \tag{3.2}$$

There are several widely used linear filters for smoothing, noise removal, and sharpening. The most simple linear filter is the normalized box filter. This filter takes the mean of a kernel of size $K \times K$ and outputs the resulting pixel value. Another useful filter is the Gaussian filter, which is used to blur images and reduce noise (Figure 3.4). The 2D Gaussian filter is described in Equation (3.3), and this 2D representation is what is most commonly used in image filtering.

$$\frac{1}{256}\begin{bmatrix} 1 & 4 & 6 & 4 & 1 \\ 4 & 16 & 24 & 16 & 4 \\ 6 & 24 & 36 & 24 & 6 \\ 4 & 16 & 24 & 16 & 4 \\ 1 & 4 & 6 & 4 & 1 \end{bmatrix}$$

Figure 3.4: 5×5 Gaussian kernel with $\sigma = 1$. The value 256 is the sum of all the values in the kernel. Figure is retrieved from [46].

$$G(x, y; \sigma) = \frac{1}{2\pi\sigma^2} e^{\frac{x^2+y^2}{2\sigma^2}} \tag{3.3}$$

σ is the standard deviation of the Gaussian distribution while x and y are the horizontal and vertical distance from the origin. The values calculated by this filter are used to make the convolution matrix that is later applied to the desired image. The Gaussian distribution has to be discretized to perform the convolution. The discretization can be done using the fact that the Gaussian distribution is approximately zero at three standard deviations from its mean, and the kernel size can then be limited to contain only these values [46].

Non-linear filters

Nonlinear filters can be applied if necessary, to achieve better performance. As opposed to linear filters, a nonlinear filter is a filter whose output is not a linear function of its input. Nonlinear filters can be used on images with noise that is not Gaussian distributed. Such noise can be referred to as *shot noise* or outliers. In these cases, a regular Gaussian filter might fail, resulting in just blurring the noise, and not removing it.

One example of a nonlinear filter is a median filter. This filer uses the median of a squared neighborhood of each pixel, making it possible to remove noise that differs a lot from the values in the neighborhood. When using the above filtering technique, the image is smoothed, and unwanted noise is filtered away [46].

3.1.3 Binarization

Binarization of an image is a result of a thresholding operation of a grayscale image, converting all pixels over a certain value to white, and those under to black. This operation is a step in the image recognition process, used to separate the background from the foreground, which is the objects of interest. This background and foreground segmentation can be used on images where the objects of interest have a brightness that differs from the background. In the threshold operation shown in Equation (3.4),

$$\theta(f,t) = \begin{cases} 1, & \text{if } f \geq t \\ 0, & \text{otherwise} \end{cases} \tag{3.4}$$

f is the binary image and t is the threshold value. If the pixels in f are above the threshold value, they become white; otherwise, they are declared black. θ is the output binary pixel.

The thresholding operation described above uses a global threshold value t. In situations where the image has different light conditions in different areas, adaptive thresholding can be useful. For this case, the algorithm calculates the threshold for a small region of the image. Thus, different regions of the image use a different threshold value, giving better results for images with different illumination [46].

3.1.4 Morphological operations

Morphological operations (analysis and processing of geometrical structures) are one of the most common image processing operations on binary images. Mathematical morphology is used to simplify image data by preserving the shape of interest and eliminate irrelevant features. Before performing mathematical morphological operations, the image is often binarized, using Equation (3.4), by following the procedure described in Section 3.1.1. When performing such operations, the binary image is convolved with a binary structuring element, and the output value is dependent on the thresholded result. Examples of structuring elements are boxes or circles. Some operations within binary morphology include dilation and erosion [49].

Dilation and erosion are the most common morphological transformations. These operations are used to remove noise, separate two elements in an image from each other, or to find holes (intensity bumps) in an image [46].

Dilation

Dilation is an operation that causes bright regions in an image, often the foreground, to grow. In that way, the objects of interest can get an increased area, and the dark background will be reduced. The dilation operation is done by convolving a region of an image with a kernel, often a square or a disk (Figure 3.5). The kernel can be thought of as a local maximum operator that replaces the image pixel under an anchor point in the kernel with the maximum value. If this is done on a binary image, the dilation process goes as follows: if at least one pixel under the kernel is 1, the pixel element is 1 [50].

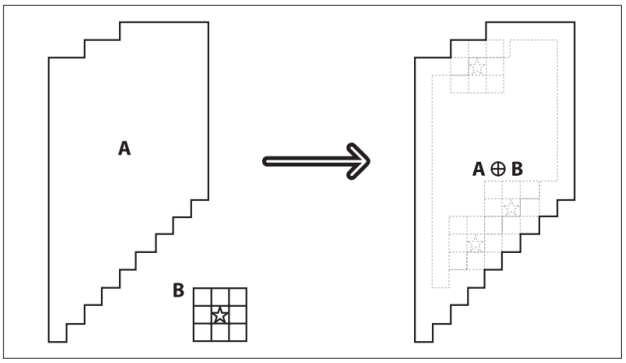

Figure 3.5: Dilation operation with an image region A and the kernel B. The star symbolizes the anchor point in the kernel. The figure is retrieved from [50].

Erosion

The opposite operation of dilation is erosion, which, together with dilation, is the most basic morphological operation. The local minimum over the kernel area is computed, and the result is illustrated in Figure 3.6. The erosion operation is mainly used to eliminate noise that occurs at speckles, often in the edge of the object of interest. With this method, visually significant content will stay in the image, while noise is eroded.

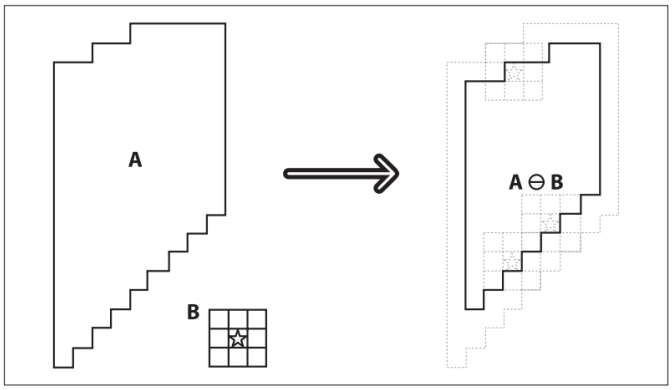

Figure 3.6: Erosion operation. An image A is convolved with the kernel B to minimize the pixel value under the anchor point. The figure is retrieved from [50].

3.1.5 Object detection

The techniques presented up until now are basic imaging techniques to improve the image and let the most important features stand out. The resulting images can be used for object detection and tracking in order to extract new and relevant information. This section will present theory on one object detection, whereas tracking of objects will be presented in Section 3.1.6.

Contour detection

Contours are lists of points that represent a curve in an image, by joining all consecutive points along a boundary having the same color or intensity [51]. To detect the contours of the objects of interest, border following algorithms can be implemented. Suzuki and Be [52] purposed two algorithms for border following that are still relevant for object detection today. These detection algorithms can effectively be used to count components and do a topological structural analysis of binary images such as finding the coordinates and the number of objects of interest. The following explanation describes an algorithm that finds the outermost border of a binary picture, which is useful in shape analysis of objects that do not contain holes. This algorithm is implemented using the OpenCV library and can be used to detect the boundaries of objects of interest.

The following description is based on [52]. The image being processed is a rectangular grid of pixels with value 0 or 1. The pixels in the image can be accessed with the index (i, j), representing the row and column numbers in the rectangular grid. i increases from top to bottom of the image, and j increases from left to right. In Suzuki and Bes algorithm, the border of the connected components and the surroundness is defined as: a border point between a 1-component S_1 and a 0-component S_2 exist if (i, j) is a member of S_1 and (p, q) is a member of

S_2. The term 0-component and 1-component refers to the connected components of pixels with values 0 and 1, respectively. If a 0-component S contains the frame, S is called the background; otherwise, it is called a hole. When it comes to sourroundness, it is said that S_2 surrounds S_1 directly if there exists a border point between them. An outer border is defined as the set of border points between a 1-component, and a 0-component which surrounds the border directly. A hole border is the set of border points between a hole and the directly surrounding 1-component. As stated by Suzuki and Be [52], the hole border and the outer border is a set of 1-pixels. Suzuki and Be define a parent border as *the hole border between S_2 and the 1-component which surrounds S_2 directly if S_2 is a hole and the frame of the picture, if S_2 is the background* (Figure 3.7).

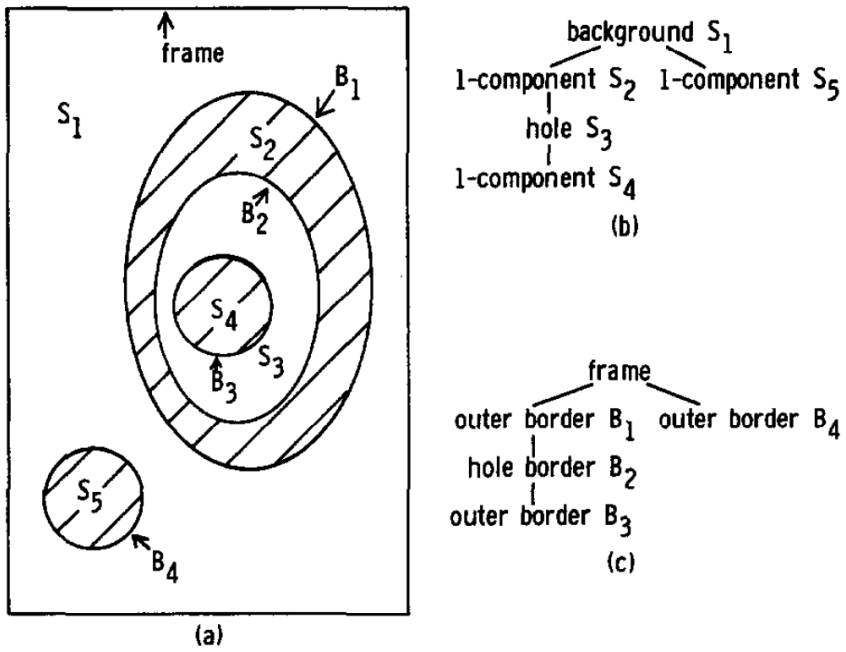

Figure 3.7: Surroundness for contour detection. S_3 is a hole and S_4 is a 1-component. S_4 surrounds S_3 directly, and the parent border between S_3 and S_4 is defined as the outer border between S_4 and the 0-component surrounding S_4 directly. The figure is retrieved from [52].

The algorithm for border following, that extracts the outermost borders of a binary picture can be found in Appendix 2 in [52]. The rationale of this algorithm is described below and is taken from [52].

The parent border of the outermost border is the frame of the picture. Therefore, the border point (i, j) immediately at the right of a 0-pixel is on an outermost border if and only if (i, j) satisfies either of the following conditions: 1) all the pixels $(i, 1)...(i, j-1)$ are 0-pixels 2) The border point (i, h) which has been encountered most recently is an outer border and the pixel $(i, h+1)$ belongs to the background [52].

Moment calculations

Moments are polygon shape descriptors, widely used in recognizing planar objects, and can be used as a feature descriptors. When the contours of objects in a frame are found, the moments of these can be taken into account. According to Flusser et al. [53], moments are used to characterize a function and capture their significant features. They have been used in pattern recognition to identify objects in images since they are independent of translation, rotation, scale, and general linear transformations of an image. From a mathematical perspective, they can be looked at as projections of a function onto a polynomial basis. Geometric moments are computed by integrating over all the pixels of a contour [50] (Equation (3.5)).

$$m_{pq} = \int_{-\infty}^{\infty} \int_{-\infty}^{\infty} x^p y^q f(x,y) dx dy \tag{3.5}$$

$f(x,y)$ is the object of interest in the continous case. Digital images require descrete representation, so Equation (3.5) needs to be rewritten to rather take the sum, resulting in Equation (3.6).

$$m_{pq} = \sum_{x=0}^{\infty} \sum_{y=0}^{\infty} x^p y^q f(x,y) \tag{3.6}$$

p is the x-order and q is the y-order. For binary images p and q are equal to 1. $r = p + q$ is said to be the order of the moment. In the simplest case, $m_{pq} = 1$ if a point (p,q) is inside the object, and $m_{pq} = 0$ if (p,q) is outside the object [53]. Low ordered geometrical moments often have an intuitive meaning. For binary images, $m00$ is the area of the object, described by Equation (3.7).

$$A = m_{00} = \sum_{x=0}^{\infty} \sum_{y=0}^{\infty} f(x,y) \tag{3.7}$$

The x- and y-coordinate of the center of gravity, also called the centroid, is defined as $\frac{m10}{m00}$ and $\frac{m01}{m00}$ [54]. When applying this to the detected contours, the centroids of the contours can be stored, and used later for further analysis such as calculations of distance and movement towards the light.

3.1.6 Tracking

When information such as position and area of objects is extracted from each frame, this can be used to retrieve time-dependent information. For some purposes, it can be valuable to follow each object from frame to frame and thus obtain information about the tracks and motions of

the objects. To identify light sensitivity of salmon lice, velocity and movement of the individual lice are of interest.

Handling changes in the appearance of the object such as out of plane rotations, shape and illumination are common problems in object tracking. Changes in the background can also appear, which gives another challenge in terms of separating the target object from the background [55].

By measuring the distance between objects from one frame to another, one can define tracks by assuming that the smallest distance between two objects in two following frames is the same object.

The distance d is measured in pixels. This can be done in several ways, but any distance metric should satisfy the requirements in Equations (3.8a) to (3.8c) for all pixels x, y and z [45].

$$d(x, y) \geq 0 \ and \ d(x, y) = 0 \quad iff \quad x = y \tag{3.8a}$$

$$d(x, y) = d(y, x) \tag{3.8b}$$

$$d(x, z) \leq d(x, y) + d(y, z) \tag{3.8c}$$

Some of the common ways to measure distance are by using Euclidean, city-block, or chessboard distance (Figure 3.8). Equations (3.9a) to (3.9c) are used to calculate the three distances.

$$d_{Euclidean([i_1,j_1],[i_2,j_2])} = \sqrt{(i_1 - i_2)^2 + (j_1 - j_2)^2} \tag{3.9a}$$

$$d_{city} = |i_i - i_2| + |j_1 - j_2| \tag{3.9b}$$

$$d_{chess} = max(|i_1 - i_2|, |j_1 - j_2|) \tag{3.9c}$$

In Equation (3.9) $i_1 - i_1$ and $j_1 - j_2$ represent the distance in x and y direction from the start position to the end position.

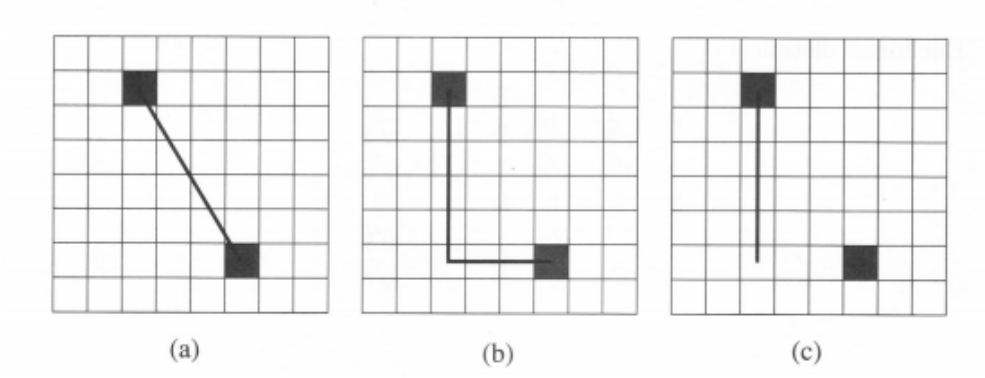

Figure 3.8: The way of measuring the different metrics for (a) Euclidean distance, (b) city-block distance, and (c) chessboard distance, retrieved from [45].

Computationally, the Euclidean distance is the most expensive choice of metric and results in real-valued distances. However, this is the distance that is closest to the continuous case and was the distance used for object tracking in both Sirisha et al. [39] and Tharanidevi et al. [40] as described in Section 2.3.

3.2 Light propagation

In order to understand the propagation of light in water, some basic theory about light is essential. This chapter will, therefore, describe the fundamentals of light and its behavior and how it interacts with its environment.

3.2.1 Light as waves and particles

Light is electromagnetic radiation. The light visible to the human eye belongs only to a specific portion within the electromagnetic spectrum, usually defined as having wavelengths from 400 nm (violet) to 700 nm (dark red). Shorter wavelengths are defined to be ultraviolet light, whereas infrared light is defined to have longer wavelengths [56]. The wavelength is the distance that light travels in one oscillation.

Light can be defined as tiny packets called photons (light quanta), having wave-like properties [57]. For a sinusoidal wave moving along the x-axis, the wave amplitude is defined as seen in Equation (3.10),

$$E(x,t) = E_0 \sin(kx \pm \omega t) \tag{3.10}$$

where E_0 represents the maximum amplitude, $k = \frac{2\pi}{\lambda}$ is the propagation number, and $\omega = \frac{2\pi}{T}$ is the angular frequency. The wave is repeated periodically with period $T = \frac{\lambda}{v}$ where λ is the wavelength, v is the speed of light, t is time [58].

It is not possible to observe the wave mode and particle mode simultaneously. While the wave mode is described by having different frequencies and wavelengths, the particle mode is described by the particle flux and energy per particle. The intensity of light can be associated with the flux of photons or the wave height. The wave and particle modes of electromagnetic radiation are linked by Planck's law, which states that the energy of a photon is linearly proportional to its frequency (inverse proportional to the wavelength). Thus, a photon belonging to blue light carries approximately 1.6 times more energy than a photon belonging to red light [57].

3.2.2 Terminology

Light intensity is often used when talking about light; however, the terminology is used in different ways in the literature. In this thesis, it is chosen to interpret light intensity as power emitted per unit solid angle in a specific direction [56]. Irradiance, on the other hand, refers to the radiant flux (power) received by a surface per unit area, and has the symbol E. A commonly used unit of irradiance is watt per unit area W/m^2, however; in the field of biology, μ mol photons m^{-2} s^{-1} is also typically used.

3.2.3 Behavior of light in vacuum

When light travels in a vacuum, it gets weaker with increased distance from the light source. This is due to the decreasing concentration of electromagnetic radiation. As the light gets further away from its source, the area it must cover increases and is proportional to the square of the distance it has traveled. The relationship between the light intensity (I) and distance (z) can be seen in Equation (3.11), E refers to the irradiance. This is called the inverse square law for light propagation [56]. When light travels through a medium like air or water, other factors do also influence the intensity.

$$E = \frac{I}{z^2} \tag{3.11}$$

3.2.4 Behavior of light in water

As described, when light propagates in a vacuum, only the distance reduces the intensity. When it travels through a medium, other factors such as absorption and scattering also impact the light intensity. There are similarities between optical propagation above and below the sea surface. Light in both air and water is affected by absorption and scattering, however; the scale of absorption and scattering in the underwater environment is much shorter, with extinction coefficients measured in inverse meters rather than inverse kilometers [59].

Absorption

Absorption is an irreversible thermal process whereby photon energy is lost due to interaction with water molecules or other organic or non-organic particulates. The absorption coefficient is numerically equal to the fraction of energy absorbed from a light beam when traveling a unit distance in an absorbing medium [60]. Blue and green wavelengths can be selected to minimize absorption, as the absorption coefficient in water is bigger for light of longer wavelengths within the visible light spectrum. However, scattering also has a significant effect of light propagation in water [59].

Scattering

Scattering is described as a process where a photon's path is changed due to interaction with particles, without changing the wavelength of the light. Rayleigh scattering represent the smallest contribution to scattering, and is a phenomenon that arises due to particles being much smaller than the wavelength of light. In water, this refers to water molecules and salt ions. Mie scattering, on the other hand, arises due to particles being larger than the wavelength of light. In water, this type of scattering is due to biological organisms and suspended particles [59]. The scattering coefficient can be described as the fraction of energy dispersed from a light source per unit of distance traveled in a scattering medium. The scattering of particles can be divided into forward- and backward scattering, depending on the change in the direction of the scattered particle or photon. Backward scattering occurs if the particle's direction gets reversed, while forward scattering refers to scattering involving a change of direction of less than 90 degrees [60].

Light attenuation

Light attenuation refers to the reduction in the intensity of light due to absorption and scattering of photons as it travels through a medium. The intensity decreases with distance depending on the wavelength of light, as shown in Figure 3.9 [61].

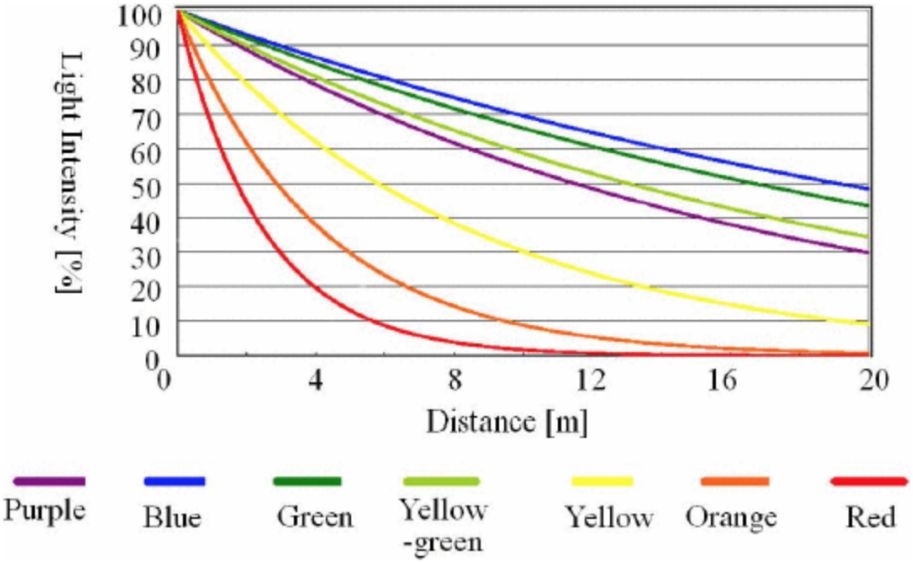

Figure 3.9: Light intensity in water whose attenuation coefficients of red, green, and blue colors are 0.4000, 0.0391, and 0.0348, respectively, used in [61].

It can be seen that red light is reduced to half the intensity at two meters, while blue light remains nearly unchanged at this distance. Red light disappears in 20 m, whereas blue light only decreases to about half of the intensity at the same distance (Figure 3.9).

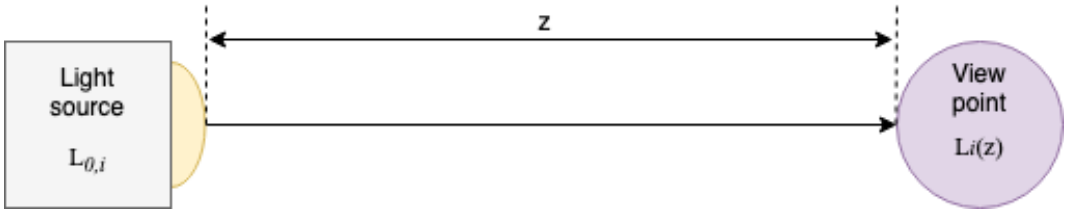

Figure 3.10: Light intensity in liquid.

The phenomenon of light attenuation can be described by Equation (3.12), and Figure 3.10 illustrates some of the involved parameters [61], [62].

$$L_\lambda(z) = L_{0,\lambda} e^{-c_\lambda z} \tag{3.12}$$

In Equation (3.12), λ refers to the wavelength of light in nm, z is the distance between the light source and the viewpoint in meters, $L_\lambda(z)$ is the light intensity of wavelength λ at distance z,

$L_{0,\lambda}$ is the light intensity at the light source, and c_λ is the attenuation coefficient.

The attenuation coefficient involved in Equation (3.12) consists of an absorption coefficient and a scattering coefficient, as light attenuation is dependent on these two phenomena. This relationship is described in Equation (3.13), where a_λ is the absorption coefficient, and b_λ is the scattering coefficient. Both are in units of m^{-1} [61].

$$c_\lambda = a_\lambda + b_\lambda \tag{3.13}$$

If the attenuation coefficient is large, it means that the beam of light is quickly attenuated as it passes through the medium. If the coefficient is small, however, it means that the medium is relatively transparent. The attenuation coefficient of water varies with the wavelength of light and the properties of the water. One example of attenuation coefficients can be seen in Figure 3.11 [61].

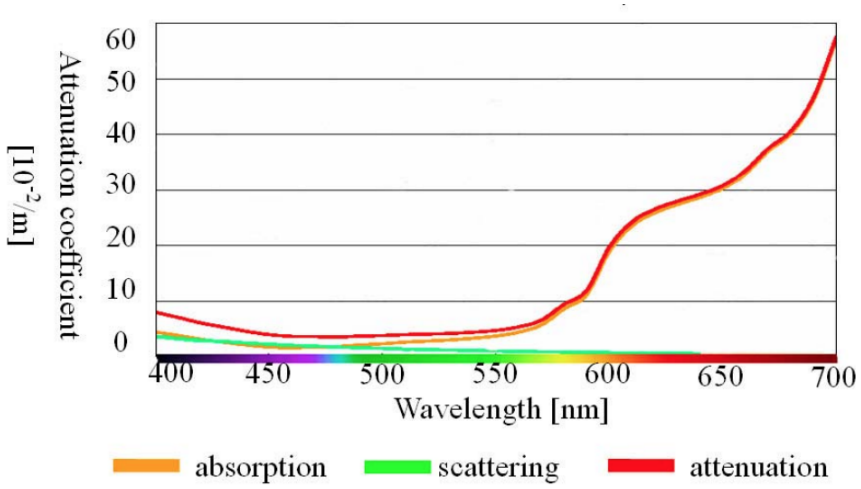

Figure 3.11: Attenuation coefficient of water whose attenuation coefficients of red, green, and blue colors are 0.4000, 0.0391, and 0.0348, respectively, as used in [61].

Absorption a_λ and scattering b_λ are inherent optical properties (IOP) which means that they only depend on the medium the light travels in; hence, they are independent of the ambient light field [63]. This means that the volume of water has well-defined properties whether or not there is light present to be absorbed or scattered [60], [64]. Typical values of absorption, scattering, and beam attenuation for different water types can be seen in Table 3.1.

Table 3.1: Values of coefficients for absorption, scattering and beam attenuation when light of wavelength λ = 514nm, corresponding to green light, is used [59].

Water Type	a(m^{-1})	b(m^{-1})	c(m^{-1})
Pure sea water	.0405	.0025	.043
Clean ocean	.114	.037	.151
Coastal ocean	.179	.219	.298
Turbid harbor	.266	1.824	2.19

Beam light versus diffuse light

The light attenuation coefficient can be calculated for beam light and vertical diffuse light, both with the use of Equation (3.12). The beam attenuation coefficient, c, is characterized by the extent to which the radiant flux is reduced with distance such that the residual beam does not contain any scattered flux. This coefficient is an IOP [65]. The coefficient is independent of existing lighting orientations, and the exponential decrease in power is accounted for in the measurements. The diffuse attenuation coefficient, K, is a measure of the extent to which diffuse downwelling daylight diminishes exponentially with depth. The diffuse attenuation coefficient has apparent optical properties (AOP), meaning it depends on both the medium and on the geometric structure of the light field [66]. For the case when the light is diffuse, the solar irradiance substitute $L_{0,\lambda}$ in Equation (3.12) [67].

Both the beam and vertical diffuse coefficients are functions of absorption and scattering; however, there are some differences. c represents the total loss, including all the absorbed and all the scattered photons, resulting in $c = a + b$. As the diffuse field propagates down through the water, both the photons which are absorbed and the photons which are backscattered are permanently lost. However, as downwelling flux is infinitely broad, the loss of photons due to forward scattering is highly reduced. It can be assumed that for the majority of photons scattered ”out,” there are photons from the adjacent region, which are scattered back ”in.” Thus, K represents the loss term, which includes all the absorbed photons and a portion of the scattered photons, resulting in $K = a + b/n$ [67].

Chapter 4

Method

The method used in this project can naturally be divided into two parts; the experimental setup and execution of experiments, and the implementation of algorithms for analysis of the experimental videos. Both are presented below. Further, the approach taken in the calculation of the light propagation under water is presented. The last subsection in this chapter presents the measurements used in order to analyze the response towards light, and the performance of the implemented algorithms.

4.1 Experimental setup

The experimental setup was based on the setup developed by Miljeteig et al. [33]. In this project, the experiments were executed by Miljeteig, Båtnes, and Vatn, and the resulting videos were provided to the authors of this thesis. The experiments can be divided into two parts. Detection experiments for detection of the overall movement of salmon lice when exposed to different light settings, and tracking experiments to map individual swimming behavior of the salmon louse. Each experiment was done with three replicates referred to as R1, R2, and R3. In this thesis, experiments were done with salmon lice in the copepodid stage, which is the free-swimming infective stage.

4.1.1 Equipment

Figure 4.1 shows the experimental setup used in Miljeteigs studies [68]. The same setup was used in this thesis; however, instead of having two IR light sources, five IR lights were used. The dimensions of the tank used for the detection experiments were 40 cm x 12.6 cm. For the tracking experiments, the length of the tank was reduced by half, resulting in a raceway of 20

cm x 12.6 cm (Figure 4.3). The tank was placed on top of a table, and IR light was directed towards the tank from an opening below. The IR lights were used to illuminate the lice in the water and make them visible in the recorded videos. IR light was used as it is invisible to the lice and therefore would not disturb the experiments. The tank was filled with filtered seawater to a depth of 4 cm. The video camera was placed 60 cm above the bottom of the tank in the detection experiments and 55 cm above the tank in the tracking experiments. An external light source was fitted to the left end of the tank to stimulate the salmon lice. The light source could be fitted with LEDs of different wavebands and was connected to a computer in order to change the light irradiance and pulsation rate without interruption of the environment (Figure 4.2). The entire setup was placed in a cooled room holding about 10 degrees Celsius. A high-speed video camera, *Oryx 5.0 MPMono 10GigE (Sony IMX250)*, was used to record the experiments in this project. This camera can record images at over 200 fps and supports transfer speeds up to 10 Gbit/s enabling the capture of 4K resolution.

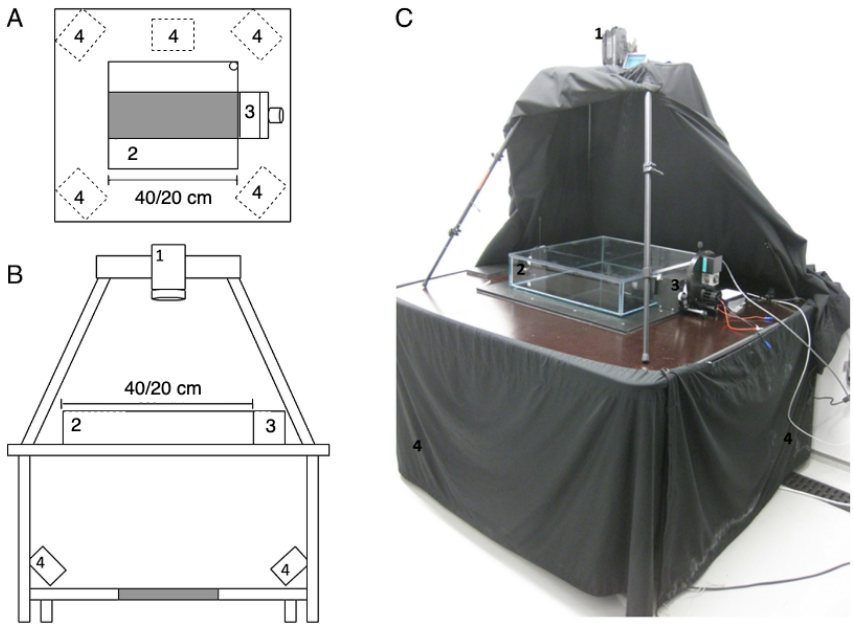

Figure 4.1: *A schematic overview of the experimental setup used to detect phototactic behavior of salmon lice from above (A) and the side (B) and a photograph of the experimental setup from the side (C). The experimental setup consisted of a camera (1), an aquarium (2) with a raceway in the middle (shaded area) fitted to the width of the light stimulus (3). A computer controlled filter wheel was fitted to the light stimulus device (3)[33].* On the table legs, five infrared (IR) lamps (4) were attached with adjustable brackets. The raceway was 40 cm long for the detection experiments, and 20 cm long for the tracking experiments.

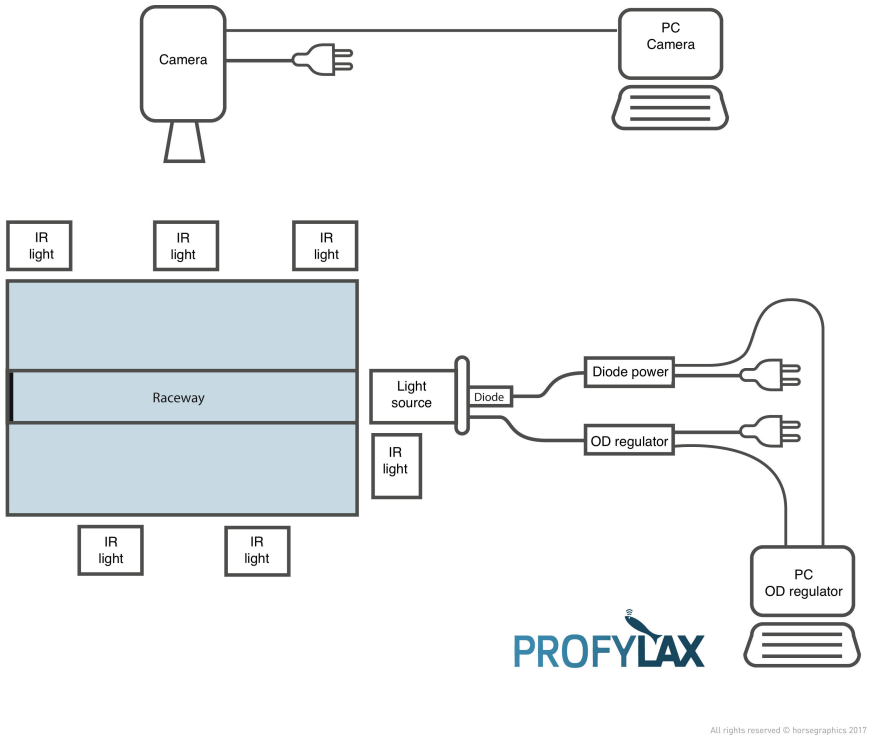

Figure 4.2: Overview of the components used in both the detection and the tracking experiments, retrieved from [69].

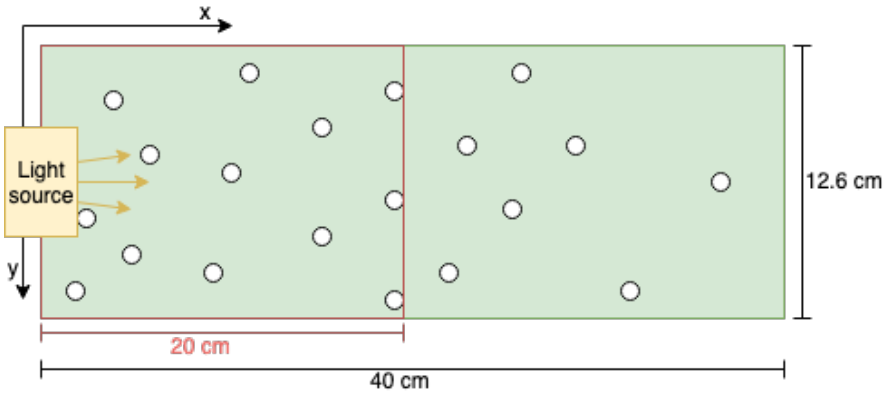

Figure 4.3: The dimensions of the experimental tank used for detection (dimensions marked in black) and tracking (dimensions marked in red). The white dots illustrate salmon lice.

4.1.2 Light settings

In the pilot project described in Section 2.5, red light showed little response for all OD levels and was therefore excluded in the main experiments. In addition, an increased response was seen with decreased OD level. OD5 was the highest OD level where a response was seen for the blue, green, and white wavebands in the pilot experiments; thus, only OD levels 1, 3, and 5 were investigated in this project.

The response of salmon lice towards light sources having three different wavebands, all in the range from 400 - 700 nm, were tested. The chosen wavebands are referred to as three different colors of light; green, blue and white, in this thesis. The wavebands for the different light sources are shown in Figure 4.4 [32]. The red part of the spectrum shown in Figure 4.4, was only used in the pilot experiments.

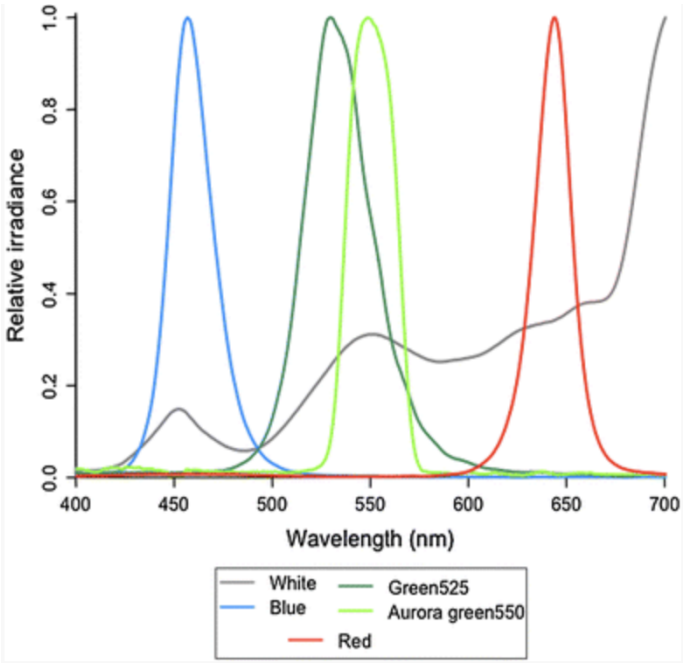

Figure 4.4: Relative spectral irradiance for white, blue and green light source based on measurements of OD5, retrieved from [32].

The irradiance values for each colored light source was varied over three different levels. This variation was controlled by an OD filter, as described in Section 2.5.

The total irradiances E was measured for OD5 for all the three different colored light sources, and the values for OD3 and OD1 were extrapolated with the use of the logarithmic relation between OD levels (Table 2.1).

Table 4.1: Total irradiance values for the different light settings with unit E (μ mol photons m^{-2} s^{-1})

	Green	**Blue**	**White**
OD1	0.3923	0.7806	0.7941
OD3	0.0039	0.0078	0.0079
OD5	3.9233E−05	7.8064E−05	7.9412E−05

Further in this thesis, the irradiance levels of the light sources, are referred to as OD1, OD3, and OD5. Practically speaking, this means high irradiance, middle irradiance, and low irradiance.

In addition to the difference in irradiance and color of the light sources, the light settings also included different pulsation rates Table 4.2.

Table 4.2: Description of the different pulsation rates used in the experiments.

	Light on [s]	**Light off [s]**
Pulsation 0 (P0)	constant	-
Pulsation 1 (P1)	0.1	0.1
Pulsation 2 (P2)	2	3
Pulsation 3 (P3)	5	5

In total this resulted in $4 \times 3 \times 3 = 36$ different light settings.

4.1.3 Procedure

Before the experiments took place, salmon lice had to be collected. For the experiments in this thesis, three different groups of copepodids were used. These include copepodids from the culture of Taskforce salmon lice (hatched at NTNU), copepodids hatched at ILAB (The Industrial and Aquatic Laboratory, Bergen), and copepodids hatched at NTNU originating from egg strings produced at ILAB.

When carrying out the experiments, the first step was to fill the tank with salmon lice. For the detection experiments, between 150 and 200 individuals were used in the tank. This number was reduced to 12-15 lice when the tracking experiments were executed. The individuals were counted the day before the experiments and stored in the dark before they were added to the experimental tank, also in the dark, ensuring complete acclimation. Further, the tank was stirred to make sure the lice were evenly distributed. Then, the tank was left untouched for 30 minutes for the currents to settle and the salmon lice to acclimate.

The experiment started when the camera was turned on. For the detection experiments, three minutes were spent with the light off before the light was turned on for seven minutes. For the tracking experiments, 30 seconds were spent in darkness before the light stimuli were on for 90 seconds. The dark period was used as a reference to test the response towards light. Each experiment was conducted with a different combination of waveband, OD, and pulsation rate. The frame rate of the recorded videos were 16 fps for the detection experiments, while the tracking experiments used a frame rate of 128 fps.

The response from the different light settings described above was tested for three different replicates, resulting in a total of 36×3 = 108 videos with detection experiments and 108 videos with tracking experiments.

In the pilot experiment, the cut-off-filter used to filter the IR-light let through visible wavelengths of light, leaving some attraction towards the IR-light. This was changed before the main experiments of this thesis. In the main experiments, the IR light as stimuli was tested to check for potential responses to the light used for illuminating the lice. This confirmed no response towards the IR light source.

The order for which the different types of light settings were tested was randomized. In addition, there were three replicates to ensure the quality of the experiment. The detection experiments were executed on January 10th, 11th, 14th, 16th, 18th and 19th, while the tracking experiments were done on February 6th, 7th, 8th, and 11th, all in 2019.

An example of a layout for one experiment is shown in Table 4.3. This information was provided to the authors, along with the experimental videos.

Table 4.3: Layout for a detection experiment with white light, OD3, and pulsation P1. The same setup is used for tracking, but with a shorter duration.

16.01.19 - White-OD3-P1-R1				
Temperature air 09:30: 9.5°C - Temperature water 09:30: 9.0°C				
09:00 - darkness acclimatization started				
09:30 - Filming started				
Duration [minutes]	OD setting	Pulse rate	Color	Number of lice
10.05	OD3	P1	White	210

A frame rate of 16 fps resulted in 9600 frames for each video of the detection experiments. For the tracking experiments, a frame rate of 128 fps gave videos of around 15360 frames. Due to a big amount of experimental videos, each video was given a name based on the configurations of OD settings, pulsation rate, and color. For instance, Blue-OD1-P1-R3 was the name of the experiment where blue light was tested with OD1, pulsation rate 1, and the third replicate. Throughout the rest of this thesis, the different light settings will be referred to using these names.

4.2 Algorithm

The detection and tracking of lice were done using two separate algorithms. First, the implementation steps of the detection algorithm is presented, followed by the implementation of the tracking algorithm.

This project required custom-made methods that could be scaled and adapted to the conducted experiments, giving room for specific response analysis of position and movement of the objects

in desired time intervals. Hence, it was chosen to implement a detection and tracking algorithm with the help of the built-in library in Python, OpenCV [51], which provides a framework to use computer vision techniques efficiently.

The following sections contain an overall approach for how the videos of the experiments were analyzed, and how the results were extracted.

4.2.1 Detection

The following section describes how the detection algorithm was implemented. The implementation was based on the theory described in Section 3.1. Figure 4.6 show the results after each step in the developed algorithm. The same images are included in Appendix B in a larger scale.

File conversion

The videos that were provided in this project consisted of images in raw format. One of the main reasons for choosing to shoot the videos in this format was due to the automatic compression that takes place when using JPEG. When this compression happens, one can risk losing important information.

Before the feature detection took place, prepossessing of the image frames needed to be done. The first step was to read the raw files and handle the pixels by converting each image to uint8, giving them a range from 0 to 255.

Cropping

In Figure 4.5 one can see one of the original images that were provided to the authors. This image show that there are areas near the sides of the image that are brighter than the rest of the image. These bright areas show light reflections in the walls of the tank.

The original video frame for the detection videos had dimensions of 2448×814 pixels. With a tank of dimensions 40×12.65 cm, the length of the pixels in x-direction became 0.0163 cm and 0.0155 cm in the y-direction. The frame was cropped to 2170×650 pixels to remove some of the light reflections seen in Figure 4.5, and thus avoid error detections.

Figure 4.5: Video frame of detection video. The dotted line marks where the video frame was cropped in the preprocessing steps of the detection algorithm.

Coordinate system

Before implementing the rest of the detection algorithm, a coordinate system needed to be defined in order to specify the locations of the detected objects. The origin of the coordinate system was chosen to be in the upper left corner of the images, with positive x-axis towards the right side, and positive y-axis directed downwards (Figure 4.3).

Background subtraction

The median of the pixel values was calculated from the 1000 last frames of the video. The calculated median was then subtracted from every frame in the video to remove the static background form the foreground. In the videos in this project, the background could contain dust particles and air bubbles that were of the same size and brightness as the salmon lice. These objects needed to be removed in order to reduce the detection error, and this was done by median subtraction. The image without the static background can be seen in Figure 4.6b.

Due to the pulsating light used in the experiments, the background in the videos changed brightness every light period. Hence, a median for both bright frames and dark frames had to be calculated. Whether the frame was bright or dark was decided by calculating the mean of all pixels in the current frame and check if it was above or below an average mean throughout the video.

Noise removal

After removing the static background from the images, a Gaussian filter was used on the frames to remove Gaussian noise as explained in Section 3.1.2, with the use of a Gaussian kernel of size 3×3 (Figure 4.6c).

Thresholding

A prerequisite for the input frame in the method used to find contours was that it had to be binary. Binarization was done by calculating a threshold for each frame. This threshold was tuned and adapted for each OD based on the pixel values in the image, due to different illumination in the videos. The result from the threshold operation can be seen in Figure 4.6d.

Morphological operation

When an image is converted to a binary image, all the pixels are either black or white. Even though feature detection could be performed on the binary image, it was preferred to increase the area of the white parts in the image (the foreground). A salmon louse has a diameter of approximately 0.7 mm. This means that it covered 3.88 pixels if the circumstances were perfect. Since the lice moved around and shifted between horizontal and vertical orientation, the pixel area it covered were sometimes even less than 3.88 pixels. By dilating the white areas in the image, the area of the lice increased, and the object detection became more stable. The dilated image can be seen in Figure 4.6e.

Feature detection

When the above processes were done, the salmon lice could be detected. OpenCV has a method based on Suzuki's algorithm for finding contours which are intuitive and easy to use, and is convenient when the objects of interest are small [52]. Thus, as the lice in the experimental videos only covered around 4 pixels (10 pixels in the tracking videos), it was the chosen method for the detection of the salmon lice. The found contours are seen in Figure 4.6f.

Contour features

When the contours were detected, the centroids could be extracted. This was done by calculating the moments of the contours, as explained in Section 3.1.5. The size range for which the objects could reside in was decided empirically from the dataset. If the area of the detected object was within this range, the object was accounted for as a louse. The x- and y-coordinates were then extracted and used for further analyses.

Pseudocode

The following pseudocode summarizes the implemented detection algorithm.

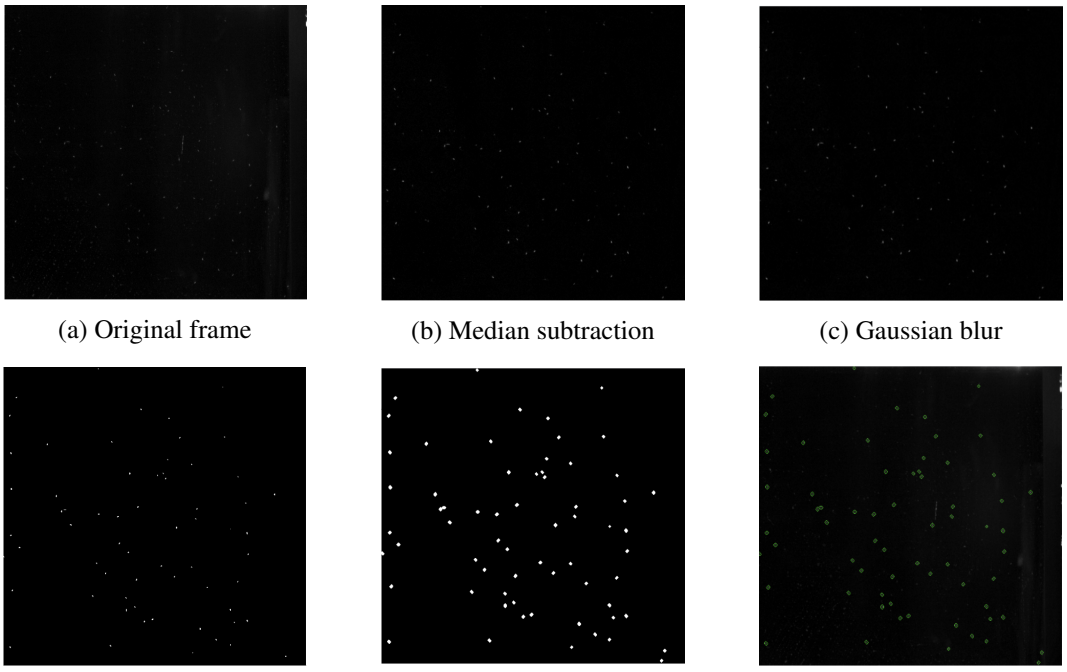

(a) Original frame (b) Median subtraction (c) Gaussian blur

(d) Threshold (e) Dilation (f) Contours

Figure 4.6: Step by step processing of each frame in the video. (a) show that the original frame had a low contrast, and that the lice appear small. (b)-(e) show the enhancing image processing steps. (f) show the detected contours marked with a green boundary.

Algorithm 1 Salmon lice detection

$frames = list(video)$ ▷ Get list of video frames
$num\_frames = length(frames)$
$median\_bright = median(bright\_frames)$ ▷ Take median of all bright frames
$median\_dark = median(dark\_frames)$ ▷ Take median of all dark frames
$all\_centeroids = [\,]$ ▷ Allocating list for centeroid coordinates in video
for frame **in** frames **do**
    if $bright\_frame\_detected$ **then**
        $frame- = median\_bright$ ▷ Remove bright background
    else
        $frame- = median\_dark$ ▷ Remove dark background
    end if
    $frame.crop()$
    $frame.increase\_brightness()$
    $frame = GaussianBlur(frame)$ ▷ Remove Gaussian noise
    $frame = threshold(frame, lower, upper)$ ▷ Binary conversion of image
    $contours = findContours(frame)$
    for contour **in** contours **do**
        $moment = moments(contour)$ ▷ Calculate moments
        $area = contourArea(contour)$ ▷ Find area of contour
        $centroids = [\,]$ ▷ Allocating list for storage of coordinates in frame
        if min $<$ area $<$ max **then** ▷ Decide range of area
            $x = \frac{m['m10']}{m['m00']}$
            $y = \frac{m['m01']}{m['m00']}$
            $centroids.append((x, y))$
        end if
        $all\_centroids.append(centroids)$
    end for
end for

4.2.2 Tracking

The tracking algorithm implemented in this project was an extension of the detection algorithm described in Section 4.2.1. For the videos of the tracking experiments, a higher resolution was obtained as the size of the tank was reduced, and the camera lens got closer to the lice. With a tank of dimensions 20×12.65 cm and a resolution of 2200×1560 pixels the length of one pixel in x and y-direction became 0.0091 cm and 0.0081 cm, respectively. The tracking experiments were executed using around 12 lice in the tank.

The tracking algorithm utilized the fact that the videos were recorded with a relatively high frame rate of 128 fps, making the change in position of the salmon lice from frame to frame small. The center coordinates of all detected objects found with the detection algorithm were used in order to match the coordinates from frame to frame. This was done by allocating a list of tracks and initialize the list with lists of the coordinates of detected objects in the first video frame. For each of the following frames, the retrieved coordinates were matched to the closest coordinate in the previous frame and added to the associated track. If the distance to the closest object in the previous frame was larger than approximately twice the length of the louse, a new track was added to the list instead of connecting the louse position to one of the previous tracks.

Distance calculations

The Euclidean distance (Equation (3.9a)) was used to compute the distance from the detected lice in frame i to all end coordinates, belonging to frame $i-1$, of the registered tracks. The computed distances were then used to connect the lice to their belonging tracks.

The distance from each coordinate to all previous coordinates was calculated in order to match the object to the correct track. In the case where the number of detected objects was higher than the number of stored tracks, a new track containing the coordinate furthest away from previous tracks was added as a new element to the list of tracks. For the case where the number of detected objects were lower than the number of stored tracks, only the tracks containing the coordinates close to the current detections were updated with new coordinates. The rest of the tracks were updated with the same coordinate as in the previous frame. From this data, information about velocity and direction was retrieved.

Velocity calculations

For velocity calculations, the same approach as described by Bianco et al. [34] was used. Velocities in x- and y-direction were calculated according to Equation (4.1),

$$u(x_i) = \frac{x_{i+1} - x_{i-1}}{2\Delta t} \tag{4.1a}$$

$$v(y_i) = \frac{y_{i+1} - y_{i-1}}{2\Delta t} \tag{4.1b}$$

where x is the x-coordinate and y is the y-coordinate of the salmon louse. Δt is the time step between each data point. With 128 fps, Δ t = 1/128 s.

The total velocity was calculated using Equation (4.2).

$$V(x_i, y_i) = \frac{\sqrt{(x_{i-1} - x_{i+1})^2 + (y_{i+1} - y_{i-1})^2}}{2\Delta t} \tag{4.2}$$

Algorithm 2 shows the steps in the tracking of salmon lice. It should be noted that the centroid coordinates were retrieved from the detection algorithm shown in Algorithm 1.

Pseudocode

Algorithm 2 Salmon lice tracking

```
video = path
centeroid_coordinates = detect_lice(video)        ▷ List of coordinates in each frame
tracks = [ ]                                      ▷ Allocating list for tracks
tracks.append([x, y]for[x, y]incenteroid_coordinates[0])
for each frame in centeroid_coordinates do
    for each cooridate in frame do
        min_distance, track = compute_distance(coordinate, tracks)
        if min_distance > lice_size then
            track.append(coordinate)              ▷ Add closest coordinate to each track
            update(tracks)
        end if
    end for
end for
for each track in tracks do
    speed = compute_speed(track)
    arc_length = compute_arc_length(track)
    distance = compute_distance(track)
    track.update(speed, arc, distance)
end for
```

This tracking algorithm was chosen because it works well when tracking objects in a video with a high frame rate. When objects cross, however, the track ID might be exchanged.

4.3 Light propagation

To calculate how far the light sources used in this project propagate under water, Equation (3.12) in Section 3.2.4 was used with irradiance E, instead of light intensity L. This equation shows how the irradiance $E_\lambda(z)$ decreases with distance z (m) away from the light source. $E_\lambda(z)$ is dependent on the attenuation coefficient K_λ, and the wavelength (λ) of the light. In this thesis, only wavelengths in the waveband 400-700 nm were used.

To be able to estimate $E_\lambda(z)$ values for the OD levels used in this project, initial irradiance $E_{0,\lambda}$ was needed for OD5, OD3 and OD1, as well as corresponding attenuation coefficients K_λ. The sum of all initial irradiances $E_{0,\lambda}$ is referred to as the total irradiance in this thesis.

Calculating initial irradiance values

With the use of the logarithmic relation between OD levels, the total irradiance values for OD3 and OD1 was calculated with the measured values for OD5 (Table 2.1) as a basis. The resulting extrapolated total irradiances for OD3 and OD1 can be found in Table 4.4.

Table 4.4: Extrapolated values for total irradiance (400-700 nm) for OD3 and OD1.

OD	**Green**	**Blue**	**White**
1.0	0.392	0.781	0.794
3.0	0.0039	0.0078	0.0079

By assuming that the ratios between the different initial irradiance values, $E_{0,\lambda}$, are independent of OD, new spectral $E_{0,\lambda}$ values for OD3 and OD1 in the waveband 400-700 nm could be calculated. The values for $\sum_{\lambda=400}^{700}(E_{0,\lambda})$ in (Equation (4.3)) were taken from Table 4.4.

$$\frac{relative\_irradiance_\lambda}{\sum_{\lambda=400}^{700}(relative\_irradiance_\lambda)} = \frac{E_{0,\lambda}}{\sum_{\lambda=400}^{700}(E_{0,\lambda})} \tag{4.3}$$

Finding attenuation coefficients

By assuming diffuse light, the vertical diffuse attenuation coefficients (K_λ) found at SINTEF ACE full-scale laboratory facility at Hosenøyan could be used. These coefficients were measured for different wavelengths than the ones used in Båtnes' [32] measurements. Thus, the needed attenuation coefficients were approximated with polynomial regression of order 3 (Figure 4.7).

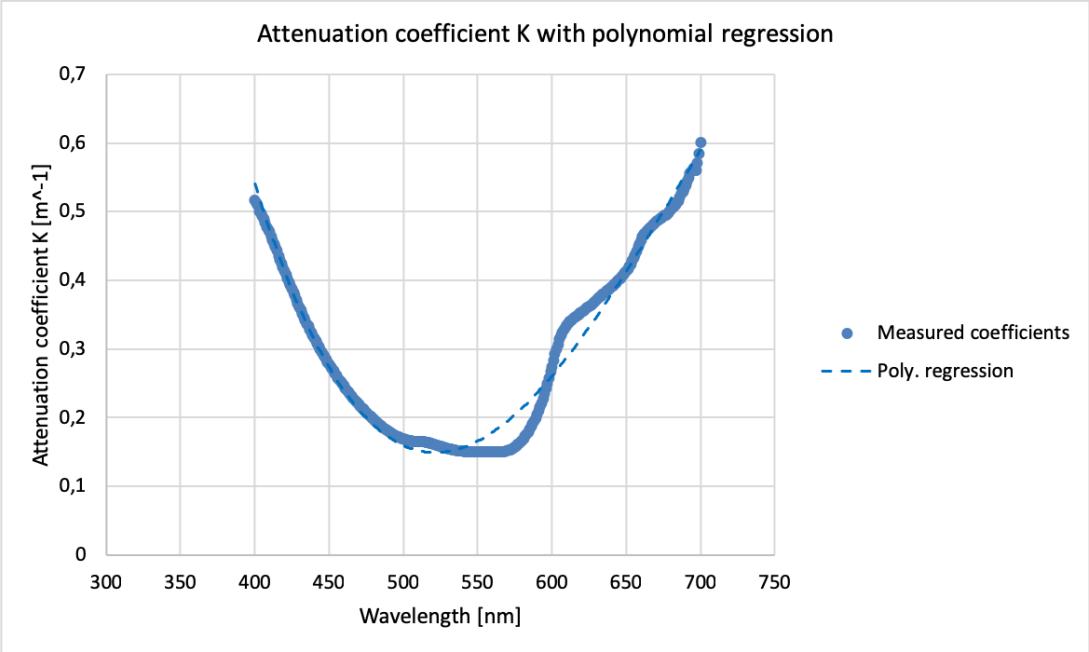

Figure 4.7: Measured values for K_λ coefficients at Hosenøyan from [41], and the approximated polynomial regression curve of 3rd degree.

Calculating irradiance values

With $E_{0,\lambda}$ and K_λ values for the waveband 400 to 700 nm, Equation (3.12) could be used to calculate spectral irradiance values $E_\lambda(z)$ for OD5, OD3 and OD1. The z values were chosen in the interval 0 to 60 m.

The sum of the calculated irradiances $E_\lambda(z)$ for each z value represented the total irradiance E at z meters away from the light source.

4.4 Motion measurements

The measurements described in this section were used for quantifying the light response of the salmon lice.

4.4.1 Detection experiments

Three different measurements were used to get an overview of the salmon lice response in the detection experiments.

Mean displacement

The mean distances from the lice to the light source was calculated to measure the phototactic response among the lice (Equation (4.4)). In the time dependent response measurements, the mean normalized sum of distances of all lice was calculated and plotted against time. Additionally, regression lines were calculated for each experiment. This was done for both the dark control period and the period of light stimulus, indicating the change of movement throughout the video. A least-squares method was used for calculating the regression line. Only the movement in x-direction was considered in this project, as the x value denoted the mean distance to the light source.

$$d_i = \frac{1}{N}\sum_{k=1}^{N}(x_{light} - x_{louse_k}) \tag{4.4a}$$

$$avg = \frac{1}{n}\sum_{i=1}^{i+n} d_i \tag{4.4b}$$

In Equation (4.4), N is the number of lice in each frame, x_{louse_k} is the x-position of louse k, and d_i is the resulting total distance from the light source for all lice in the specific frame. The mean distances were calculated for all frames in an interval $[i, i+n]$ and the average, avg, of these taken and plotted. The interval used in the mean calculations was $n = 160$ frames, corresponding to 10 seconds.

Area dependent movement

In addition to calculating the mean position of all the lice over time for the detection experiments, the number of lice in certain areas of the tank was calculated(**??**). Specifically, the change of the number of lice in the area closest to the light source, marked by the dotted line in Figure 4.8 was calculated and plotted in Section 5.1. The percentage of lice in this area was calculated with Equation (4.5).

$$percentage\_of\_lice = \frac{n\_close}{N} \times 100 \tag{4.5}$$

In Equation (4.5), n_close denote the number of lice in the area closest to the light source, and N is the total number of lice detected in the current frame.

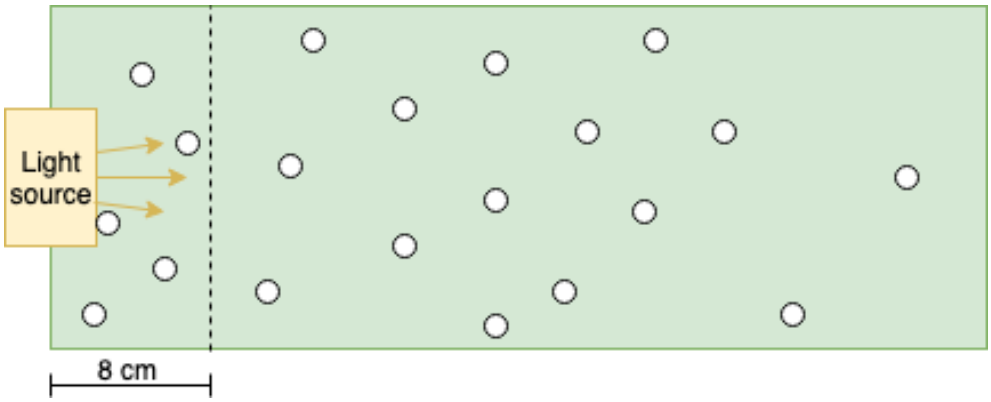

Figure 4.8: The 20 % closest area to the light source is marked with a dotted line. The white dots illustrate lice.

Total displacement

For the detection experiments, box plots were used to illustrate the total displacement of the salmon lice throughout the experiment. The distance from a baseline was calculated for each louse in the tank and presented. The baseline was calculated as the median position of all the lice in the first minute before the light was turned on. As the lice were approximately evenly spread out in the tank, this value was typical close to 20 cm from the light source (in the middle). In the 7th minute of light stimuli, the distances from the baseline to each louse were calculated, and the median of these distances were plotted in each box (Figure 4.9).

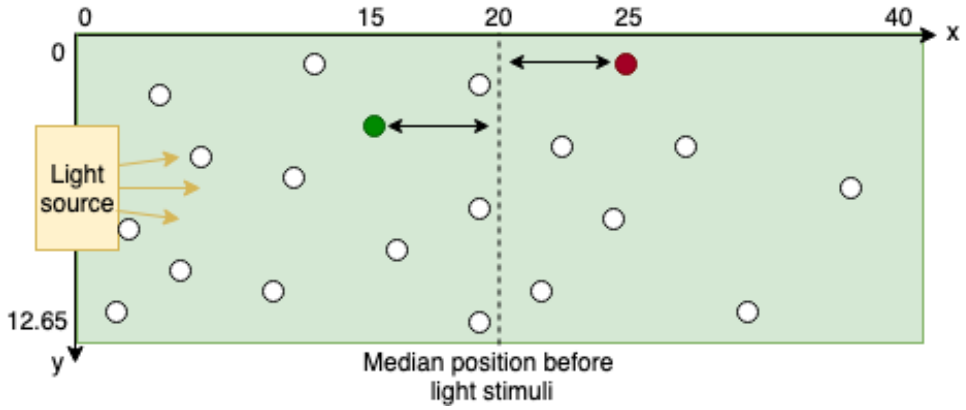

Figure 4.9: Distance from baseline to the salmon lice(white dots). The dotted line (referred to as baseline) is an example of a median position of all lice before the light was turned on, typically found to be around 20 cm.

For the green louse in Figure 4.9, the resulting distance from baseline is $20 - 15 = 5$ cm while the red lice have the distance $20 - 25 = -5$ cm. This means that positive values indicate a response towards the light source, while negative values show a displacement away from the light source.

4.4.2 Tracking experiments

To map the response seen for the salmon lice in the tracking experiments, two different measurements were used.

Determined swimming motion

In the tracking experiments, a determination factor for the swimming behavior of the salmon lice was calculated. The determination factor was calculated for each track, using Equation (4.6). High values implied that the salmon lice had a determined swimming behavior, but whether the direction was towards or from the light source was not taken into account. The only distinguishing factor was the distance traveled when swimming from one place in the tank to another other.

$$det\_factor = \frac{distance}{arc\_length} \tag{4.6}$$

$distance$ refers to the Euclidean distance from the first to the last coordinate of the track, while arc_length is the length of the track.

The determination factor was calculated for each track before and after the light was turned on, to show how the swimming pattern changed with light stimuli present. High values imply that the lice had determined swimming behavior.

Velocity profile

The formulas for velocity calculation are described in Section 4.2.2. The velocity of each salmon louse was calculated before and after the light was turned on to gain knowledge about the change in behaviour with different light stimuli.

Chapter 5

Results

The results in this chapter quantify the phototactic swimming behavior of salmon lice when exposed to 36 different light settings, by showing overall movement, as well as velocity and direction of the lice before and during the exposure time. More results can be found in appendix and in an attached folder.

5.1 Detection

Only the main findings from the detection experiments will be presented in this section. The work of this thesis, regarding detection, includes analysis of all the experiments where each experiment has been evaluated using some of the measurements described in Section 4.4. Due to the high amount of results, only the main findings will be presented in this section. Blue-OD1-P2 is used as an example to show the results obtained from the analyses of all light settings. See attached folder for similar results for the other light settings.

5.1.1 Blue-OD1-P2

Figure 5.1 and Figure 5.2 show the response of salmon lice over time for the three replicates using the light setting Blue-OD1-P2. A decrease in distance from the light source was seen for all replicates, with a higher decrease for R2 (Figure 5.1). R1 and R3 showed a more similar pattern; however, there were relatively big variations among the three replicates.

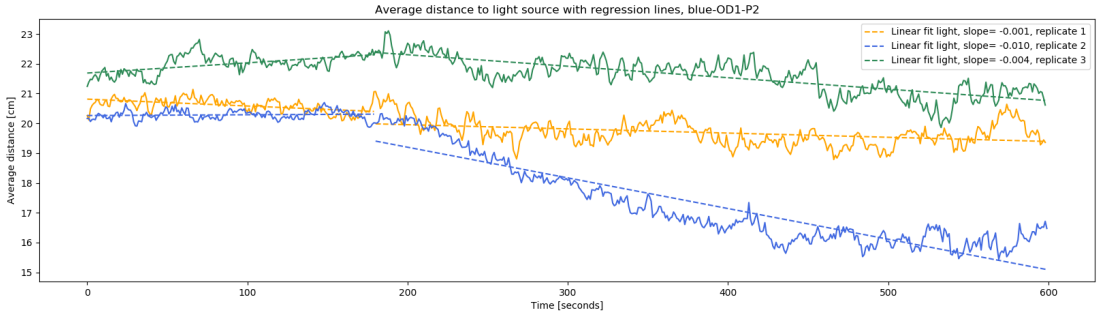

Figure 5.1: Mean distance from lice to light source for R1 (yellow), R2 (blue) and R3 (green), Blue-OD1-P2. The information in the legend corresponds to the time period of the light stimuli, starting after three minutes. A decrease in mean position implies that the distance from the lice to the light source decreases.

The percentage of lice residing in the area closest to the light source increased over time for all three replicates (Figure 5.2). The highest increase in the percentage of lice in the area close to the light source was reached with R2. Similar trends were seen for R1 and R3 (Figure 5.2). For R2, the percentage of lice in this area increased from around 10% to around 25%.

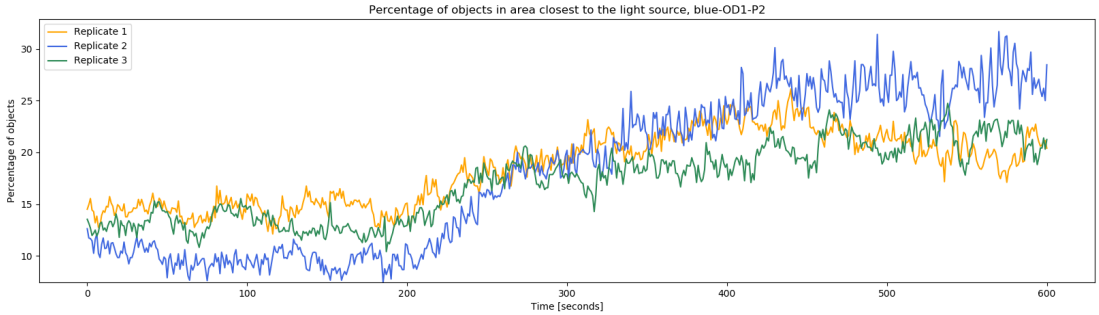

Figure 5.2: Percentage of lice in area closest to the light source for R1 (yellow), R2 (green) and R3 (blue), Blue-OD1-P2. An increase in percentage means that the amount of lice in the area closest to the light source increased.

5.1.2 Summarized results

The figures in this section show the distance between the median position (baseline) before the light was turned on and after the light had been on for 7 minutes, as explained in Section 4.4. An illustrative demonstration of this calculation can be found in Figure 4.9. The detected response for all light settings within each color of light is presented, followed by a comparison of the responses across all 36 light settings.

Green

With green light, OD1-P0 gave the highest displacement from baseline with a median of 3.07 cm, followed by OD1-P2 with a displacement from baseline of 2.59 cm. The light setting Green-OD1-P0 showed less dispersion than the result for Green-OD1-P2 (Figure 5.3), having SDs of 1.50 cm and 3.91 cm, respectively.

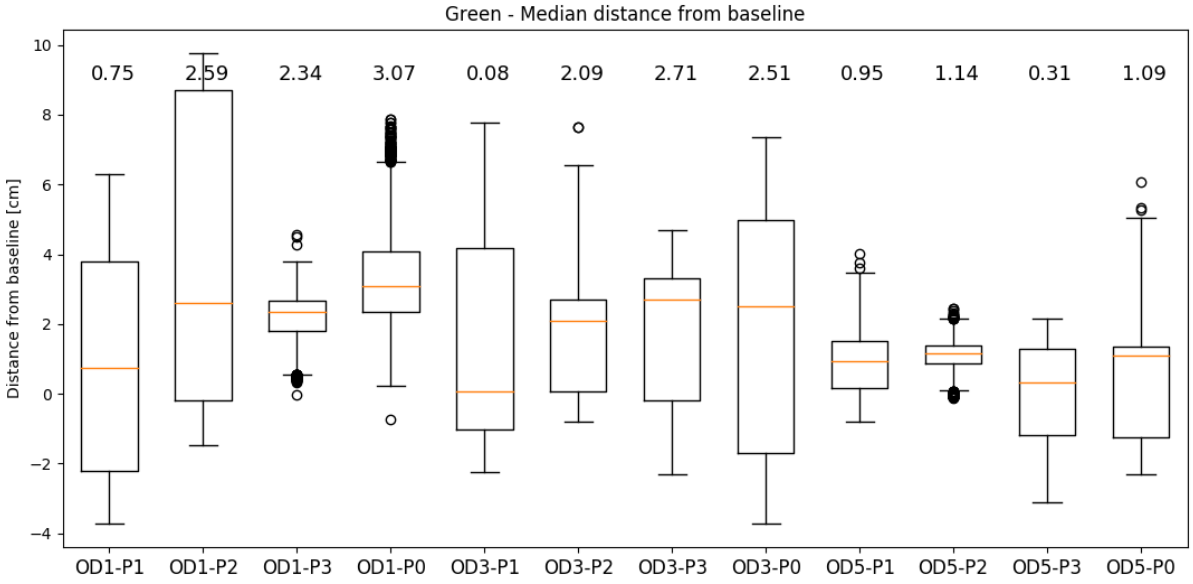

Figure 5.3: Box plot showing the median distance (number placed above the boxes) to baseline with respect to the color green, OD and pulsation. Positive numbers show that the median distance from the baseline to the salmon lice increase, meaning that the distance towards the light source decrease. Each box includes median values for the salmon lice positions in each frame in the 7th minute of the experiments, giving a data set of approximately 960×3 values (960 frames and 3 replicates) in each box. Whiskers are defined as 1.5×IQR.

Blue

When looking at the total displacement from the baseline for all the experiments done with blue light, the light setting Blue-OD1-P0 gave the overall highest result, with SD of 2.05 cm. The second largest displacement was seen for Blue-OD5-P0, with a lower SD of 1.87 compared to Blue-OD1-P0. For Blue-OD1-P1 and Blue-OD5-P3, the displacement was negative, meaning that the median position of the salmon lice after 7 minutes was further away from the light source than before the light was turned on (Figure 5.4). The SDs were 1.79 cm and 1.57 cm, respectively.

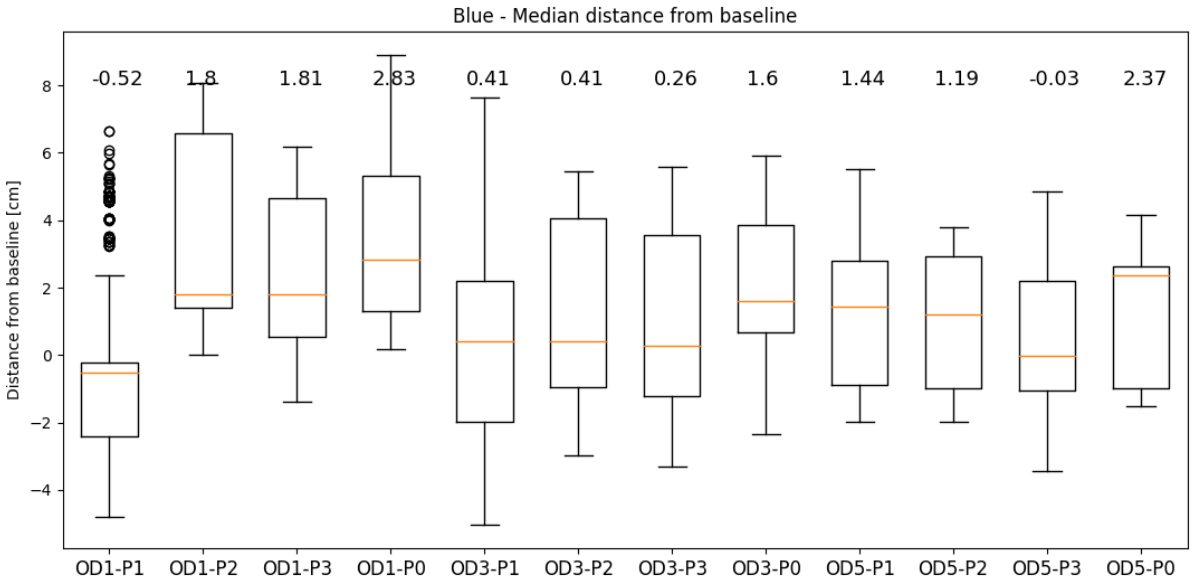

Figure 5.4: Box plot showing the median distance (number placed above the boxes) to baseline with respect to the color blue, OD and pulsation. Positive numbers show that the median distance from the baseline to the salmon lice increase, meaning that the distance towards the light source decrease. Each box includes median values for the salmon lice positions in each frame in the 7th minute of the experiments, giving a data set of approximately 960×3 values (960 frames and 3 replicates) in each box. Whiskers are defined as 1.5×IQR.

White

For the experiments done with white light, the light setting that gave the highest response was White-OD3-P0 with a total displacement from baseline at 6.28 cm, followed by White-OD1-P0 with a displacement of 5.29 cm (Figure 5.5). The Standard deviations (SD) for these light settings were 4.13 and 3.20, respectively.

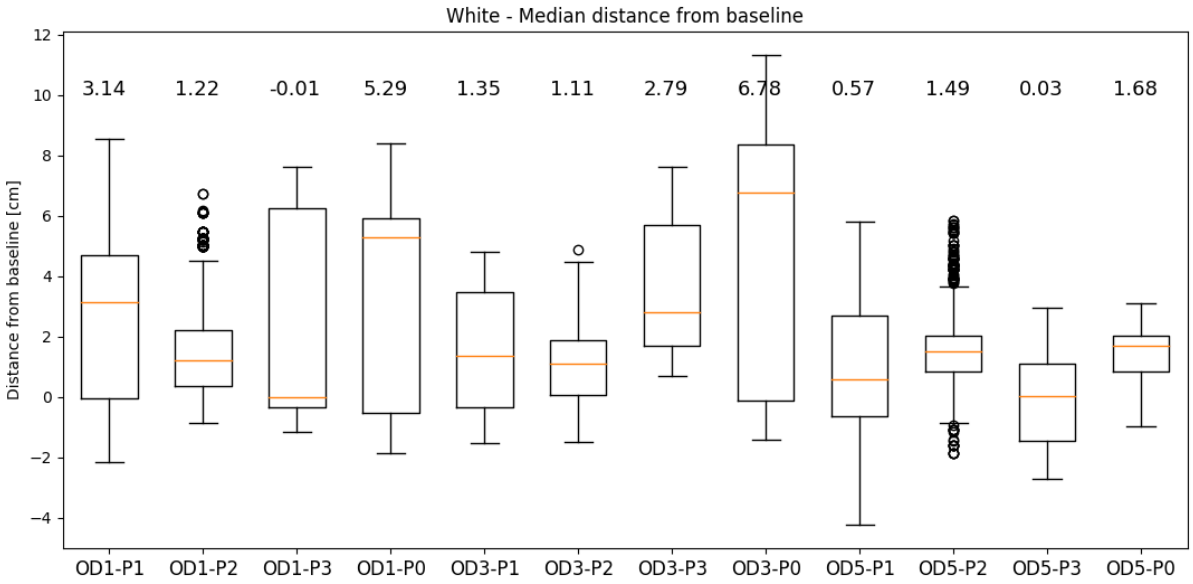

Figure 5.5: Box plot showing the median distance (number placed above the boxes) to baseline with respect to the color white, OD and pulsation. Positive numbers show that the median distance from the baseline to the salmon lice increase, meaning that the distance towards the light source decrease. Each box includes median values for the salmon lice positions in each frame in the 7th minute of the experiments, giving a data set of approximately 960×3 values (960 frames and 3 replicates) in each box. Whiskers are defined as 1.5×IQR.

Comparison

Table 5.1 summarizes the median displacements from baseline for all the experiments. Comparing all the displacements, White-OD3-P0 gave the overall highest response among the salmon lice, but this light setting was also the light setting with the highest standard deviation (SD) (Table 5.2).

Table 5.1: The median displacements from baseline calculated for each frame in the 7th minute of the detection videos. All values are in cm.

	OD1-P1	**OD1-P2**	**OD1-P3**	**OD1-P0**	**OD3-P1**	**OD3-P2**	**OD3-P3**	**OD3-P0**	**OD5-P1**	**OD5-P2**	OD5-P3	**OD5-P0**
Green	0.75	2.59	2.34	3.07	0.08	2.09	2.71	2.51	0.95	1.14	0.31	1.09
Blue	-0.52	1.8	1.81	2.83	0.41	0.41	0.26	1.6	1.44	1.19	-0.03	2.37
white	3.14	1.22	-0.01	5.29	1.35	1.11	2.79	6.78	0.57	1.49	0.03	1.68

Table 5.2: Standard deviation (SD) in cm of the median displacements from baseline calculated for each frame in the 7th minute of the detection videos. The values are in cm.

	OD1-P1	**OD1-P2**	**OD1-P3**	**OD1-P0**	**OD3-P1**	**OD3-P2**	**OD3-P3**	**OD3-P0**	**OD5-P1**	**OD5-P2**	**OD5-P3**	**OD5-P0**
Green	2.86	3.91	0.72	1.50	2.77	1.58	1.89	3.33	0.79	0.43	1.29	1.35
Blue	1.79	2.54	2.06	2.05	2.51	2.50	2.50	1.87	1.90	1.85	1.57	1.80
white	2.34	2.46	3.15	3.20	1.80	0.99	1.91	4.13	1.83	0.90	1.25	0.66

5.2 Tracking

An excerpt of the light settings were investigated further in terms of tracking. The three light settings Green-OD1-P2, Blue-OD1-P0, and White-OD1-P3 were chosen based on the results presented in Section 5.1. From the detection experiments it was shown that Green-OD1-P2 and Blue-OD1-P0 showed a relatively big response towards the light, whereas White-OD1-P3 showed to have a negative response. Further, the highest SD of the median displacement for all light settings was shown for Green-OD1-P2. The observed differences in swimming behaviour among the three light settings is interesting to investigate further. In addition, the chosen light settings represent all colors of light, as well as three different pulsation rates, showing robustness of the algorithm.

The results from these tracking experiments include a plot of all the tracks with a table of associated information, speed calculations, and calculation of a determination constant, as explained in Section 4.4. In this section, only the tracks of one replicate within each light setting is shown, and a velocity plot corresponding to only one of the salmon lice in each experiment. See Appendix C for more results.

The names of the following subsections are based on the respective light settings, where the involved parameters are explained in Section 4.1.2.

5.2.1 Green-OD1-P2

For green light with OD1 and pulsation P2, R1 was chosen as an example. Figure 5.6 shows the tracks in the two-minute long video. Average and maximum speed were among the investigated performance indicators, as well as the arc lengths and at which time each track was first registered (Table 5.3).

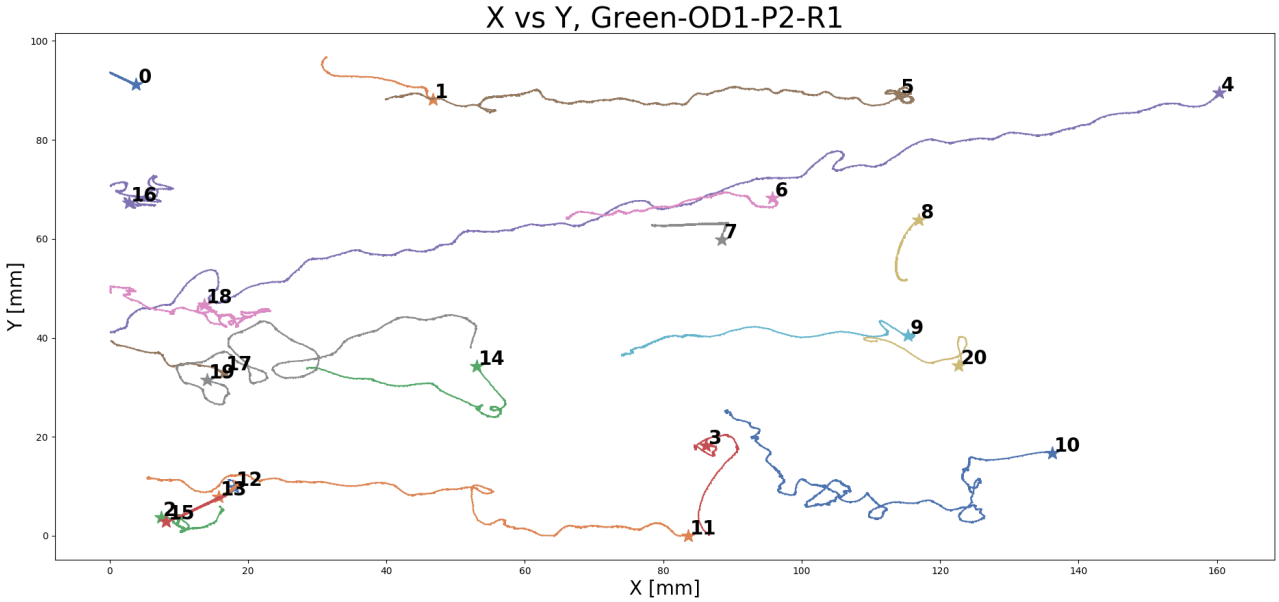

Figure 5.6: Tracks found in the two minute long experimental video for Green-OD1-P2-R1. Stars denote the start of each track.

Table 5.3: Information corresponding to tracks for Green-OD1-P2-R1. Start time indicates when the track was first registered.

Track ID	Start time [s]	Arc length [mm]	Average speed [mm/s]	Maximum speed [mm/s]
0	0.00	46.69	0.44	6.63
1	0.00	117.76	1.14	39.81
2	0.09	197.00	1.56	44.52
3	0.00	91.56	0.84	79.77
4	36.59	315.08	3.27	60.92
5	0.00	317.94	1.88	44.82
6	0.00	272.72	1.61	22.42
7	1.06	266.92	1.70	19.47
8	13.80	42.38	0.30	11.61
9	87.75	90.94	2.17	99.20
10	0.00	352.62	2.43	88.83
11	56.61	194.36	2.47	74.88
12	90.40	85.27	1.89	11.39
13	67.03	138.37	2.05	18.51
14	37.20	68.80	1.16	74.69
15	22.84	216.28	1.75	23.85
16	0.08	92.69	1.02	30.05
17	51.62	52.89	0.79	36.02
18	0.00	157.30	1.34	27.51
19	0.00	172.77	1.81	47.74
20	0.00	265.76	0..96	94.19

The majority of the salmon lice moved from right to left in the experimental tank, meaning they

had a directional movement towards the light source. The arc lengths varied from 42.38 mm (track 8) to 352.62 mm (track 10), where the mean arc length among all tracks was 169.48 mm. The maximum speed obtained for the different tracks was in the range from 6.63 mm/s (track 0) to 99.20 mm/s (track 9), with a mean maximum speed of 45.56 mm/s (Table 5.3).

Each track was investigated further by looking at the total speed over time, as well as the velocity in x- and y-direction. It is chosen to look at the velocity profile for track 4, as the salmon louse belonging to this track ID has a long arc length, swimming across the entire tank towards the light source. The total speed for was plotted, as well as corresponding velocity in x-direction as this is the most relevant direction with regards to the movement towards the light source (Figure 5.7).

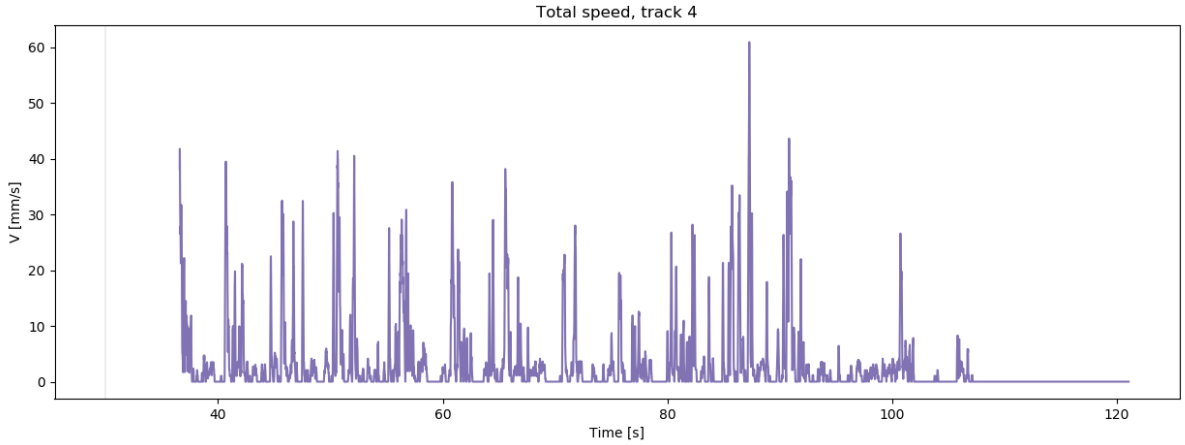

(a) Total speed in mm/s.

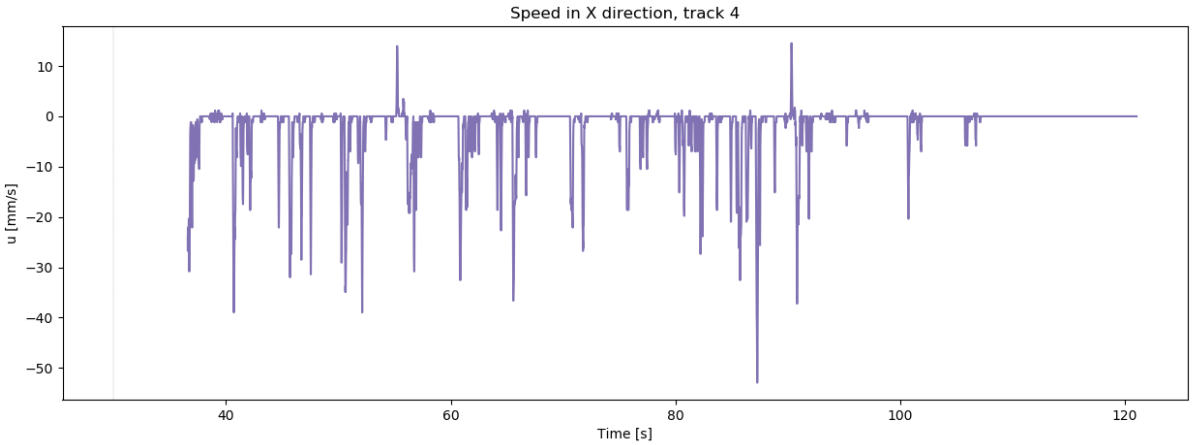

(b) Velocity in x-direction in mm/s. Negative velocity implies that the salmon louse move towards the light source.

Figure 5.7: Velocity of track 4 in Green-OD1-P2-R1. The light was turned on after 30 s.

The movement of the salmon louse was somewhat periodic as seen from the speed calculations (Figure 5.7). This may be related to the pulsation rate P2, with on/off ratio 2.0/3.0 s.

The above figures represent results from one out of three replicates for light setting Green-OD1-P2-R1. These three replicates were combined to look for trends and consistency of the experiments. The calculated determination coefficients explained in Section 4.4.2 showed that the swimming behavior was more determined when the light was turned on for all three replicates (Figure 5.8). The most significant response occurred for R2.

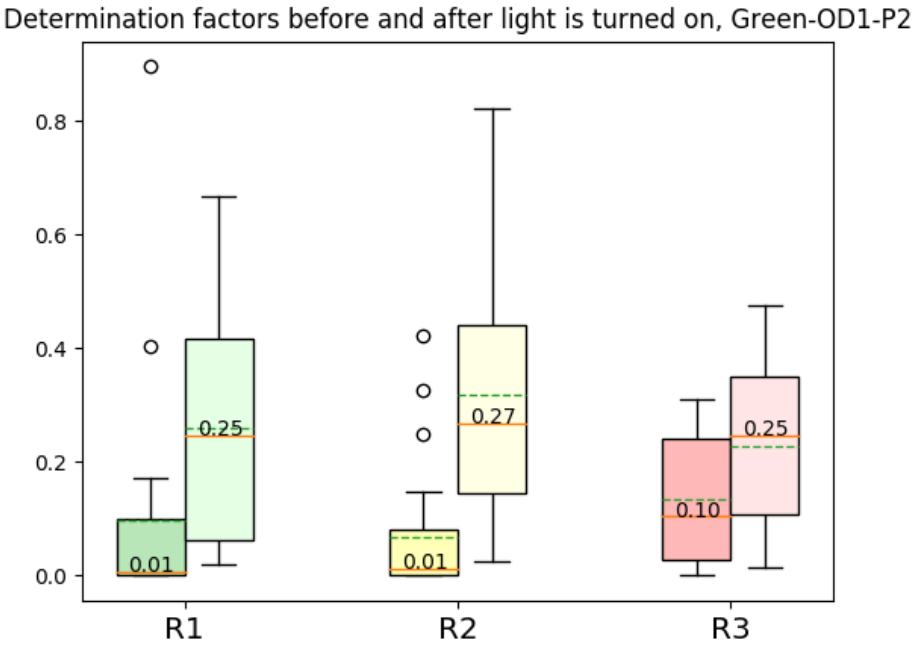

Figure 5.8: Determination factor (distance/arc_length) before and after light was turned on, for R1, R2 and R3. The orange lines mark the median of the data, with the median value printed above the line. The dotted lines mark the mean of the data. Whiskers are defined as 1.5×IQR.

A similar box plot was used in order to distinguish between the three replicates with respect to speed. The total speed increased after the light was turned on for all three replicates (Figure 5.9). The velocity in x-direction after the light was turned on reached approximately the same maximum as the total speed for all three replicates. This indicates that the swimming direction was targeted towards the light source.

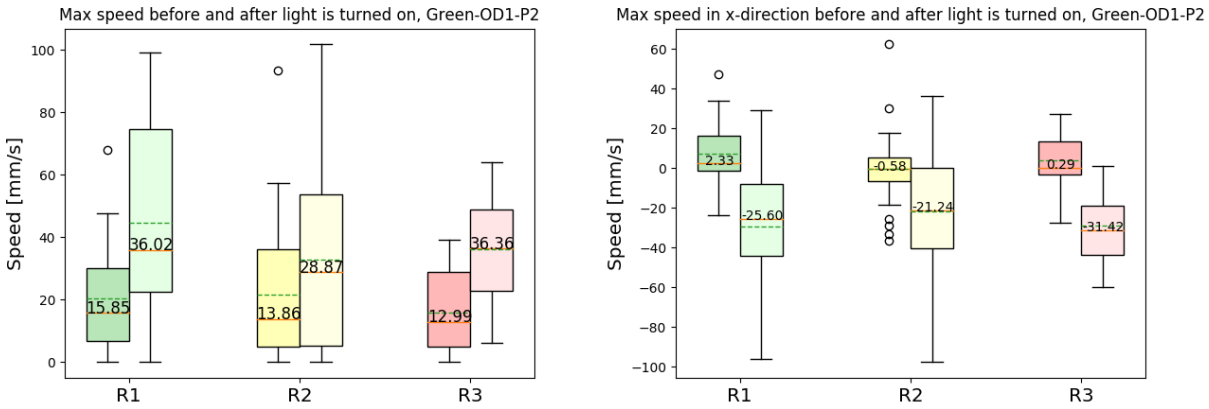

(a) Total speed.

(b) Velocity in x-direction.

Figure 5.9: Maximum speed and maximum velocity in x-direction before and after light was turned on, for R1, R2 and R3. Negative values in (b) imply that the lice moved towards the light source. The orange lines mark the median of the data, and the median value is written in the boxes. The dotted lines mark the mean of the data. Whiskers are defined as 1.5×IQR.

For all replicates with the Green-OD1-P2 light setting, the maximum total speed detected was 101.80 mm/s, with a velocity in the x-direction of 97.75 mm/s. This result was obtained with R2. This indicates that salmon louse holding this maximum speed had a determined swimming direction during the corresponding period.

5.2.2 Blue-OD1-P0

Compared to the tracks found for Green-OD1-P2-R1, the arcs of the tracks corresponding to the lice in Blue-OD1-P0-R2 were less directed (Figure 5.10). However, most of the lice had an overall movement towards the light source.

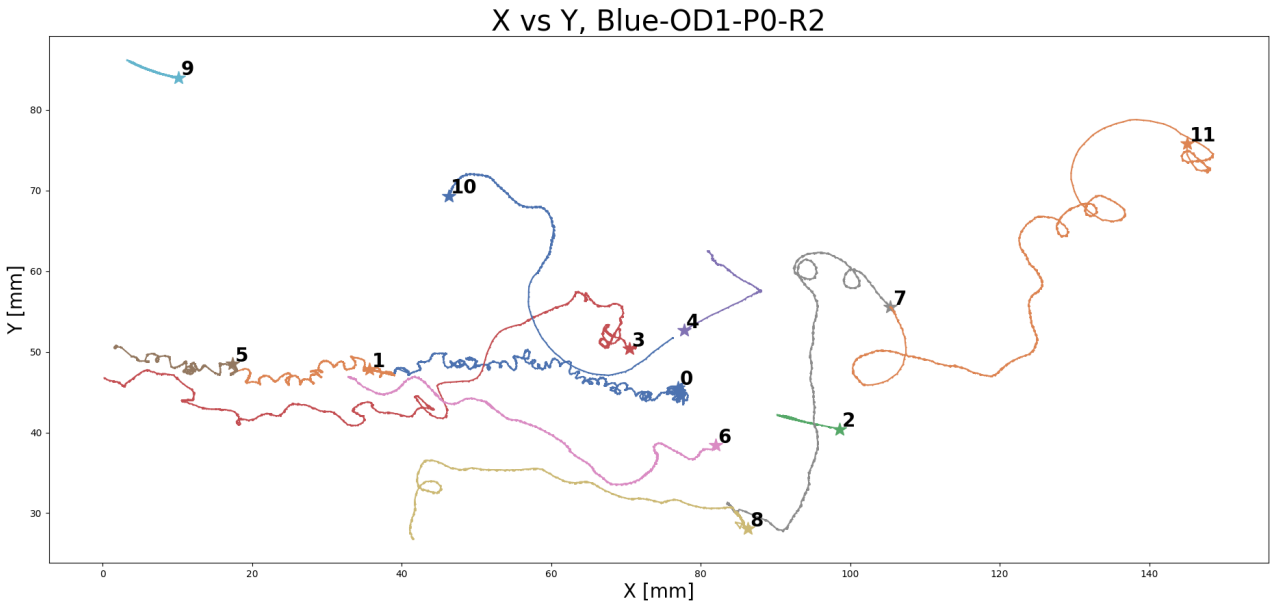

Figure 5.10: Tracks found in the two minute long experimental video for Blue-OD1-P0-R2. Stars denote the start of each track.

Table 5.4: Information corresponding to tracks for Blue-OD1-P0-R2. Start time indicates when the track was first registered.

Track ID	Start time [s]	Arc length [mm]	Average speed [mm/s]	Maximum speed [mm/s]
0	0.00	242.57	1.97	46.18
1	0.00	97.66	0.98	20.19
2	96.79	36.85	1.33	15.44
3	0.00	190.79	1.82	98.51
4	180.60	34.44	1.96	99.69
5	0.08	83.02	0.76	23.62
6	29.93	201.57	1.64	18.58
7	77.55	140.56	2.61	17.51
8	29.93	272.46	2.37	32.49
9	0.00	96.37	0.67	6.41
10	29.93	177.84	1.46	83.62
11	0.00	230.74	1.93	115.64

The arc lengths of the registered tracks varied from 34.44 mm (track 4) to 272.46 mm (track 8), where the mean arc length among all tracks was 150.41 mm. The maximum speed obtained for the different tracks were in the range from 6.41 mm/s (track 9) to 115.64 mm/s (track 11), with a mean maximum speed of 48.16 mm/s (Table 5.4).

For the light setting Blue-OD1-P0, the periodic motion as seen with the light setting Green-OD1-P2 was no longer present. The lack of periodic motion can be seen for track 11 in Figure 5.11a and Figure 5.11b. There were a few high peaks in the swimming speed, otherwise,

the speed was found to be steadily below 30 mm/s (Figure 5.11)

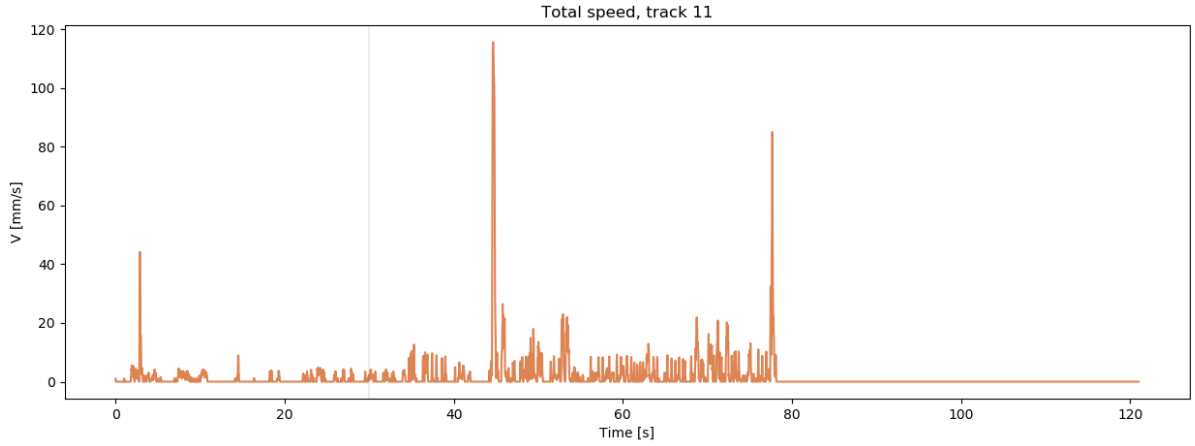

(a) Total speed in mm/s.

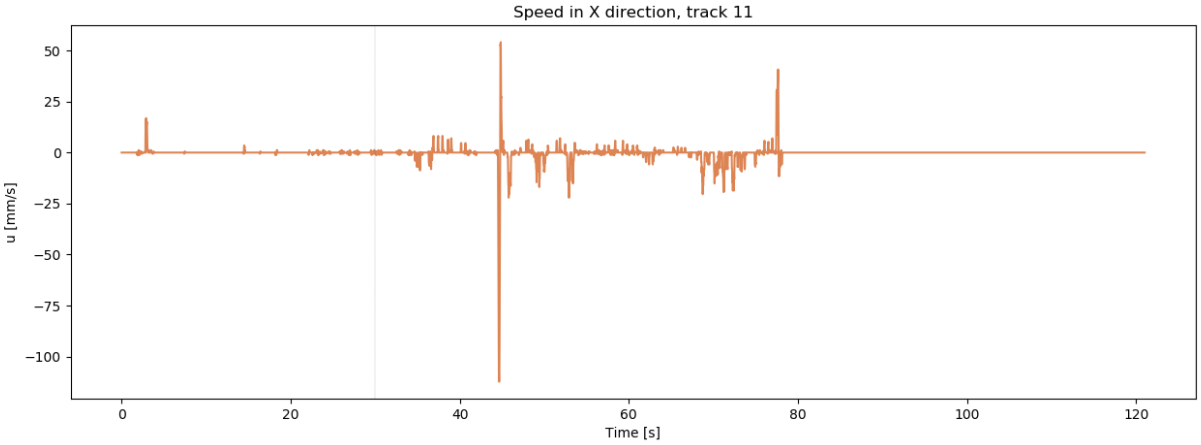

(b) Velocity in x-direction in mm/s.

Figure 5.11: Velocity of track 11 in Blue-OD1-P0-R2. The light was turned on after 30 s.

The swimming behavior was more determined when the light was turned on for all three replicates (Figure 5.12). The most significant response occurred for R2.

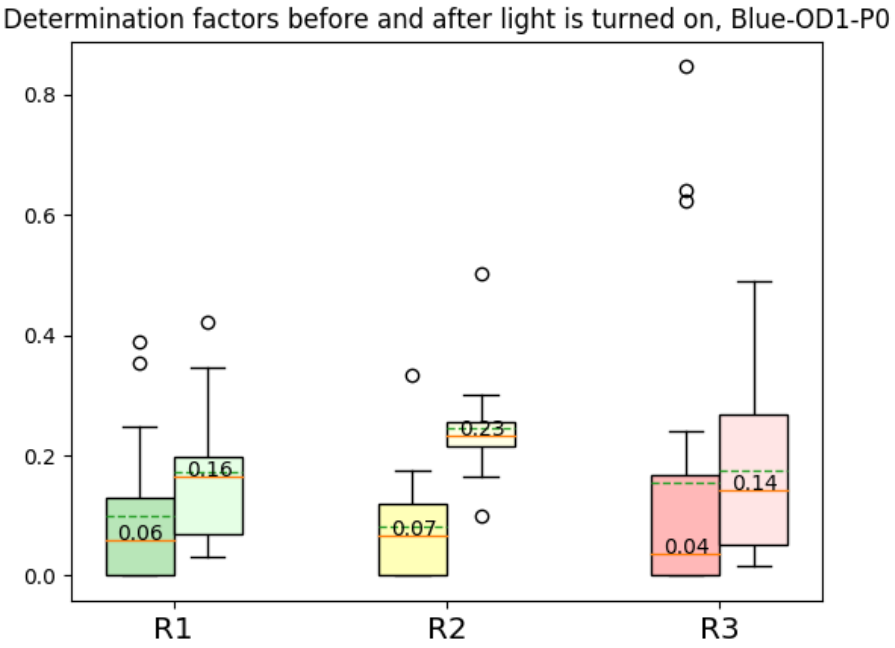

Figure 5.12: Determination factor (distance/arc_length) before and after light was turned on, for R1, R2 and R3. The orange lines mark the median of the data, with the median value written above the median line. The dotted lines mark the mean of the data. Whiskers are defined as 1.5×IQR.

The overall biggest change in speed occurred for R1; however, the maximum speed was found for one of the lice in R2 (Figure 5.13). When looking into the velocities in the x-direction, the median velocity for both R1 and R3 was 0.00 mm/s before the light was turned on. For R3, the median velocity remained the same during light stimuli, but with more dispersion in the data. For R2, the change in median velocity in x-direction went from 0.29 mm/s with the light off to -18.04 mm/s with the light on, resulting in the biggest change in speeds among the three replicates. In addition, a low dispersion in the data was seen for R2 in Figure 5.13b, with only some outliers corresponding to the maximum speed, found for Blue-OD1-P0.

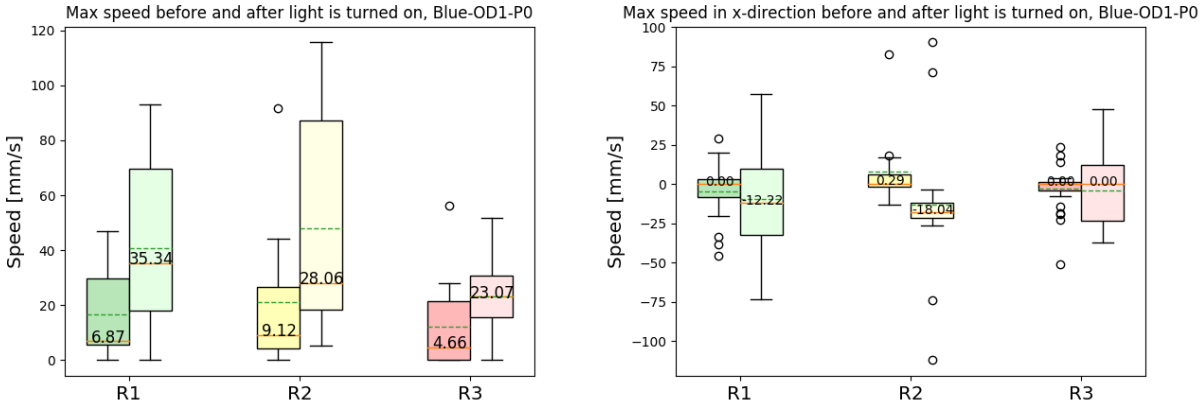

(a) Total speed.

(b) Velocity in x-direction.

Figure 5.13: Maximum speed and maximum velocity in x-direction before and after light was turned on, for R1, R2 and R3. Negative values in (b) imply that the lice moved towards the light source. The orange lines marked the median of the data, with the median value written above the median line. The dotted lines mark the mean of the data. Whiskers are defined as $1.5 \times$IQR.

When comparing all three replicates with the Blue-OD1-P0 light setting, the maximum speed detected was 115.64 mm/s with a velocity in the x-direction of 112.29 mm/s, occurring in R2.

5.2.3 White-OD1-P3

The tracks found for White-OD1-P3 show variations in the behavior of the lice. While some lice moved from the opposite end of the tank to the light source, other lice seemed to have a circular swimming behavior (Figure 5.14).

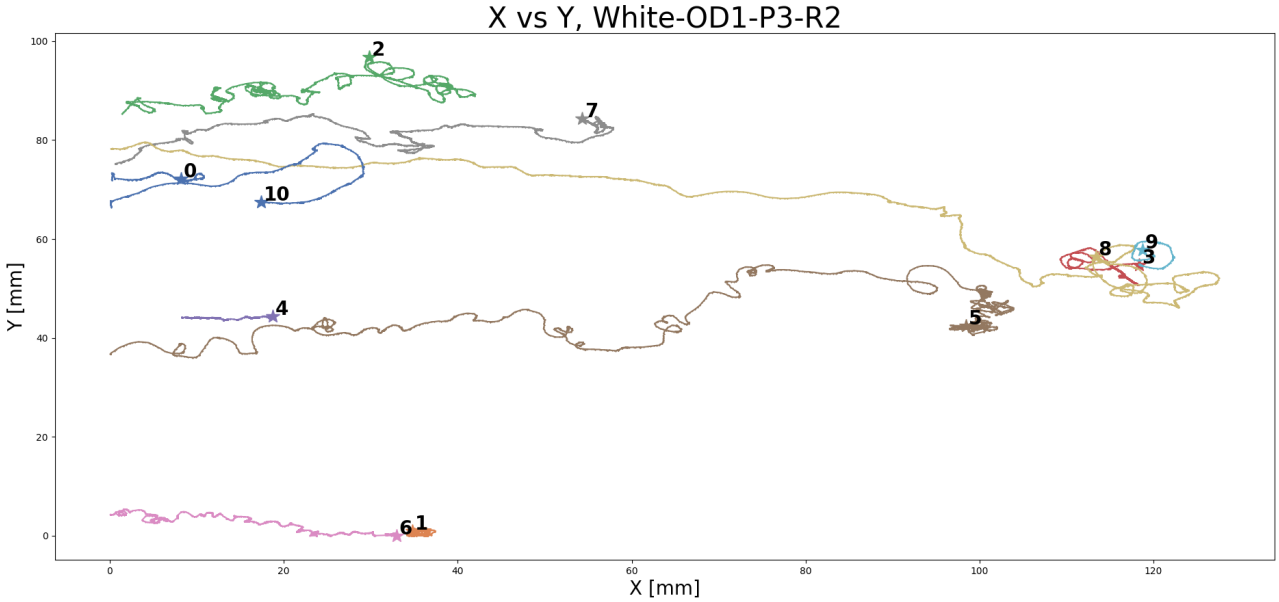

Figure 5.14: Tracks found in the two minute long experimental video for White-OD1-P3-R2. Stars denote the start of each track.

Table 5.5: Information corresponding to tracks for White-OD1-P3-R2. Start time indicates when the track was first registered.

Track ID	Start time [s]	Arc length [mm]	Average speed [mm/s]	Maximum speed [mm/s]
0	0.00	131.51	1.13	30.47
1	0.00	84.15	0.82	24.12
2	2.89	316.51	2.04	47.53
3	6.99	172.19	1.07	31.01
4	5.89	98.26	0.82	15.82
5	0.34	404.69	3.55	73.06
6	34.57	175.02	1.66	20.61
7	0.00	228.55	1.50	35.54
8	0.00	318.82	2.56	73.17
9	0.00	28.17	0.35	31.01
10	0.05	102.66	0.90	53.93

The arc lengths of the registered tracks varied from 28.17 mm (track 9) to 404.66 mm (track 5), where the mean arc length among all tracks was 187.32 mm. The maximum speeds obtained for the different tracks were in the range from 15.82 mm/s (track 4) to 73.17 mm/s (track 8), with a mean maximum speed of 39.66 mm/s (Table 5.5).

When looking into the speed of the salmon louse corresponding to track 8, it can be seen that this was somewhat periodic. The periodic change in speed after 60 s may be related to the pulsating light having an on/off ratio of 5.0/5.0 s (Figure 5.15).

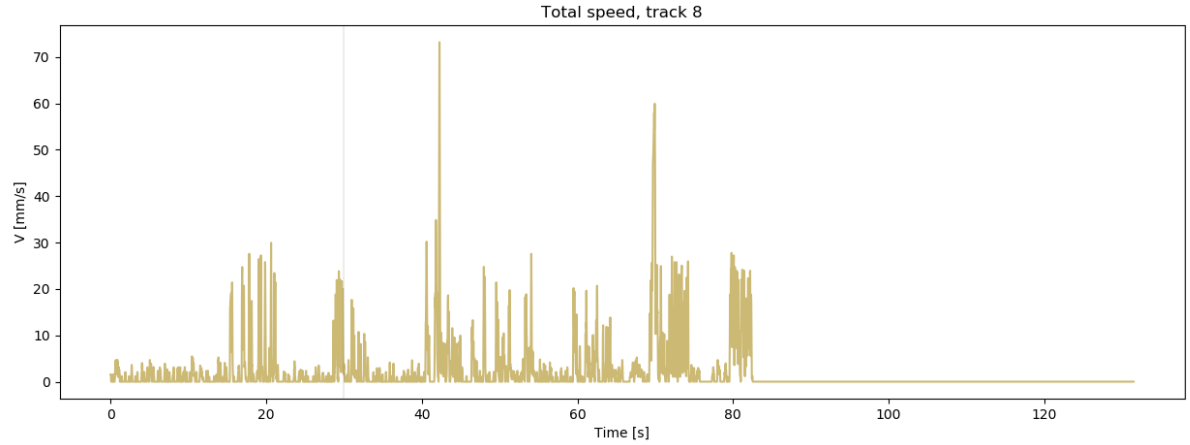

(a) Total speed in mm/s.

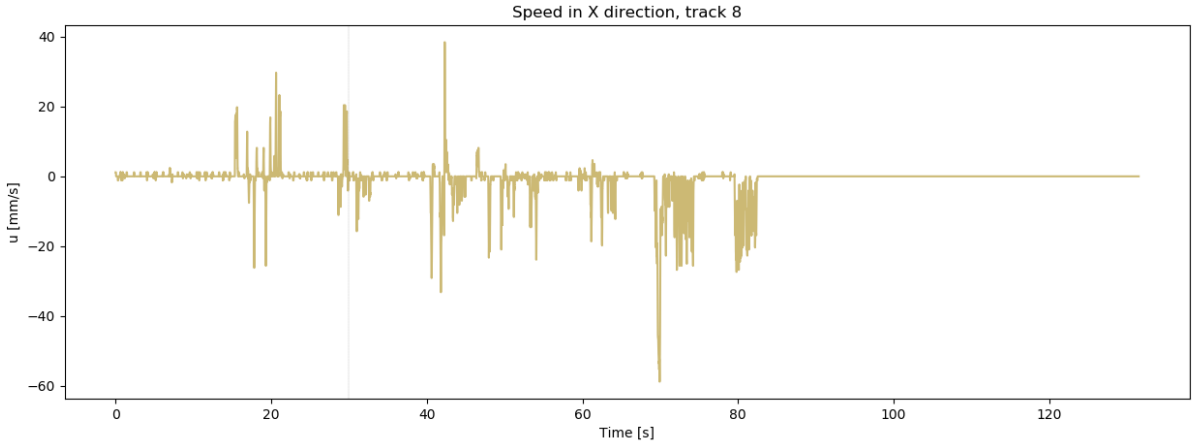

(b) Velocity in x-direction in mm/s.

Figure 5.15: Velocity of track 8 in White-OD1-P3-R2. The light was turned on after 30 s.

As for Green-OD1-P2 and Blue-OD1-P0, the determination factor increased after the light was turned on for all three replicated, where the most significant increase occurred for R1 (Figure 5.16).

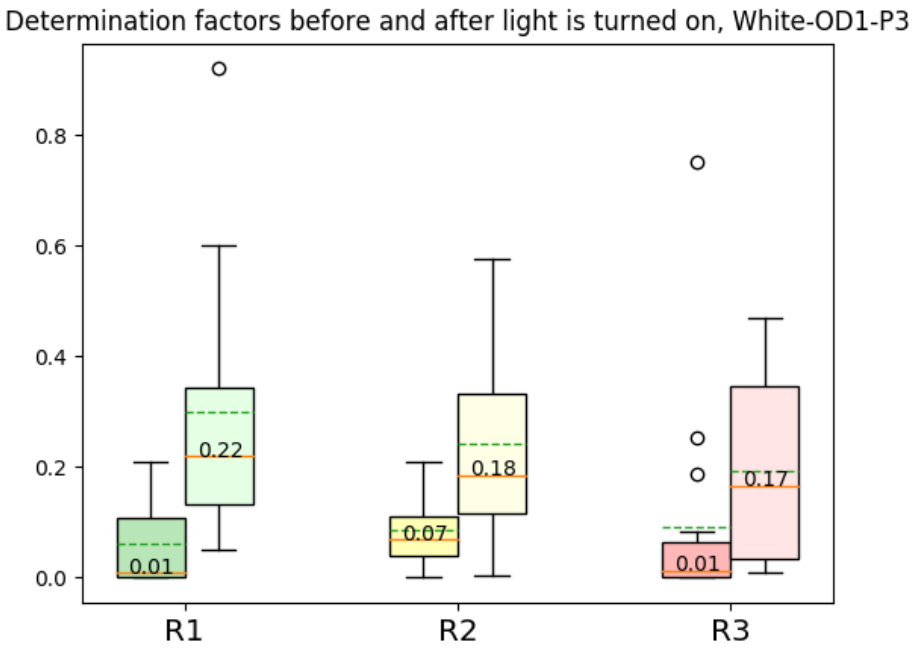

Figure 5.16: Determination factor (distance/arc length) before and after light was turned on, for R1, R2 and R3. The orange lines mark the median of the data, with the median value written above the median line. The dotted lines mark the mean of the data. Whiskers are defined as 1.5×IQR.

The maximum speed increased for all replicates after the beginning of light stimuli. The median maximum total speed was relatively high for both R1 and R2 before the light was turned on. R2 only showed a slight increase in total speed from during the light stimuli, while the increase for R1 was bigger. R3 had a bigger increase in total maximum speed compared to R1 and R2. By comparing the maximum total speed and maximum velocity in the x-direction for R2, it was seen that the swimming direction was changed drastically after light stimuli, obtaining a change in velocity in the x-direction of 27.92 mm/s (Figure 5.17).

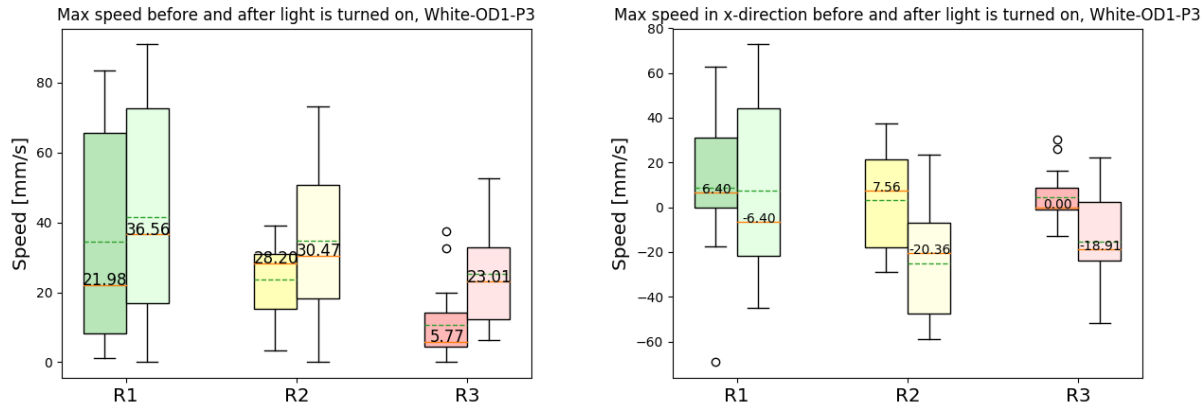

(a) Total speed.

(b) Velocity in x-direction.

Figure 5.17: Maximum speed and maximum velocity in x-direction before and after light was turned on, for R1, R2, and R3. Negative values in (b) imply that the lice moved towards the light source. The orange lines mark the median of the data, and the median value is written above the median line. The dotted lines mark the mean of the data. Whiskers are defined as $1.5 \times$IQR.

For all three replicates of blue light with OD1 and P3, the maximum detected total speed, and maximum detected velocity in x-direction, was 90.97 mm/s and 69.24 mm/s, respectively, both for R1.

5.3 Light propagation of artificial light at Hosenøyan

By theoretically calculating the irradiance at different distances away from a diffuse light source with Equation (3.12), an impression of how the light settings used in these experiments will propagate in the ocean can be obtained. The irradiance values were calculated with the use of diffuse attenuation coefficients measured at Hosenøyan in Norway [41]. OD5 was excluded from this analysis as no information about the light response towards light intensities lower than what corresponds to OD5 was retrieved from the conducted experiments.

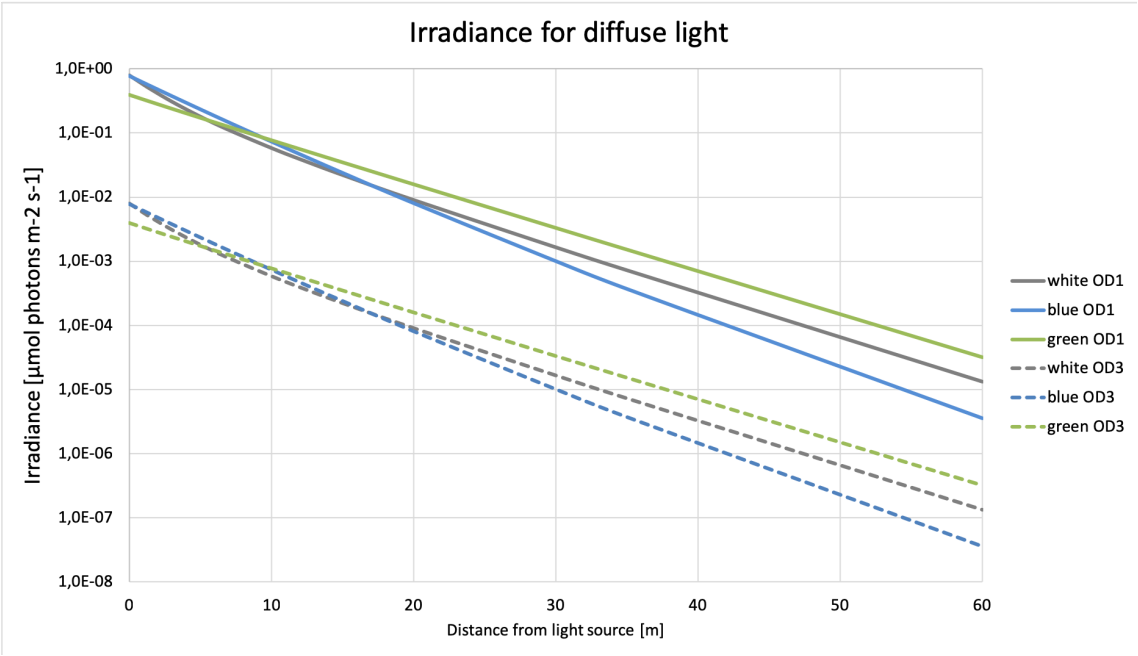

Figure 5.18: Irradiance in oceanic water at Hoseanøyan in Norway, for six different light sources. The bold lines illustrate the irradiance for three light sources with white, blue, and green light, with irradiance value corresponding to OD1 in this project. The dotted lines illustrate the irradiance of three light sources with color white, blue, and green for light with irradiance value corresponding to OD3 used in this project. The scale is logarithmic.

With the light sources of irradiance value corresponding to OD1, the results indicate that green light propagates furthest before it is attenuated to an irradiance level corresponding to OD5 (3.923E−05 E), with a distance of 58 m. The results also show that blue light will propagate 42 m, while white light will propagate 47 m before the irradiance values are below OD5 (Figure 5.18, Table 5.6).

Table 5.6: Calculated distances that light sources with irradiances 0.794 E, 0.781E and 0.392E, corresponding to OD1 in this project, can travel before the irradiances are lower than 7.94E-05, 7.81E-05 and 3.923E-05, corresponding to OD5 in this project.

Distance to reduced intensity levels			
	White	**Blue**	**Green**
OD2	9 [m]	10 [m]	14 [m]
OD3	21 [m]	20 [m]	29 [m]
OD4	34 [m]	31 [m]	44 [m]
OD5	47 [m]	42 [m]	58 [m]

For the light setting with irradiance value corresponding to OD3, the results indicate that green light will theoretically propagate 31 m before the irradiances are below what corresponds to OD5. Blue and white light is shown to propagate 21 m before the irradiances are lower than OD5 for the respective colors (Table 5.7).

Table 5.7: The table show the calculated distances that light sources with irradiances 0.00794E (white), 0.0078E (blue) and 0.0039E (green) corresponding to OD3 can travel before the irradiance levels are below OD5 for the respective colors.

Distance to reduced intensity levels			
	White	**Blue**	**Green**
OD4	10 [m]	10 [m]	17 [m]
OD5	21 [m]	21 [m]	31 [m]

Chapter 6

Discussion

Limitations in the experimental setup, biological unpredictability, and restrictions in the implemented algorithm are all areas that are important to consider. In this chapter, these areas are discussed before a discussion of the implemented method and the results follows.

6.1 Experimental setup

Before interpreting the results, limitations, and potential errors of the experimental setup should be considered.

6.1.1 Light reflection

Light reflections were one of the main problems in the experimental setup in the pilot project-Section 2.5, so a matte black plate was used to cover the wall on the opposite side of the light source to prevent reflections in the tank used in the main experiments. Even though this preventive measure was included, there were still some reflections present. As a result, the lice may have been attracted towards the reflections rather than the light source. This effect needs to be considered when interpreting the results.

6.1.2 Deviations from ocean environment

As explained in section Section 2.1.3, the swimming velocities of salmon lice is lower than the velocity of the ocean currents [10], [22]. When the light response was tested in the experimental tank, no currents were present. As includin currents were not part of the scope of this project.

Thus, it cannot be known whether the salmon louse can override the current velocities when exposed to light, despite showing determined swimming behavior and relatively high velocities in the experimental environment. This should be kept in mind when considering the results and the use of light stimuli as an attractive source to handle salmon lice in the areas of the fish pens.

6.1.3 Biological restrictions

As this project was conducted with the use of living organisms, biological effects need to be considered. There are many factors to consider when evaluating how reliable the results are. The environmental factors such as levels of minerals, oxygen, and currents are different than in the real habitat of the salmon lice. This might have had an impact on the behavior of the salmon lice, meaning that they might behave differently in the ocean than what they did in the experimental environment. When it comes to salinity and temperature, the levels should be the same as in the ocean, as the water was collected from the sea, and the temperature was controlled.

To test for a response towards different light settings, acclimation relative to light stimuli becomes essential. In the experiments, 30 minutes were used in complete darkness in order for the lice to reset and be ready for the next experiment with different light settings. This was considered to be enough time; however, this cannot be known for sure. The time of acclimation should be kept in mind when considering the results.

The density of lice should also be considered. Around 210 lice shared 2024 cm^3 of water in the experimental tank. With this density, the lice might have acted differently than groups of lice in the ocean, where the density is different. Their motion might have affected each other to some degree, but this was not taken into account when analyzing the results.

Different groups of salmon lice were used throughout the experiments. The variation in population was probably the most significant biological error source in this project and may have caused differences in the behavior of the salmon lice [69]. In the pilot project described in Section 2.5, differences between the replicates were observed, where R2 showed a higher response than R1 and R3. A possible reason for this difference was that the salmon lice in R1 and R3 were used in several experiments over two days, but R2 was only used in experiments over one day. According to [70], the salmon lice energy levels are reduced after extended periods of swimming, and energy levels below a certain point will cause the lice to die. Therefore, it is reasonable to think that the salmon lice in R1 and R3 would be more exhausted than those in R2. In the main experiments, variations in the response among the replicates were also observed. The reasons for these variations can assumably be related to the differences in the salmon lice population, day of hatching and potential diseases in addition to variations in energy level [69],

[70].

The natural swimming pattern of the salmon lice is in the vertical direction, as described in [12]. However, in these experiments, it was tested for swimming patterns in the horizontal direction, which are not part of the natural behavior of the salmon louse and is usually only obtained due to currents. This means that the results obtained in this project are not affected by the passive motion of the salmon lice, which, for example, occurs due to gravity. This is different from the experimental setup used in [10], where the salmon lice response to artificial light was tested in the vertical direction.

6.1.4 Detection experiments

In the experiments done by Bron et al. [8] and Gravil [22], a tank of 15 x 3 x 3 cm was used and divided into five equal sized areas separated by thin partitions. In [8], 10 lice were used in the experiment, whereas 50 were used in [22]. To determine the phototactic response of the individuals used in the experiment, manual counting of the lice in each area was done before and after light stimuli [8]. Automatic detection and counting of lice, as used in this thesis, allowed for the experiments to be conducted using a higher volume of lice. The experiments performed in this project used approximately 20 times as many lice as in [8] and four times as many lice as in [22], making the results less prone to errors related to individual differences within the group of lice.

Compared to the experimental setup of this project where the horizontal movement of salmon lice was tested, Fields et al. [10] tested for vertical movement of salmon lice towards an on/off stimulus frequency. Every second, an image was captured from three vertically aligned cameras, and the lice that were visible in each view were counted. Compared to their method, the position of all lice was retrieved every 0.0625 s in the experiments conducted in this project, revealing more information about the movement of lice over time. With a horizontal experimental setup, the impact of gravity did not disturb the behavioral response among the salmon lice towards the light. However, this impact will occur in a real environment, which means that the experimental setup in this project did not reflect the natural environment in the same way as in [10].

6.1.5 Tracking experiments

Bianco et al. [34] used a telecentric 3D computer vision system to characterize the swimming behavior of the copepod, *Clausocalanus furcatus*, as explained in Section 2.3. Compared to the experimental setup used in this project, they were able to map the swimming motion in the vertical direction, not only in the horizontal direction. In their experiments, they used 30-37

individuals, leaving a bigger statistical basis for the results than what has been obtained with 10-12 individuals. However, as occlusion became a problem with a high density of lice when only considering the horizontal plane, fewer lice were chosen in the tracking experiments. The camera used in [34] used a frame rate of 15 fps, which is significantly lower than 128 fps as used in this project. This confirms the ability of the algorithm to track the salmon louse at its maximum velocities.

6.2 Algorithm

The algorithms developed, as part of the method for quantifying the light response among the salmon lice, should be discussed. Strengths and weaknesses of the developed method should be kept in mind when considering the results in this thesis. It is also interesting to compare the developed method to the methods found in the literature on similar topics. The discussion is divided into two sections; first is a discussion of the detection algorithm, before a discussion of the tracking algorithm follows.

6.2.1 Detection algorithm

The detection algorithm developed in this project was based on standard image processing techniques for feature detection as described in Section 3.1. These techniques are commonly used when the goal is to detect multiple objects in video frames, as stated in the literature in Section 2.2.

Performance

The algorithm seemed to perform sufficiently for the detection of a group of lice in the experimental videos. The algorithm worked well for the videos without pulsating light. When pulsation was present, it worked better for the videos with OD1 than for those with OD3 and OD5. However, it can be seen that the algorithm was able to detect the overall movement of the salmon lice (Figure 5.1, Figure 5.2). As seen in these figures, the salmon lice positions were mapped over time for the whole experiment, giving insight in when the lice started to respond, and whether they swam towards or away from the light source. Despite these results, there are some limitations to discuss.

As seen in Figure 4.6, the original video frame was of low contrast making it challenging to separate the salmon lice from the background. The low contrast between the salmon lice

and the other noise in the image, such as dust particles and water bubbles did also lead to difficulties when trying to detect only the salmon lice. For the same images in a larger scale, see Appendix B.

A Gaussian filter was used to remove the Gaussian distributed noise in the images. This filter did not remove all the noise, so a nonlinear median filter was tested. However, as the dimensions and pixel values of the salmon lice were similar to the shot noise seen in the images, important information got lost when applying this filter, hence this was not used.

A threshold on the contour area was chosen to differ between remaining noise and the salmon lice. When the salmon lice swam downward, the body area became smaller; hence, the algorithm was not able to differentiate between the salmon lice and, e.g., floating dust particles. This effect did also contribute to an irregular number of detections. Other particles with the same size as the salmon lice that was not subtracted by the background subtraction were also sometimes detected and accounted as salmon lice, leading to some deviations in the measured salmon lice positions. Despite othis ccurence of misdetections, the number of detected lice in the tank was relatively stable throughout the experiments.

The experiments in this project included response analysis with pulsating light that led to variations in the background luminance throughout the videos. These irregularities were partly taken care of by dividing the background subtraction into two parts; one for bright frames and one for dark frames. This solution worked well for the experiments with OD1 since the difference in dark and bright pixel values were significant. For the experiments with OD3 and OD5, it was more complex to detect the difference in bright and dark frames, hence more challenging to get a robust background subtraction. This led to irregularities in the number of detected lice throughout the videos.

The varying luminance gave the need for a variable threshold in order to separate the objects of interest from the background. Adaptive thresholding was tested, without obtaining useful results, hence the threshold was varied based on the pixel values measured in each image instead.

The algorithm implemented in this project did not focus on solving the problem of occlusion. Hence, salmon lice lying close to each other, or on top of each other, were detected as one individual. This effect became apparent when the lice moved close to the light source and the local density of lice increased; hence, the number of detected lice decreased in the last minutes of the videos.

Comparison with other methods

Similarities of the implemented algorithm in this thesis and the detection process described in [31] for the detection of biological cells, and in [29] for detection of plankton in the ocean, can be seen. For the detection stage, Kocack et al. [29] used an active contour model, referred to as snakes, in order to detect plankton in an underwater video with good results. Such an active contour model could also be used in this project; however, it was chosen to use a border following algorithm as described in Section 3.1.5 instead, due to its simplicity and availability.

Detection of moving objects in videos has also been done using image analyzing software such as ImageJ [68], [32]. This software provides many of the same image processing techniques for object detection as the ones implemented in this thesis. However, by implementing a custom-made algorithm for analysis of the experiments conducted in this project, scalability was achieved. A drawback with this custom-made method is that it can be tricky to adapt to other problems, as changes in several parameters then need to be done.

In [32] median subtraction was used to remove the static background from an image, and [31] used a thresholding operation to convert the image to binary scale. Dilation was used in [29] to increase the area of interest. These image processing techniques were used before detecting the objects of interest, and were also implemented in the developed algorithm before the contour detection took place, showing an overall good performance.

6.2.2 Tracking algorithm

The tracking algorithm mapped the coordinates from frame to frame, obtaining tracks of each salmon louse during the time of the experiments. From these tracks, the algorithm was able to retrieve information such as velocity, distance traveled, and how directed the swimming behavior of the salmon lice were.

Performance

Due to the erratic swimming characteristic seen for the salmon lice, it is difficult to keep track of each louse over time manually. With an automatic tracking system and videos recorded with a frame rate of 128 fps, it was possible to obtain continuous tracks despite the quick and random jumps.

It can be observed that the number of tracks is different between the three replicates shown in Section 5.2. This partly has to do with the requirements made for adding coordinates to a given track. If the distance from one track to the closest coordinate in the next frame was too long, a

new track was created. By observing the videos, it was seen that some lice moved too close to the wall to be detected by the camera, and stayed there over multiple frames before it appeared in a different location. Thus, the current track of this louse was interrupted, and a new track was created. Another reason for the different number of tracks was the vertical motion of the lice. As salmon lice are elongated, the area of the louse visible to the camera decreased when the louse swam in the vertical direction, causing it to no longer be detected as a louse. When it appeared, it had in some cases moved past the limit of distance where it would be connected to its current track; thus, a new track was created. Another reason for the difference in the number of tracks is that there were different numbers of lice in each experiment, even though this was tried to be avoided.

Comparison with other methods

As explained in Section 2.3, methods were proposed for handling the problem of interacting targets, referred to as occlusion. Khan et al. [37] proposed a method that used a particle filter to solve this problem. However, with only 10-12 lice in a tank of 253 cm^2 in the horizontal plane, this was not found to be needed.

Walter et al. [35] used a separate linear Kalman filter to estimate the position of the detected objects and track their centroids over the image plane, and Straw et al. [36] used an extended Kalman filter (EKF) for tracking of insects. Regarding this project, the main reason for making the tracking algorithm more complex would be to handle occlusion. A single Kalman filter would not be able to handle this phenomenon, because each time two lice collide, the probability distribution would be bimodal, as each louse can follow both tracks, as the swimming motion is assumed to be random. One way to handle this would be to create one Kalman filter for each path, leaving the point of occlusion for each louse, and then resolve the most probable path based on behavioral traits. Another reason why a Kalman filter was not used in this thesis was that it would not handle the problems related to the discontinuities any better than the currently implemented algorithm. Lastly, the Kalman filter would filter out the peaks of the sporadic, fast jumps of the salmon louse, leaving a tradeoff between smoothing and losing information. Despite being able to gain information about overall trends, such as general movement towards the light source, this smoothing would leave out valuable information for the purpose of this thesis.

Sirisha et al. [39] and Tharanidevi et al. [40] used the knowledge about the position of objects in each frame together with Euclidean distance measures. This was found to be a convenient way of tracking the salmon lice in the experimental videos obtained from the tracking experiments, as occlusion was rarely present. This method was shown to accurately track the salmon lice

from frame to frame.

6.3 Detection results

The movement towards the light source was bigger for R2 than for R1 and R3 (Figure 5.1, Figure 5.2). This tendency is repeating, but can not be seen for all the experiments. The salmon lice in R2 belonged to the population hatched at ILAB, and had lived longer compared to the salmon lice used in R1 and R3. As stated in [14], the salmon lice live for approximately 12 days. Because the salmon lice in R2 were at the end of their life cycle, one would assume that these lice had a lower energy level than the younger salmon lice. However, one can also question whether the salmon lice become more desperate to find a host, and thereby the response towards an attractant gets bigger at the end of their infective copepodid stage.

For the green light source, the highest response was seen for OD1-P0 with a median displacement from baseline of 3.07 cm. The result for this light setting was less dispersed than the results for the second highest displacement of 2.71 cm, which was seen for OD3-P3. The SD for OD1-P0 and OD3-P3 was 1.50 cm and 1.89 cm, respectively, leaving a more reliable result for OD1-P3 (Figure 5.3, Table 5.2).

For the blue light source, the highest response was also seen for OD1-P0, with a total displacement of 2.83 cm from baseline. However, compared to Green-OD1-P0, this result had a higher dispersion and a higher SD of 2.05. The lowest SD for the experiments with blue light was 1.57 cm found for OD5-P3. With blue light source, negative results occurred for OD1-P1 and OD5-P3, meaning that the total displacement of the salmon lice was away from the light source (Figure 5.4, Table 5.2). As discussed about the experimental setup, some light reflections were present during the experiments. These reflections led to uncertainty when interpreting the results, as remains unknown whether the salmon lice swam towards the reflections, or tried to escape from the light stimuli when negative displacements were observed.

For white light, the highest displacement occurred for OD3-P0, followed by OD1-P0, with displacements at 6.78 cm and 5.29 cm, respectively. Despite having large displacements towards the light source, the standard deviations were large for these light settings, with 4.13 and 3.19, respectively (Figure 5.5, Table 5.2).

The highest displacement among all colors occurred for white-OD3-P0 with a median value of 6.78 cm from the baseline, towards the light source. Even though this light setting gave a high median value of the salmon lice displacements, it also had the highest SD at 4.13 cm, meaning that the measured displacements were dispersed. In general, the results with green light had lower SD, but also lower overall displacement than the results obtained with white light. An

attraction of salmon lice was seen for most light settings; however, many light settings showed high dispersion in the data. Thus, there are uncertainties of the results. Since the salmon lice are living organisms with individual behavior, the dispersion was to some degree expected. As discussed in Section 6.1.3, the different replicates used different populations of lice, which may substantiate the high variation in the results. Another reason for the high dispersion in some of the results might have been the observed reflections in many of the experiments, where one hypothesis is that some lice moved towards these rather than the light source, as discussed in Section 6.1. This could have affected the median displacement, meaning that the measured displacement might have been bigger if the light reflections were not preset.

Both similarities and differences can be seen when comparing the results from this project with the literature. First of all, it has been seen that the overall movement of the salmon lice was towards the light source, for most light settings. This coincides with the findings in [10], [8] and [22].

In [8], the highest response towards artificial light among the salmon lice was obtained with light stimuli of wavelength 550 nm, which corresponds to green light. Similar results were shown in [22], where the highest responses were reached for wavelengths between 500 - 560 nm. The results in this thesis show that the total displacement was not as big for green light as for white light; however, green light was shown to give attraction for most of the light settings, with lower SDs than for white light.

Gravil [22] did also show that the salmon lice in their copepodid stage were attracted to a light source simulating artificial daylight. The same positive response was shown for light simulating daylight in the study done by Fiels et al. [10]. In this project, white light was most similar to daylight. This light source also gave the most significant response among the salmon lice when looking at the median displacement.

As stated in [22], the salmon lice copepodids are sensitive to many levels of irradiance. This was also shown in the results in Section 5.1.2, where some response can be seen for all irradiance levels.

When considering how the pulsation rate impacts the salmon lice response, the study done by Fields et al. [10] and this study can be compared. Fields et al. stated that the highest response was obtained with an on/off pulsation rate of 3.7/5.5 s. The results from the detection experiments in this project show that the highest response was obtained without any pulsation in the light stimuli, which contradicts the study done in [10]. However, it can be seen in Section 5.1.2 that pulsation rates of 2.0/3.0 s and 5.0/5.0 s obtained higher response than the pulsation rate of 0.1/0.1 s. This result is similar to what was found in [10], where they showed that high pulsation frequency gave a lower response compared to low pulsation frequancies.

6.4 Tracking results

The swimming behavior of the salmon lice (*L. salmonis copepodids*) showed to be different from the swimming behavior found for the copepod *Clausocalanus furcatus*, explained in Section 2.3. While *C. furucatus* showed a regularity in the swimming behavior when exposed to food, having a triangular or circular pattern [34], the salmon lice showed a less regular, but more determined swimming behavior. The trajectories found from the experiments of the salmon lice showed differences within the groups of lice. While some of the lice were determined in their swimming pattern, with swimming direction towards the light source, other lice moved in random patterns, staying in the same area for a longer time. However, the determination coefficient for the group of lice increased after the light was turned on for all three replicates, meaning that the group of lice became more determined in their swimming motion. A reason for the different swimming patterns between the two copepods, both belonging to the subclass called Copepoda, might lie in the positive phototaxis of the salmon lice. The experiment performed with *C. furucatus* only used food to attract the copepods, and did not involve light as an attractive source. While the salmon louse was fooled to think that food can be found near the light, *C. furucatus* might have needed to map a bigger area to find food.

The *C. furucatus* copepods showed to move faster when the concentration of food was higher [34]. The same trend was found for the salmon lice during light stimuli. For all the experiments presented in Section 5.2, the maximum velocities increased after the light was turned on. In box plots showing total maximum velocity, that the mean velocity lies above the median velocity, which implies that few lice had a much higher maximum velocity than the group of lice as a whole (Figure 5.9, Figure 5.13, Figure 5.17). Compared to the *C. furucatus* copepods, having a maximum velocity at around 10 mm/s with a short duration, some of the salmon lice showed to have a maximum velocity at around 100 mm/s with a short duration. For all the copepods in the experiments presented, the average velocity of the salmon lice showed to be below 4 mm/s. Like the *C. furucatus* copepods, the salmon louse showed a jumping swimming pattern. The jumps of the salmon louse, however, were longer and with a higher velocity.

It was seen that the majority of the lice moved towards the light source, with some exceptions (Figure 5.6, Figure 5.10, Figure 5.14). Approximately half of the salmon lice ended up in the area of the light source. However, it cannot be known whether this number would be higher with increased time of the experiments. From a total of 41 tracks presented in the results, the maximum velocity detected was 115.64 mm/s, found for Blue-OD1-P0-R2. However, the median maximum velocity of the lice in the nine experiments lied in the range of 23.01 mm/s - 36.56 mm/s (Appendix C). Comparing these results to the results obtained in [22], one can see a similar trend. Gravil calculated that the maximum obtained velocity was 10.23 cm/s = 102.23

mm/s and that the maximum average velocity was 2.14 cm/s = 21.4 mm/s.

The swimming motion can be considered to distinguish between the light settings. One way to distinguish between the response towards light, is by looking at the mean difference between the median determination factor before and after the light was turned on for the three replicates within each light setting. For Green-OD1-P2, Blue-OD1-P0, and White-OD1-P3, this difference was 0.22, 0.11, and 0.16, respectively. Thus, the assumption that the swimming pattern is more determined towards the Green-OD1-P2 light setting can be made. One can also look at the mean difference in the maximum velocity detected before and after the light was turned on. For Green-OD1-P2, Blue-OD1-P0 and White-OD1-P3, these differences were 19.52 mm/s, 21.94 mm/s and 11.36 mm/s, respectively.

By looking into the swimming velocities of each salmon lice presented in Section 5.2, the periodic increase and decrease in velocity is an interesting discovery. For Green-OD1-P2, track 4 had an oscillating velocity, going from approximately 5 mm/s to 30-40 mm/s in almost regular intervals with approximately the same periodic pulsation as P2 (Figure 5.7). The same applied to track 8 in White-OD1-P3, where the general velocity pattern had periods corresponding to the on/off ratio of P3, after some time with light stimuli (Figure 5.15). For Blue-OD1-P0, the same oscillating behavior was not seen, which can be related to the fact that there was no pulsating light present (Figure 5.11). These results coincide nicely with the findings of Fields et al. [10], which proved a significant attraction towards light flicker frequency having pulsations with on/off ratios of 3.7/5.5 and 3.7/16.5. These light pulsations simulated the flickery reflections of light from the salmon skin or shadows caused by groups of fish swimming above the lice. Thus, the periodic increase in velocity when applying pulsating light seems reasonable, as this might fool the salmon louse to think that there is a host nearby.

When comparing the results from the detection experiments for Green-OD1-P2, Blue-OD1-P0, and White-OD1-P3 with the results from the tracking experiments, some differences can be seen. For example, White-OD1-P3 showed to have a negative response in the detection experiments, which could be interpreted as an escape from the light. However, as the tracking experiments with the same light setting showed a clear attraction, the hypothesis of attraction towards the light reflections rather than an escape from the light source can be confirmed.

It should be kept in mind that the velocities were registered for salmon lice in an experimental tank, with few external forces present. Thus, it cannot be known whether the salmon lice when exposed to, e.g., ocean currents, can obtain a higher maximum speed than what has been measured, in order to override the current forces if an attractant is nearby.

6.5 Light propagation in the ocean

How the light propagates in the ocean can be used together with the results from the detection and tracking experiments to look for new methods for reducing the problems associated with salmon lice in the fish farming industry. Before elaborating further on this topic, error sources of the calculations of light intensities should be considered.

6.5.1 Error sources of irradiance calculations

When investigating the possibilities of using light to attract salmon lice in water, artificial light sources can be used. These light sources can be approximated to be diffuse; however, they will work as point light sources in practice. The attenuation coefficients (K_λ) found at Hosenøyan, which were used in the calculations of irradiance, $E_\lambda(z)$, are vertical diffuse attenuation coefficients. They are a measure of to which extent the diffuse downwelling daylight diminishes at different depths. The initial light irradiances, $E_{0,\lambda}$, were measured at the light source used in this project, which was collimated to approximate diffuse light. Thus, beam attenuation coefficients should have been used in the calculation of $E_\lambda(z)$. With no access to this data, the attenuation coefficients measured at Hosenøyan were used as an approximation to look at the propagation of the light sources found to attract salmon lice most efficiently. Despite this assumption, the use of the vertical diffuse attenuation coefficients (K_λ) in the calculations of $E_\lambda(z)$ could be correct if the light sources are placed close to each other, by for instance constructing a grid in the area of interest, approximating a diffuse light source.

An assumption made when calculating $E_{0,\lambda}$ for OD3 and OD1, from the measured values for OD5, was that the OD filter was logarithmic. If there were disturbances on the filter, the calculated values for $E_{0,\lambda}$ would deviate from the actual values.

Measurement noise could also have influenced the initial values for light irradiance and attenuation coefficients. In addition, some assumptions had to be made in the preprocessing of the data, which might have caused errors. These include the assumption that the OD filter was logarithmic, and that the attenuation coefficients could be approximated to be a polynomial of 3rd degree (Figure 5.18).

6.5.2 Results

In Table 5.6 and Table 5.7, the distances for which the different light sources can propagate before their total irradiance value E is reduced by one OD level is shown for oceanic water at Hosenøyan. From the detection experiments, it was seen that the response was generally lower

for OD5 than for OD3 and OD1. The results from the pilot experiments presented in Section 2.5 showed little response towards irradiance corresponding to OD levels above OD5. Thus, to get information about the effect of each light source with respect to the attraction of salmon lice, the distance it takes before the light irradiance is reduced to OD5 is of interest.

Among White-OD1, Blue-OD1, and Green-OD1, the results imply that green light propagates furthest, 58 m, before it reaches the irradiance level corresponding to OD5. White light reaches OD5 after 47 m, and blue light reaches OD5 after 42 m. This does not correspond to the plotted attenuation lengths in Figure 3.9, where blue light propagates further than green light [61]. However, it conforms well with the attenuation coefficients provided to the authors, as the attenuation coefficient is largest for blue light, meaning the light is attenuated at a shallower depth for blue light than for both white and green light. This difference has to do with the variations in the waters where the attenuation coefficients were measured. If there were colored dissolved organic matter and other biological material present, the attenuation coefficient for blue light would increase. Thus, it makes sense that the coefficient was larger for blue light as the measurements were done outside of a fish farming cage at Hosenøyan.

For White-OD1, the light propagates 34 m before it reaches OD4 and 46 m before it reaches OD5, where the attraction of lice still occurs, but with a generally lower response. This corresponds well to the findings of Fields et al. [10], where it was estimated that the copepodids of salmon lice can detect light/shadows from a depth of 31-37 m.

6.5.3 Natural light versus artificial light

In these experiments, the response among the salmon lice was measured when they were exposed to artificial light stimuli, without the impact of other light sources such as natural daylight. How the salmon lice will perceive the artificial light source in combination with natural daylight was not tested for in this project; hence, the salmon lice response to such an artificial light source will not be known when placed in their natural environment.

Chapter 7

Conclusions and further work

7.1 Conclusions

A method involving a customized algorithm for analyses and quantification of the swimming behavior, velocity, and swimming direction of the salmon louse copepodid has been developed using computer vision.

The phototactic swimming behavior of salmon lice was quantified with the use of feature detection and object tracking. An algorithm was developed using image processing techniques such as median subtraction, Gaussian filtering, thresholding, and morphological operations. The objects of interest were detected using a border following algorithm, and the centroid coordinates were extracted in each frame and used in the analyses of the salmon lice behaviour. Further, the tracking algorithm mapped the coordinates from frame to frame, obtaining the track of each salmon louse during the time of the experiments. Parameters such as velocity and distance were then computed for each salmon louse.

The developed method was able to distinguish between salmon lice behavior when exposed to different light settings. An overall attractive response towards light stimuli was seen. When tracking each salmon louse, it was seen that the swimming behavior differed with different pulsation rates and irradiance levels. From a total of nine experiments with three different light settings, the median maximum swimming velocities were in the range 23.01-36.56 mm/s, where the maximum velocity registered was 115.64 mm/s. These swimming velocities coincide with previous findings in the literature. The results imply that the salmon lice have more directed swimming behavior during light stimuli than in the dark for all the tested light settings.

In addition to detection and tracking of salmon lice in experimental videos, the light attenuation for six different light settings used in the experiments was calculated in oceanic water at

Hosenøyan in Norway to investigate the potential effects of artificial light in the ocean. With the given attenuation coefficients, green light shows to propagate furthest before the irradiance is reduced to a level where the attraction of salmon lice is reduced to a minimum, propagating 58 m before it is reduced from Green-OD1 to Green-OD5. The same reduction is seen after 47 m and 42 m for white and blue light, respectively.

The authors have been concerned whether light can be used as an attractant in water due to the attenuation of light. However, with the given results, light as an attractive source may be suitable, with precautions. If the artificial light source can be approximated to be diffuse, by for instance constructing a grid of light in the area of interest, it may be used as a salmon lice attractant. By fooling the lice to swim towards the light rather than the fish, it may contribute to reducing the increasing problem regarding salmon welfare in the fish farming cages.

7.2 Further work

Further analyses should be done in order to determine the exact light source that achieves the highest response among salmon lice. Further, it can be investigated whether this light setting will work as an attractant for salmon lice in the ocean. How this light setting can be used as an aid in the handling of salmon lice in the fish farming industry can be further explored. Traps using artificial light and filters for collecting the lice is one such idea. As part of research on this topic, investigating the use of 3D tracking to obtain information about swimming behavior in all directions might prove important. In addition, it is a question of future research to investigate the effect of natural daylight in combination with a potential artificial light source in the ocean.

Future research could examine the use of machine learning and convolutional neural networks, in particular, to learn to recognize the salmon lice and its behavior in each video frame. Hence, a more robust detection method can be obtained, reducing the number of error detections.

Bibliography

[1] K. Boxaspen, "A review of the biology and genetics of sea lice," *ICES Journal of Marine Science*, vol. 63, pp. 1304–1316, 8 2006.

[2] "Fakta om lakselus og lakselusbekjempelse — Mattilsynet," 2016. Available at https://www.mattilsynet.no/fisk_og_akvakultur/fiskehelse/fiske_og_skjellsykdommer/lakselus/fakta_om_lakselus_og_lakselusbekjempelse.23766, Accessed: 2019-02-29.

[3] K. Glover, Stølen, A. Messmer, B. Koop, O. Torrissen, and F. Nilsen, "Population genetic structure of the parasitic copepod Lepeophtheirus salmonis throughout the Atlantic," *Marine Ecology Progress Series*, vol. 427, pp. 161–172, 4 2011.

[4] E. Osterloff, "The problem of sea lice in salmon farms — Natural History Museum," 2018. Available at https://www.nhm.ac.uk/discover/the-problem-of-sea-lice-in-salmon-farms.html, Accessed: 2019-01-23.

[5] A. T. Baklien and T. A. Steinset, "Aquaculture - annually, final figures - SSB," 2018. Available at https://www.ssb.no/en/fiskeoppdrett?fbclid=IwAR1i1DfXBkzh5Tma1_70GqJ2E8yaVqmfIAdmG0vh-zOV3ATqcBgEHh21s-I, Accessed: 2019-01-23.

[6] B. Hjeltnes, B. B. Jensen, A. Haukaas, C. S. Walde, and G. Bornø, "Fish Health Report 2017," tech. rep., 2017. Available at https://www.vetinst.no/rapporter-og-publikasjoner/rapporter/2018/fish-health-report-2017, Accessed: 2018-11-14.

[7] I. Carr, H. Dankertsen, L. Buttle, T. Barclay, and D. Robb, "CARGILL AQUA NUTRITION SUSTAINABILITY REPORT 2016 Editorial and design team," tech. rep.

[8] J. E. Bron, C. Sommerville, and G. H. Rae, "Aspects of the behaviour of copepodid larvae

of the salmon louse Lepeophtheirus salmonis (Krøyer, 1837).," *Pathogens of wild and farmed fish: sea lice.*, pp. 125–142, 1993.

[9] R. B. Forward, "Behavioral responses of a sand-beach amphipod to light and pressure," *Journal of Experimental Marine Biology and Ecology*, vol. 102, pp. 55–74, 11 1986.

[10] D. M. Fields, A. B. Skiftesvik, and H. I. Browman, "Behavioural responses of infective-stage copepodids of the salmon louse (Lepeophtheirus salmonis, Copepoda:Caligidae) to host-related sensory cues," *Journal of Fish Diseases*, vol. 41, pp. 875–884, 6 2018.

[11] L. A. Hamre, C. Eichner, C. M. A. Caipang, S. T. Dalvin, J. E. Bron, F. Nilsen, G. Boxshall, and R. Skern-Mauritzen, "The Salmon Louse Lepeophtheirus salmonis (Copepoda: Caligidae) Life Cycle Has Only Two Chalimus Stages," *PLoS ONE*, vol. 8, p. e73539, 9 2013.

[12] J. Skarhamar, J. Albretsen, A. D. Sandvik, V. S. Lien, M. S. Myksvoll, I. A. Johnsen, L. Asplin, B. Ådlandsvik, E. Halttunen, and P. A. Bjørn, "Modelled salmon lice dispersion and infestation patterns in a sub-arctic fjord," *ICES Journal of Marine Science*, vol. 75, pp. 1733–1747, 10 2018.

[13] T. A. Schram, "Practical identification of pelagic sea lice larvae," 2019.

[14] D. o. B. University of Bergen, "The atlantic salmon louse," 2018.

[15] G. A. Boxshall and D. Defaye, *Pathogens of wild and farmed fish : sea lice*. Ellis Horwood, 1994.

[16] D. Fields, M. Weissburg, and H. Browman, "Chemoreception in the salmon louse Lepeophtheirus salmonis: an electrophysiology approach," *Diseases of Aquatic Organisms*, vol. 78, pp. 161–168, 12 2007.

[17] H. I. Browman, K. Boxaspen, and P. Kuhn, "The effect of light on the settlement of the salmon louse, Lepeophtheirus salmonis, on Atlantic salmon, Salmo salar L.," *Journal of Fish Diseases*, vol. 27, pp. 701–708, 12 2004.

[18] P. A. Heuch and E. Karlsen, "Detection of infrasonic water oscillations by copepodids of Lepeophtheirus salmonis (Copepoda Caligida)," *Journal of Plankton Research*, vol. 19, pp. 735–747, 6 1997.

[19] R. L. Genna, W. Mordue, A. W. Pike, and A. J. Mordue (Luntz), "Light intensity, salinity, and host velocity influence presettlement intensity and distribution on hosts by copepodids of sea lice, Lepeophtheirus salmonis," *Canadian Journal of Fisheries and Aquatic Sciences*, vol. 62, pp. 2675–2682, 12 2005.

[20] R. L. Genna, "The chemical ecology, physiology and infection dynamics of the sea louse copepodid, Lepeophtheirus salmonis Kroyer," 2002.

[21] K. Aarseth and T. Schram, "Wavelength-specific behaviour in Lepeophtheirus salmonis and Calanus finmarchicus to ultraviolet and visible light in laboratory experiments (Crustacea:Copepoda)," *Marine Ecology Progress Series*, vol. 186, pp. 211–217, 9 1999.

[22] H. R. Gravil, "Studies on the biology and ecology of the free swimming larval stages of Lepeophtheirus Salmonis (Kroyer, 1838) and Caligus Elongatus Nordmann, 1832 (Copepoda: Caligidae)," 1996.

[23] J.-E. Juell, A. Fernö, D. Furevik, and I. Huse, "Influence of hunger level and food availability on the spatial distribution of Atlantic salmon, Salmo salar L., in sea cages," *Aquaculture Research*, vol. 25, pp. 439–451, 5 1994.

[24] I. Huse and J. C. Holm, "Vertical distribution of Atlantic salmon (Salmo salar) as a function of illumination," *Journal of Fish Biology*, vol. 43, pp. 147–156, 12 1993.

[25] E. Hevrøy, K. Boxaspen, F. Oppedal, G. Taranger, and J. Holm, "The effect of artificial light treatment and depth on the infestation of the sea louse Lepeophtheirus salmonis on Atlantic salmon (Salmo salar L.) culture," *Aquaculture*, vol. 220, pp. 1–14, 4 2003.

[26] P. A. Heuch, A. Parsons, and K. Boxaspen, "Diel vertical migration: A possible host-finding mechanism in salmon louse (Lepeophtheirus salmonis) copepodids?," *Canadian Journal of Fisheries and Aquatic Sciences*, vol. 52, pp. 681–689, 4 1995.

[27] S. Kadri, N. B. Metcalfe, F. A. Huntingford, and J. E. Thorpe, "Daily feeding rhythms in Atlantic salmon in sea cages," *Aquaculture*, vol. 92, pp. 219–224, 1 1991.

[28] J. Bron, C. Sommerville, G. Rae, G. Boxshall, and D. Defaye, "Aspects of the behaviour of copepodid larvae of the salmon louse lepeophtheirus salmonis (krøyer, 1837)," 1993.

[29] D. Kocak, N. da Vitoria Lobo, and E. Widder, "Computer vision techniques for quantifying, tracking, and identifying bioluminescent plankton," *IEEE Journal of Oceanic Engineering*, vol. 24, no. 1, pp. 81–95, 1999.

[30] M. Kass, A. Witkin, and D. Terzopoulos, "Snakes: Active contour models," *International Journal of Computer Vision*, vol. 1, pp. 321–331, 1 1988.

[31] D. Lizanets, J. A. Dziuban, and R. Walczak, "Comparison of algorithms for detection and real-time tracking of living microorganisms in lab-on-a-chip devices," in *2017 MIXDES - 24th International Conference "Mixed Design of Integrated Circuits and Systems*, pp. 581–584, IEEE, 6 2017.

[32] A. S. Båtnes, C. Miljeteig, J. Berge, M. Greenacre, and G. Johnsen, "Quantifying the light sensitivity of Calanus spp. during the polar night: potential for orchestrated migrations conducted by ambient light from the sun, moon, or aurora borealis?," *Polar Biology*, vol. 38, pp. 51–65, 1 2015.

[33] C. Miljeteig, A. J. Olsen, A. S. Båtnes, D. Altin, T. Nordtug, M. O. Alver, J. D. Speed, and B. M. Jenssen, "Sex and life stage dependent phototactic response of the marine copepod Calanus finmarchicus (Copepoda: Calanoida)," *Journal of Experimental Marine Biology and Ecology*, vol. 451, pp. 16–24, 2 2014.

[34] G. Bianco, V. Botte, L. Dubroca, M. Ribera d'Alcalà, and M. G. Mazzocchi, "Unexpected Regularity in Swimming Behavior of Clausocalanus furcatus Revealed by a Telecentric 3D Computer Vision System," *PLoS ONE*, vol. 8, p. e67640, 6 2013.

[35] D. Walther, D. Edgington, and C. Koch, "Detection and tracking of objects in underwater video," in *Proceedings of the 2004 IEEE Computer Society Conference on Computer Vision and Pattern Recognition, 2004. CVPR 2004.*, vol. 1, pp. 544–549, IEEE.

[36] A. D. Straw, K. Branson, T. R. Neumann, and M. H. Dickinson, "Multi-camera real-time three-dimensional tracking of multiple flying animals," *Journal of The Royal Society Interface*, vol. 8, pp. 395–409, 3 2011.

[37] Zia Khan, T. Balch, and F. Dellaert, "MCMC-based particle filtering for tracking a variable number of interacting targets," *IEEE Transactions on Pattern Analysis and Machine Intelligence*, vol. 27, pp. 1805–1819, 11 2005.

[38] Kap-Ho Seo and Ju-Jang Lee, "Real-time object tracking and segmentation using adaptive color snake model," in *31st Annual Conference of IEEE Industrial Electronics Society, 2005. IECON 2005.*, p. 5 pp., IEEE, 2005.

[39] K. Sirisha, A. Prof, and R. Patnaik, "IMPLEMEMTATION OF MOVING OBJECT TRACKING AND DETERMINATION OF VELOCITY USING DSK," *International Journal of Scientific & Engineering Research*, vol. 3, no. 11, 2012.

[40] B. Tharanidevi, R. Vadivu, and K. B. Sethupathy, "Moving Object Tracking Distance and Velocity Determination based on Background Subtraction Algorithm," Tech. Rep. 1.

[41] M. Alsvik, *The response of salmon lice nauplii and copepodids (Lepeophtheirus salmonis) to artificial light stimuli [In preparation]*. PhD thesis, Norwegian University of Science and Technology, 2019.

[42] E. Sakshaug, G. H. Johnsen, and K. M. Kovacs, *Ecosystem Barents Sea*. Tapir Academic, 2009.

[43] E. Børset, *Investigating the Phototactic Response of Salmon Lice Design and Analysis of Experiments [In preparation]*. PhD thesis, Norwegian University of Science and Techonolgy (NTNU), 2019.

[44] J. Danielsen and P. Nordenfelt, "Computer Vision-Based Image Analysis of Bacteria," pp. 161–172, 2017.

[45] R. Jain, R. Kasturi, and B. G. Schunck, *Machine vision*. McGraw-Hill, 1995.

[46] R. Szeliski, *Computer vision : algorithms and applications*. Springer, 2011.

[47] Itu-r, "Recommendation ITU-R BT.601-7 Studio encoding parameters of digital television for standard 4:3 and wide-screen 16:9 aspect ratios BT Series Broadcasting service (television)," tech. rep. Available at http://www.itu.int/ITU-R/go/patents/en, Accessed: 2019-05-29.

[48] S. Westland and V. Cheung, "RGB systems," in *Handbook of Visual Display Technology*, pp. 171–177, 2016.

[49] R. M. Haralick, S. R. Sternberg, and X. Zhuang, "Image Analysis Using Mathematical Morphology," *IEEE Transactions on Pattern Analysis and Machine Intelligence*, vol. PAMI-9, pp. 532–550, 7 1987.

[50] G. Bradski and P. Kaehler, *Learning OpenCv*. 1005 Gravenstein Highway North, Sebastopol, CA 95472: O'Rielly Media.

[51] "OpenCV opencv documentation! — OpenCV 2.4.13.7 documentation," 2019. Available at https://docs.opencv.org/2.4.13.7/, Accessed: 2019-04-13.

[52] S. Suzuki and K. A. Be, "Topological structural analysis of digitized binary images by border following," *Computer Vision, Graphics, and Image Processing*, vol. 30, pp. 32–46, 4 1985.

[53] M. H. Singer, "A general approach to moment calculation for polygons and line segments," *Pattern Recognition*, vol. 26, pp. 1019–1028, 7 1993.

[54] J. Flusser, T. Suk, and B. Zitov, *Moments and Moment Invariants in Pattern Recognition*. Chichester, UK: John Wiley & Sons, Ltd, 10 2009.

[55] H. Grabner, M. Grabner, and H. Bischof, "Real-Time Tracking via On-line Boosting," 2006.

[56] J. M. Palmer and B. G. B. G. Grant, *The art of radiometry*. SPIE Press, 2010.

[57] A. Einstein, "On a Heuristic Point of View about the Creation and Conversion of Light," tech. rep., Annalen der Physik (AdP), 1905.

[58] F. Sigernes, "BASIC HYPER SPECTRAL IMAGING," tech. rep. Available at http://kho.unis.no/doc/BASIC_HYPER_SPECTRAL_IMAGING.pdf, Accessed: 2019-05-11.

[59] L. Mullen, "Optical propagation in the underwater environment," vol. 7324, p. 732409, International Society for Optics and Photonics, 5 2009.

[60] J. Downing, "Effects of Light Absorption and Scattering in Water Samples on OBS ® Measurements," tech. rep., 2008.

[61] A. Yamashita, M. Fujii, and T. Kaneko, "Color Registration of Underwater Images for Underwater Sensing with Consideration of Light Attenuation," in *Proceedings 2007 IEEE International Conference on Robotics and Automation*, pp. 4570–4575, IEEE, 4 2007.

[62] J. Jaffe, "Computer modeling and the design of optimal underwater imaging systems," *IEEE Journal of Oceanic Engineering*, vol. 15, pp. 101–111, 4 1990.

[63] G. Johnsen, M. A. Moline, L. H. Pettersson, J. Pinckney, D. V. Pozdnyakov, E. S. Egeland, and O. M. Schofield, *Optical monitoring of phytoplankton bloom pigment signatures*, p. 538–606. Cambridge Environmental Chemistry Series, Cambridge University Press, 2011.

[64] Curtis Mobley, "Inherent Optical Properties • Ocean Optics Web Book," 2010.

[65] H. Loisel and D. Stramski, "Estimation of the inherent optical properties of natural waters from the irradiance attenuation coefficient and reflectance in the presence of Raman scattering," *Applied Optics*, vol. 39, p. 3001, 6 2000.

[66] S. Roy, C. Llewellyn, E. S. Egeland, and G. Johnsen, *Phytoplankton Pigments : Characterization, Chemotaxonomy and Applications in Oceanography.* Cambridge University Press, 2011.

[67] J. G. Shannon, "Correlation Of Beam And Diffuse Attenuation Coefficients Measured In Selected Ocean Waters," vol. 0064, pp. 3–11, International Society for Optics and Photonics, 11 1975.

[68] C. Miljeteig, A. J. Olsen, A. S. Båtnes, D. Altin, T. Nordtug, M. O. Alver, J. D. Speed, and B. M. Jenssen, "Sex and life stage dependent phototactic response of the marine copepod Calanus finmarchicus (Copepoda: Calanoida)," *Journal of Experimental Marine Biology and Ecology*, vol. 451, pp. 16–24, 2 2014.

[69] J. A. Vatn, *Method for investigating the phototactic swimming behavior of the marine copepod Lepeophtheirus salmonis [In preparation]*. PhD thesis, Norwegian University of Life Sciences, 2019.

[70] J. Cumilaf, "Energy availability during the early development of calagus rogercresseyi, delayed settlement and the imploctions for fixation success and development times," 2018.

Appendix A

OpenCV functions

A.0.1 Image processing functions

The following functions have been used from the openCV library in the image processing stages of the implemented detection algorithm. The information in retrieved from [**?**].

- *GaussianBlur()*: Removing Gaussian noise from an image by convolving the image with a specified Gaussian kernel.
- *treshold()*: Converts the image to a binary image where all pixels above a specified threshold value becomes 1 and those below becomes 0.
- *dilate()*: A pixel element becomes 1 it at least one pixel under a specified kernel is 1. It increases the white region in the image.

A.0.2 Finding contours

In openCV, a contour is represented by a *CvSeq* sequence, which is a sequence of points [50]. For increased accuracy, the input image should be binary which can be created by *cvCanny()*, which have edge pixels in them, or images created by functions like *cvThreshold()* or *cvAdaptiveThreshold()*, where the edges are implicit as boundaries between positive and negative regions [**?**]. This is also important as *cv2.findContours()* looks for white objects on a black background.

cv2.findContours() is the function used to detect the contours. It takes as input an 8-bit single-channel source image, storage location, header size, contour retrieval mode and the contour approximation method. The two last inputs clarify what is to be computed and how it is going

to be computed. The mode indicates exactly what contours that should be found, and how they should be presented.

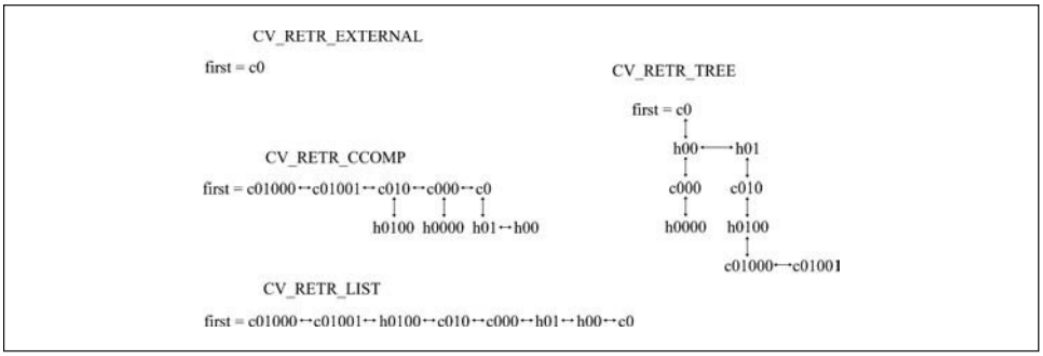

Figure A.1: cv2.findContours(). The way in which the tree node variables are used to "hook up" all of the contours located by cvFindContours() [50].

There are four different modes to consider:

- CV_RETR_EXTERNAL retrieves only the extreme outer contours.
- CV_RETR_LIST retrieves all the contours and puts them in the list.
- CV_RETR_CCOMP retrieves all the contours and organizes them into a two-level hierarchy, where the top-level boundaries are external boundaries of the components and the second level boundaries are boundaries of the holes.
- CV_RETR_TREE retrieves all the contours and reconstructs the full hierarchy of nested contours.

The two main contour approximation methods available in OpenCV are *cv2.CHAIN_APPROX_NONE* and *cv2.CHAIN_APPROX_SIMPLE*. The first method stores all boundary points, whereas the second one removes all redundant data points and thereby saves memory.

There are three output variables; the modified image, the contours and hierarchy. The contours are presented in a list where each individual contour is a Numpy array of (x,y) coordinates of boundary points.

The contours found can be used for many different purposes, among them identifying and thereby detecting objects.

Appendix B

Images from detection steps

As the images presented in this thesis are of low contrast, larger scaled images are presented here. The images illustrate the resulting frame after each step in the detection algorithm.

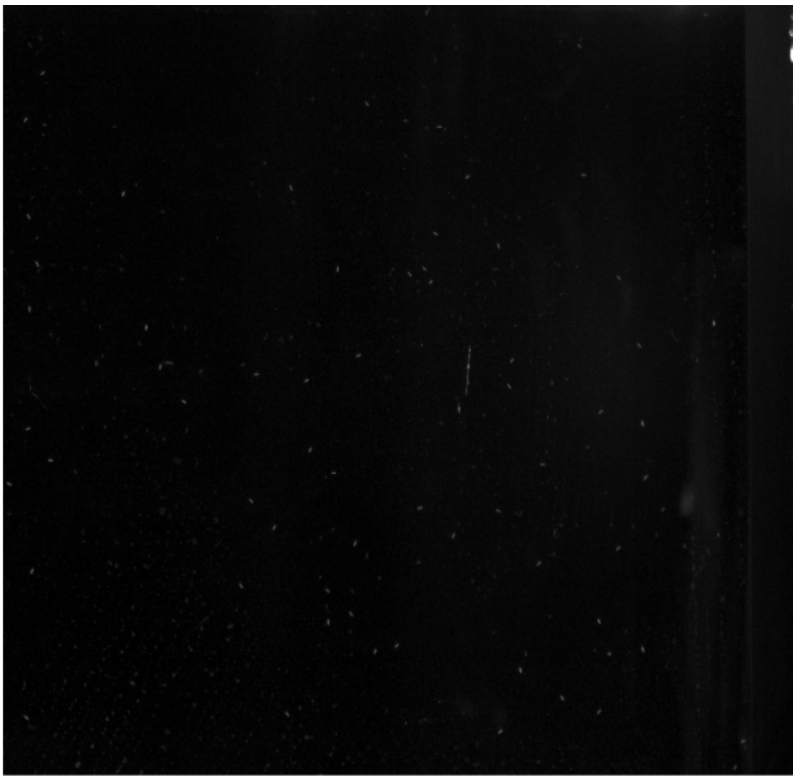

Figure B.1: Original image

Figure B.2: Image without static background

Figure B.3: Image without Gaussian noise

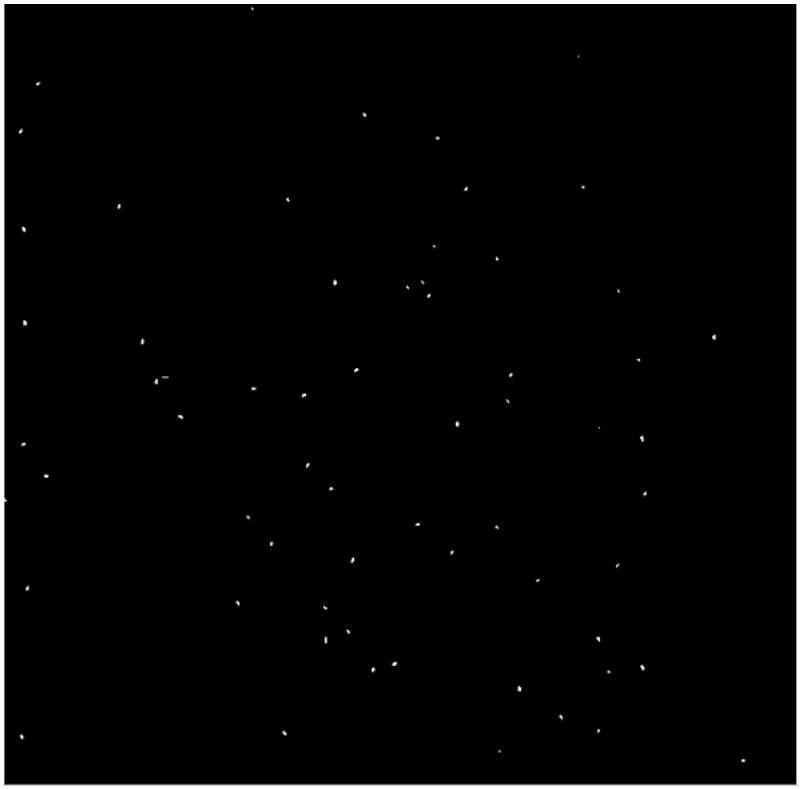

Figure B.4: Binary image

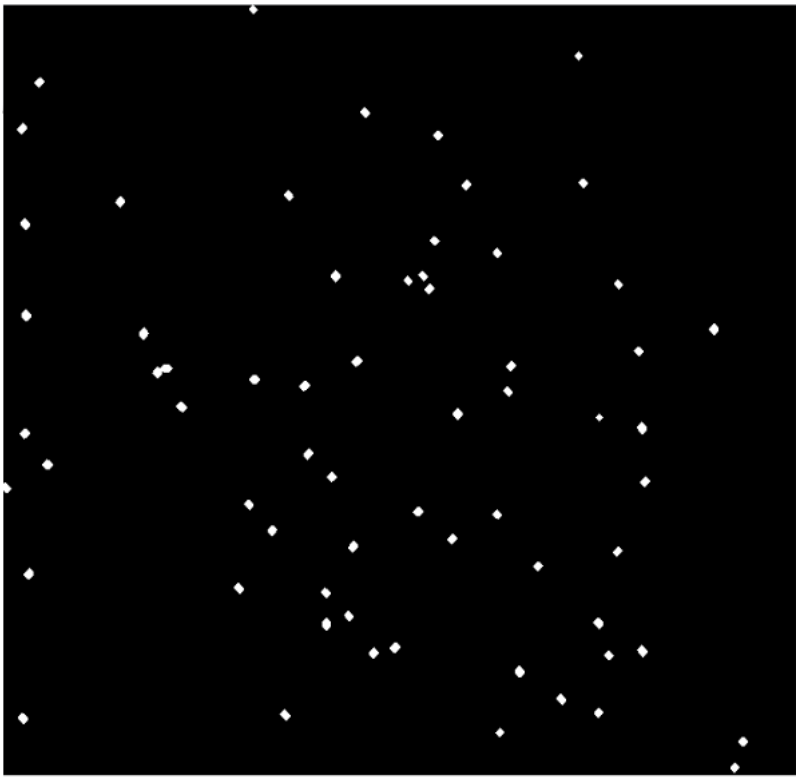

Figure B.5: Image with dilated white areas

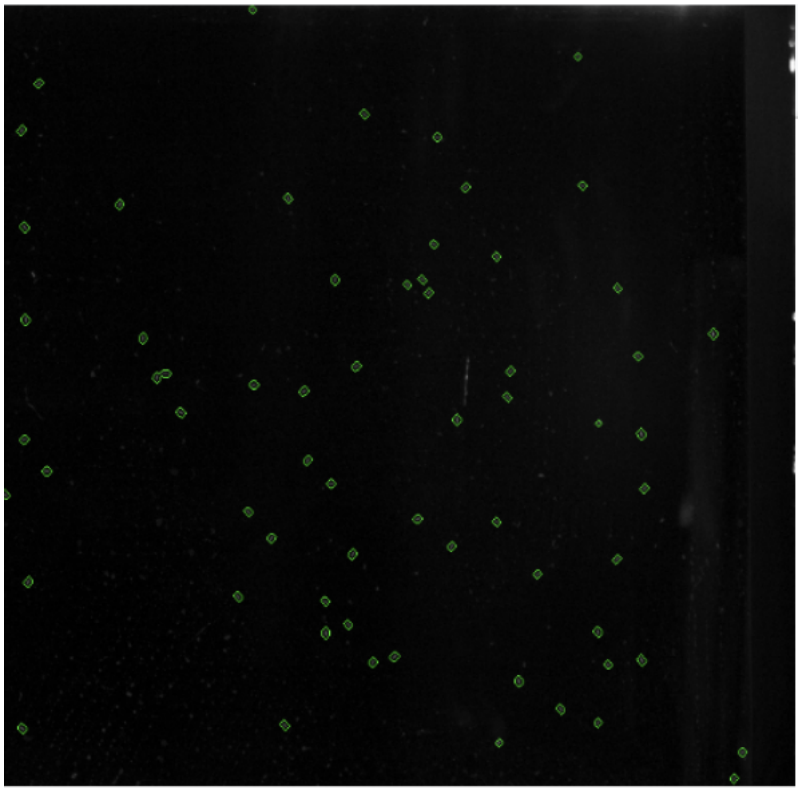

Figure B.6: Marked contours on original frame

Appendix C

Tracking results

The results from six different experiments are presented, with three replicates within each light setting.

The first figure in each section presents all the tracks found for the respective experiment. Each track has an associated description. This description includes information about start time for each track, arc length, average speed and maximum speed. The figures that follows, show the total speed and velocity in x-direction for the three salmon lice with the longest tracks for each experiment. The reason for choosing the tracks with the longest arch lengths, is that these tracks give the most information about the salmon lice behaviour throughout the experiments.

C.1 Blue-OD1-P0-R1

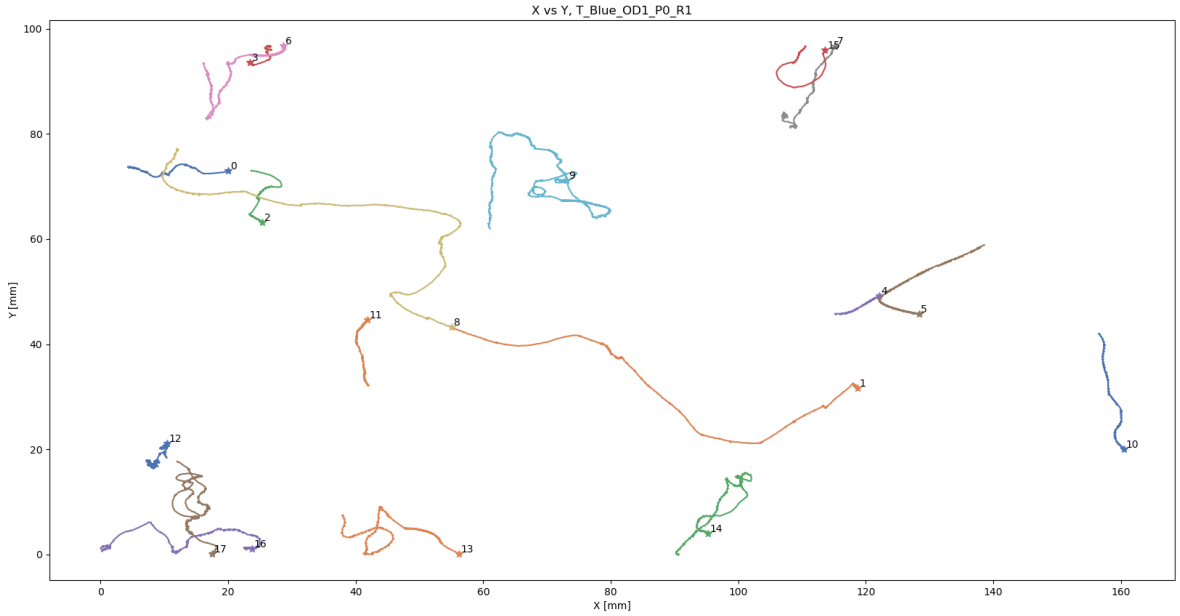

Figure C.1: Tracks found in the two minute long experimental video for Blue-OD1-P0-R1. Stars denote the start of each track.

0: Start: 39.09s, Arc length: 37.45mm, Avg speed: 0.60mm/s, Max speed: 47.67mm/s
1: Start: 0.00s, Arc length: 199.38mm, Avg speed: 1.39mm/s, Max speed: 75.08mm/s
2: Start: 0.00s, Arc length: 66.73mm, Avg speed: 0.55mm/s, Max speed: 78.37mm/s
3: Start: 0.00s, Arc length: 17.57mm, Avg speed: 0.21mm/s, Max speed: 31.87mm/s
4: Start: 3.18s, Arc length: 21.67mm, Avg speed: 0.23mm/s, Max speed: 5.82mm/s
5: Start: 0.00s, Arc length: 106.48mm, Avg speed: 0.99mm/s, Max speed: 14.22mm/s
6: Start: 25.02s, Arc length: 185.05mm, Avg speed: 1.32mm/s, Max speed: 22.61mm/s
7: Start: 76.73s, Arc length: 93.60mm, Avg speed: 1.62mm/s, Max speed: 19.80mm/s
8: Start: 77.98s, Arc length: 157.65mm, Avg speed: 3.00mm/s, Max speed: 72.40mm/s
9: Start: 0.00s, Arc length: 264.06mm, Avg speed: 1.59mm/s, Max speed: 40.51mm/s
10: Start: 65.78s, Arc length: 139.02mm, Avg speed: 1.59mm/s, Max speed: 17.27mm/s
11: Start: 0.00s, Arc length: 105.74mm, Avg speed: 0.66mm/s, Max speed: 9.94mm/s
12: Start: 0.55s, Arc length: 125.10mm, Avg speed: 1.24mm/s, Max speed: 29.12mm/s
13: Start: 54.43s, Arc length: 165.15mm, Avg speed: 1.79mm/s, Max speed: 31.31mm/s
14: Start: 26.47s, Arc length: 180.01mm, Avg speed: 1.44mm/s, Max speed: 61.09mm/s
15: Start: 29.93s, Arc length: 59.07mm, Avg speed: 0.51mm/s, Max speed: 93.14mm/s
16: Start: 0.00s, Arc length: 208.29mm, Avg speed: 1.41mm/s, Max speed: 43.33mm/s
17: Start: 42.50s, Arc length: 106.34mm, Avg speed: 1.49mm/s, Max speed: 76.56mm/s

Figure C.2: Information corresponding to tracks for Blue-OD1-P0-R1. Start time indicates when the track was first registered.

Total speed, Blue-OD1-P0-R1

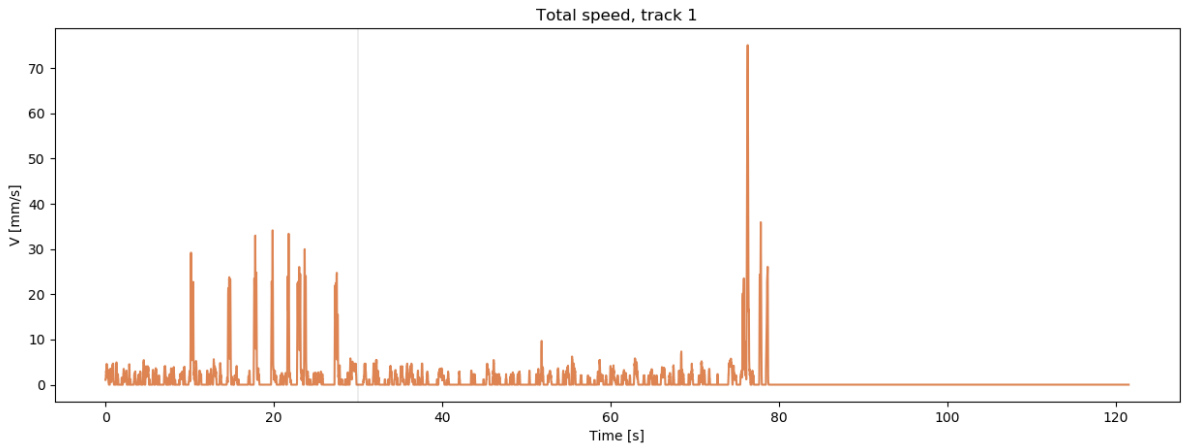

Figure C.3: Speed profile of track 1 in Blue-OD1-P0-R1. The light was turned on after 30 s.

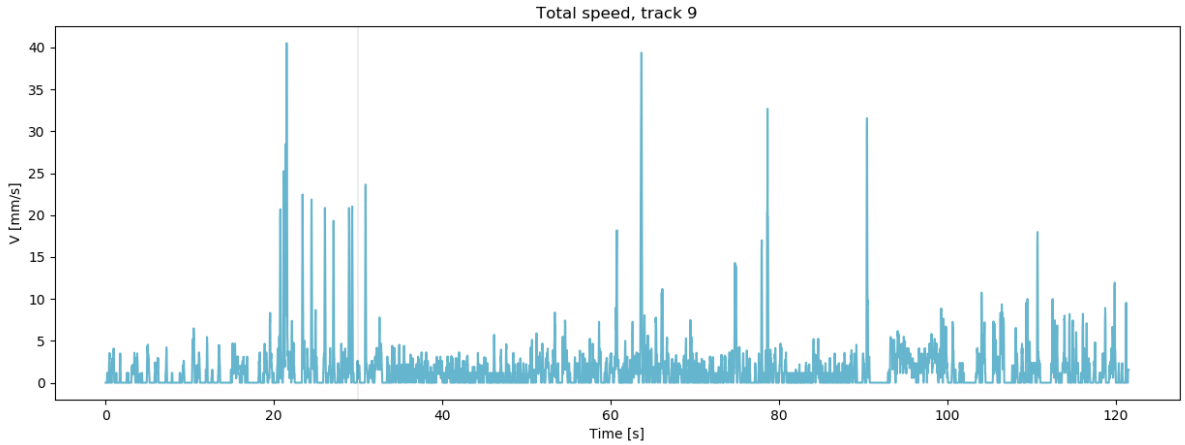

Figure C.4: Speed profile of track 9 in Blue-OD1-P0-R1. The light was turned on after 30 s.

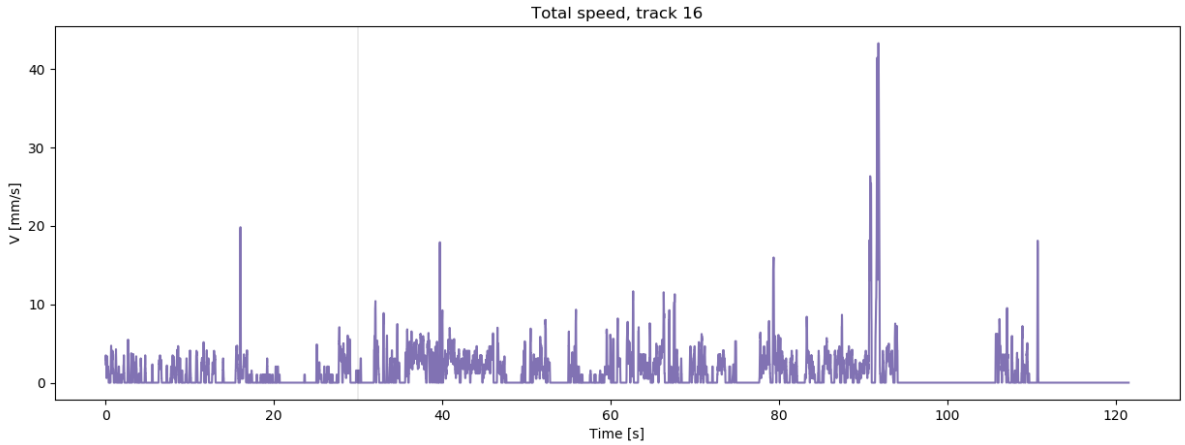

Figure C.5: Speed profile of track 16 in Blue-OD1-P0-R1. The light was turned on after 30 s.

Velocity in x-direction, Blue-OD1-P0-R1

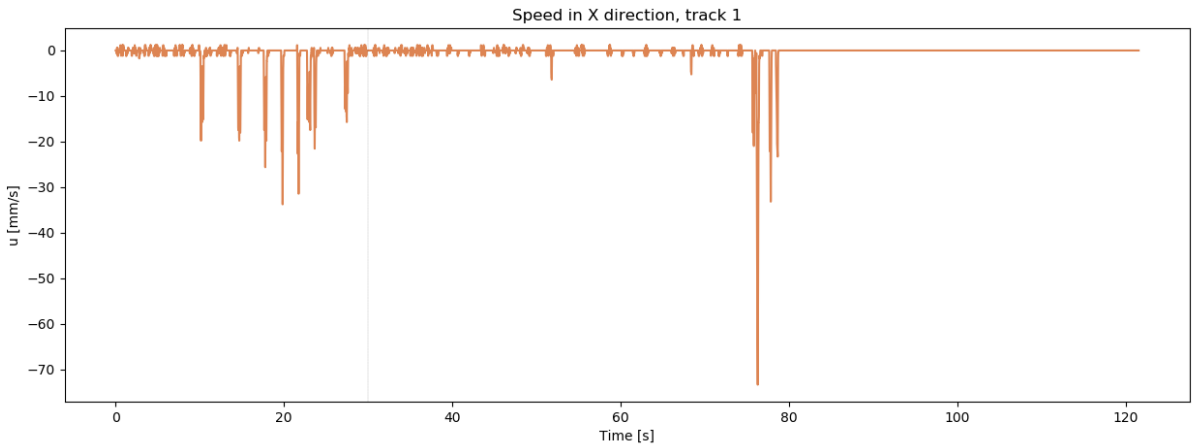

Figure C.6: Velocity profile for track 1 in Blue-OD1-P0-R1. The light was turned on after 30 s.

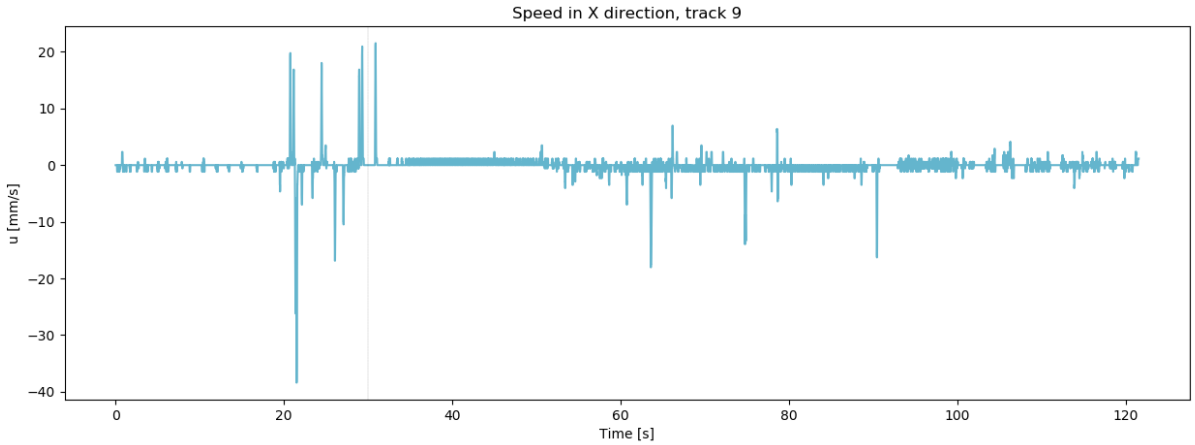

Figure C.7: Velocity profile for track 9 in Blue-OD1-P0-R1. The light was turned on after 30 s.

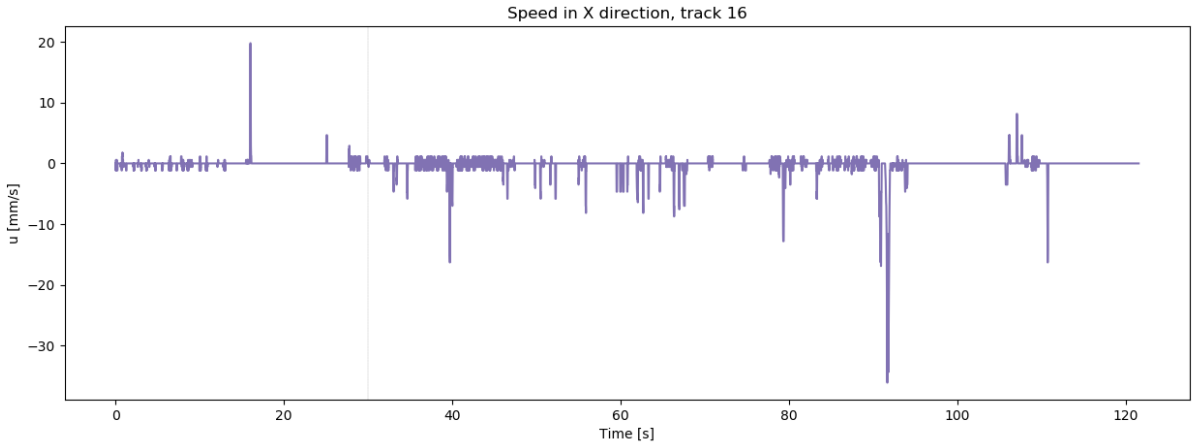

Figure C.8: Velocity profile for track 16 in Blue-OD1-P0-R1. The light was turned on after 30 s.

C.2 Blue-OD1-P0-R2

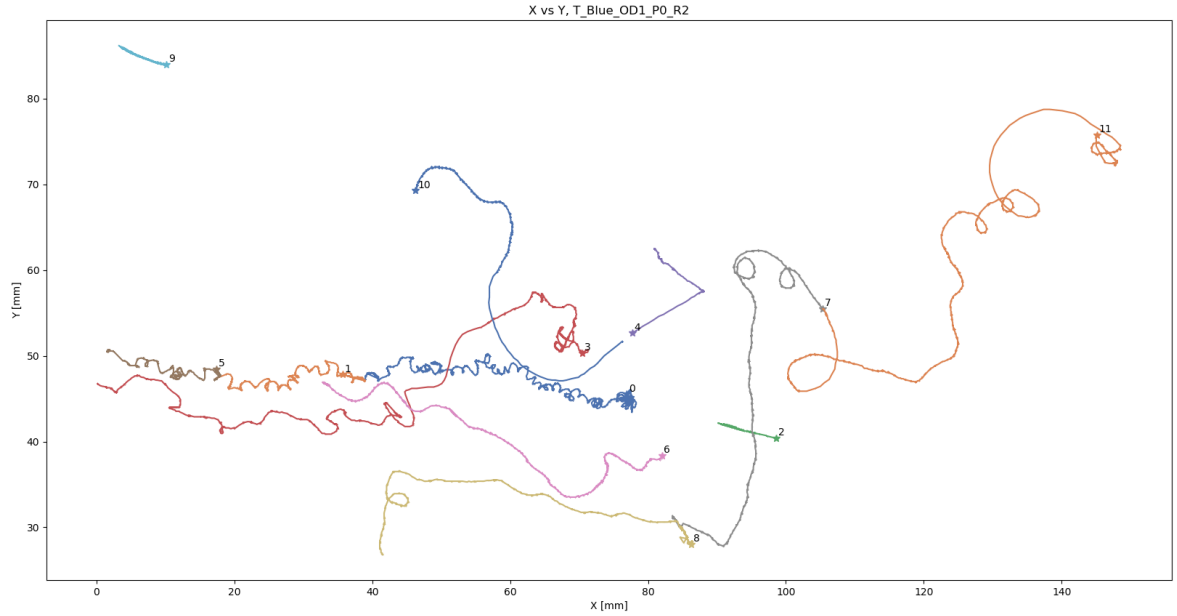

Figure C.9: Tracks found in the two minute long experimental video for Blue-OD1-P0-R2. Stars denote the start of each track.

0: Start: 0.00s, Arc length: 242.57mm, Avg speed: 1.97mm/s, Max speed: 46.18mm/s
1: Start: 0.00s, Arc length: 97.66mm, Avg speed: 0.98mm/s, Max speed: 20.19mm/s
2: Start: 96.79s, Arc length: 36.85mm, Avg speed: 1.33mm/s, Max speed: 15.44mm/s
3: Start: 0.00s, Arc length: 190.79mm, Avg speed: 1.82mm/s, Max speed: 98.51mm/s
4: Start: 108.60s, Arc length: 34.44mm, Avg speed: 1.96mm/s, Max speed: 99.69mm/s
5: Start: 0.08s, Arc length: 83.02mm, Avg speed: 0.76mm/s, Max speed: 23.62mm/s
6: Start: 29.93s, Arc length: 201.57mm, Avg speed: 1.64mm/s, Max speed: 18.58mm/s
7: Start: 77.55s, Arc length: 140.56mm, Avg speed: 2.61mm/s, Max speed: 17.51mm/s
8: Start: 29.93s, Arc length: 272.46mm, Avg speed: 2.37mm/s, Max speed: 32.49mm/s
9: Start: 0.00s, Arc length: 96.37mm, Avg speed: 0.67mm/s, Max speed: 6.41mm/s
10: Start: 29.93s, Arc length: 177.84mm, Avg speed: 1.46mm/s, Max speed: 83.62mm/s
11: Start: 0.00s, Arc length: 230.74mm, Avg speed: 1.93mm/s, Max speed: 115.64mm/s

Figure C.10: Information corresponding to tracks for Blue-OD1-P0-R2. Start time indicates when the track was first registered.

Total speed, Blue-OD1-P0-R2

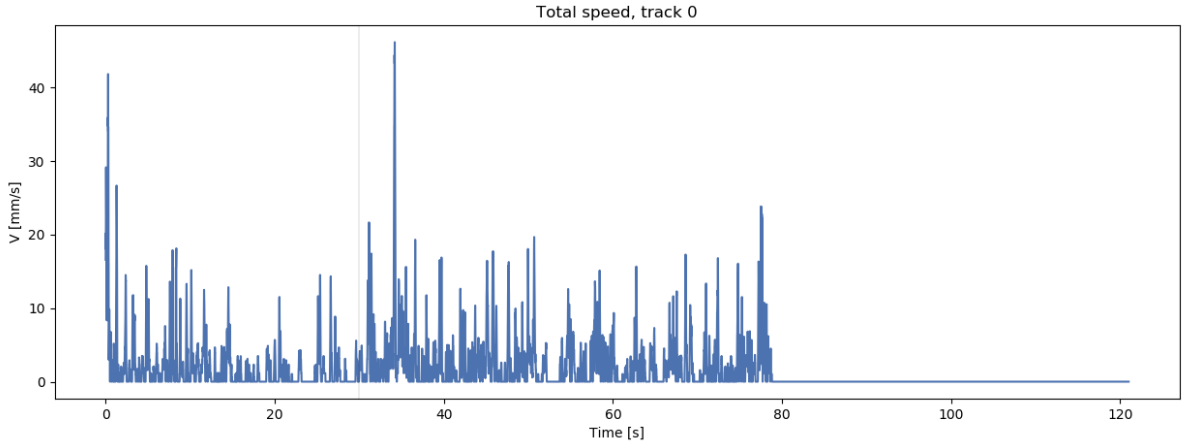

Figure C.11: Speed profile of track 0 in Blue-OD1-P0-R2. The light was turned on after 30 s.

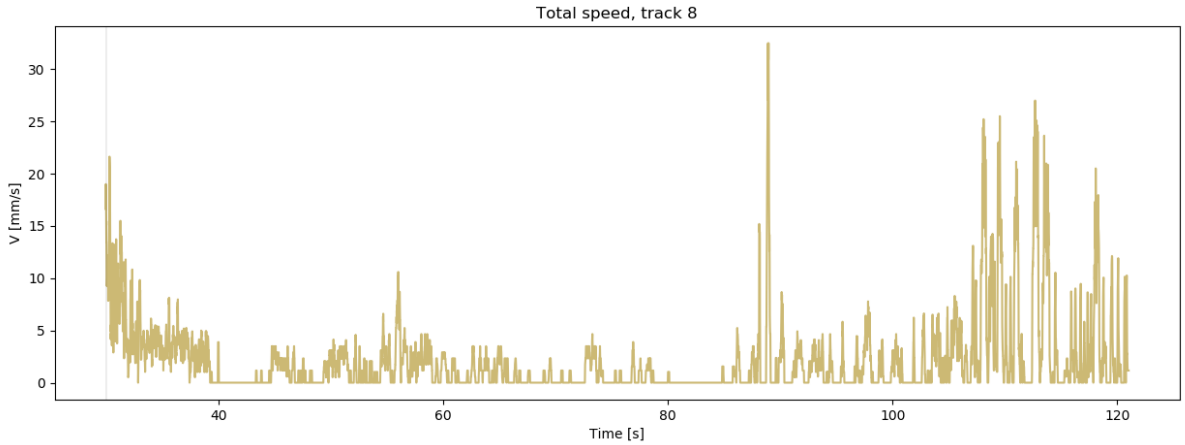

Figure C.12: Speed profile of track 8 in Blue-OD1-P0-R2. The light was turned on after 30 s.

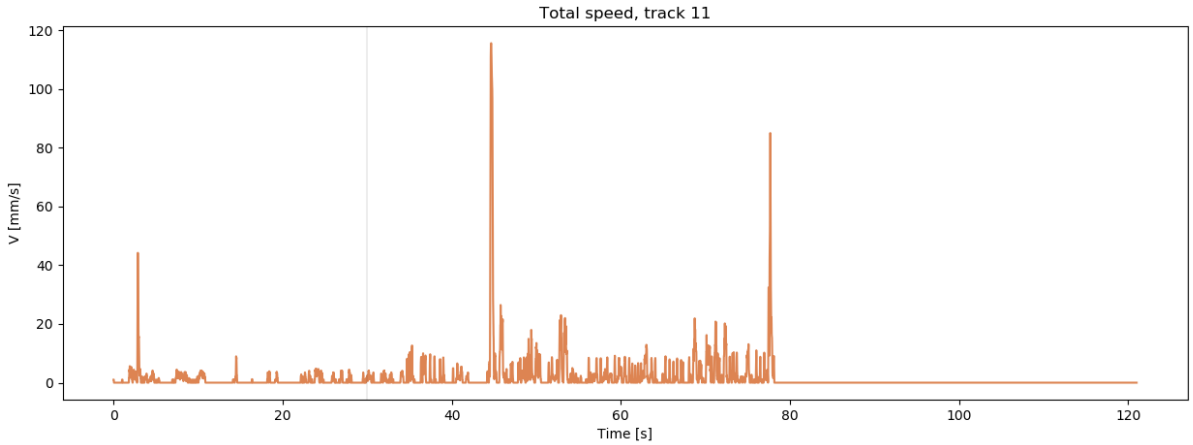

Figure C.13: Speed profile of track 11 in Blue-OD1-P0-R2. The light was turned on after 30 s.

Velocity in x-direction, Blue-OD1-P0-R2

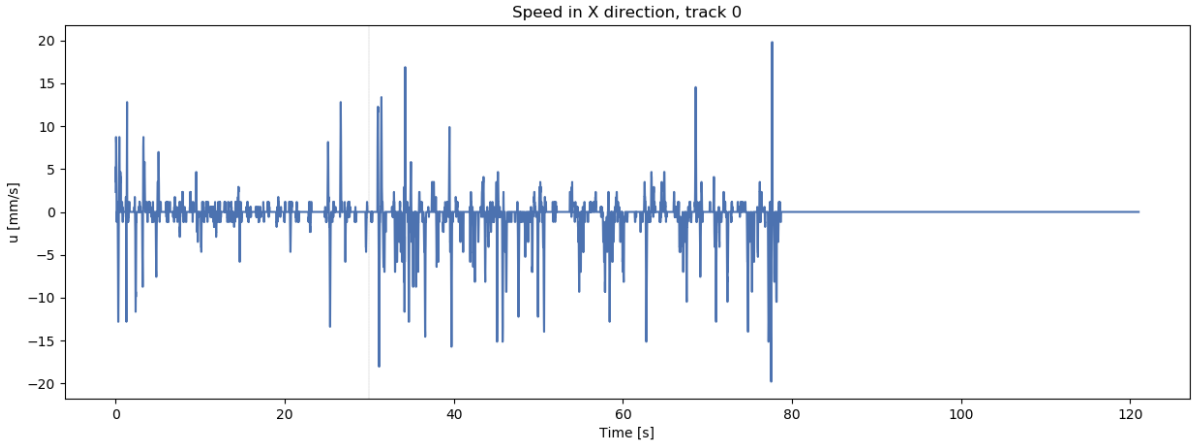

Figure C.14: Velocity profile for track 0 in Blue-OD1-P0-R2. The light was turned on after 30 s.

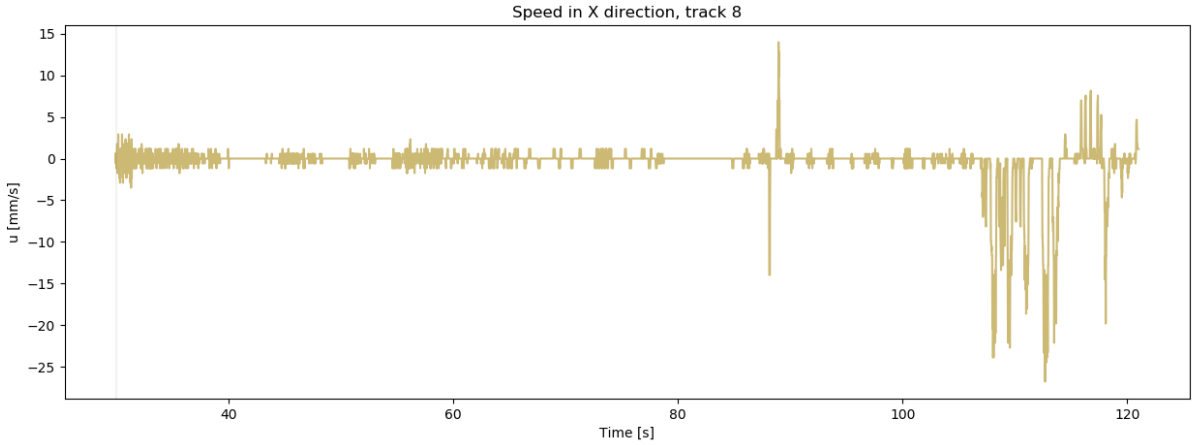

Figure C.15: Velocity profile for track 8 in Blue-OD1-P0-R2. The light was turned on after 30 s.

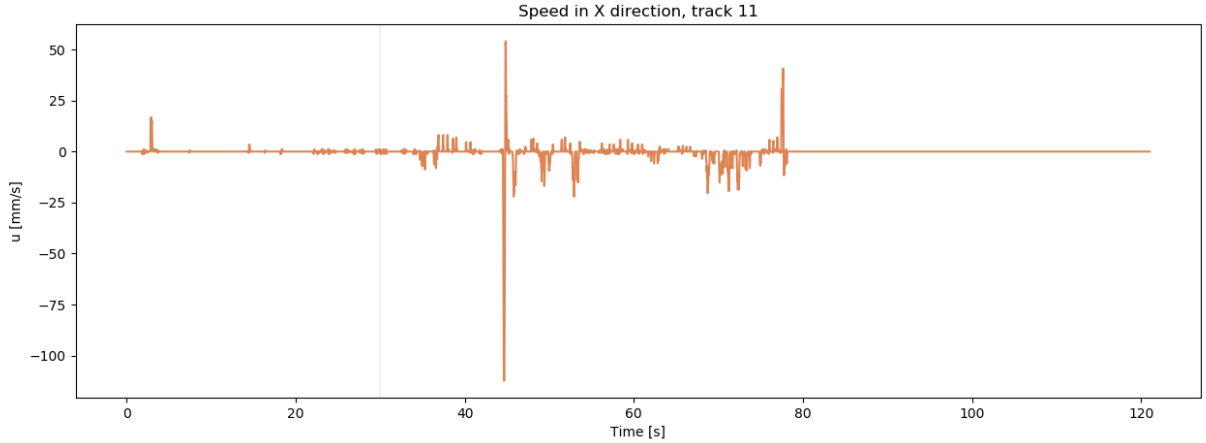

Figure C.16: Velocity profile for track 11 in Blue-OD1-P0-R2. The light was turned on after 30 s.

C.3 Blue-OD1-P0-R3

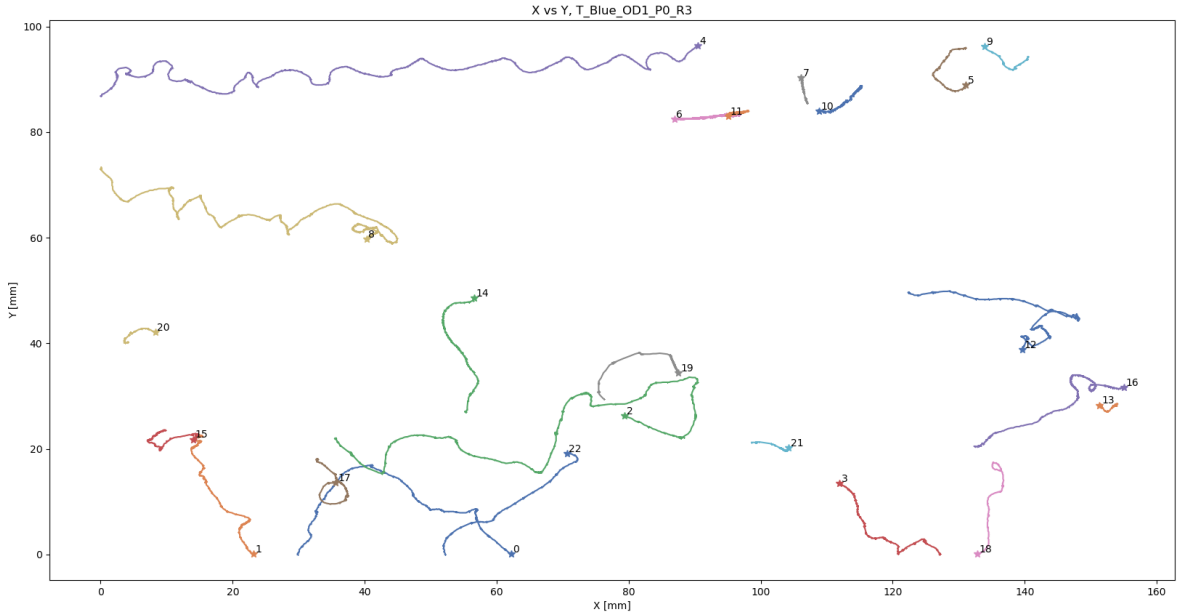

Figure C.17: Tracks found in the two minute long experimental video for Blue-OD1-P0-R3. Stars denote the start of each track.

0: Start: 25.65s, Arc length: 84.18mm, Avg speed: 1.11mm/s, Max speed: 24.73mm/s
1: Start: 71.54s, Arc length: 84.75mm, Avg speed: 1.61mm/s, Max speed: 25.44mm/s
2: Start: 29.41s, Arc length: 215.13mm, Avg speed: 1.76mm/s, Max speed: 51.80mm/s
3: Start: 29.93s, Arc length: 152.83mm, Avg speed: 1.33mm/s, Max speed: 23.71mm/s
4: Start: 51.24s, Arc length: 194.35mm, Avg speed: 2.63mm/s, Max speed: 35.86mm/s
5: Start: 29.93s, Arc length: 127.40mm, Avg speed: 1.11mm/s, Max speed: 19.46mm/s
6: Start: 0.00s, Arc length: 285.26mm, Avg speed: 1.78mm/s, Max speed: 13.82mm/s
7: Start: 6.55s, Arc length: 20.47mm, Avg speed: 0.26mm/s, Max speed: 20.94mm/s
8: Start: 0.00s, Arc length: 194.59mm, Avg speed: 1.35mm/s, Max speed: 32.20mm/s
9: Start: 104.73s, Arc length: 41.96mm, Avg speed: 1.92mm/s, Max speed: 20.35mm/s
10: Start: 50.54s, Arc length: 125.30mm, Avg speed: 1.46mm/s, Max speed: 17.32mm/s
11: Start: 78.74s, Arc length: 183.64mm, Avg speed: 2.44mm/s, Max speed: 15.71mm/s
12: Start: 0.00s, Arc length: 203.81mm, Avg speed: 1.44mm/s, Max speed: 51.85mm/s
13: Start: 22.84s, Arc length: 157.59mm, Avg speed: 0.79mm/s, Max speed: 12.46mm/s
14: Start: 29.93s, Arc length: 135.97mm, Avg speed: 1.15mm/s, Max speed: 20.15mm/s
15: Start: 101.61s, Arc length: 41.47mm, Avg speed: 1.60mm/s, Max speed: 29.02mm/s
16: Start: 29.93s, Arc length: 170.51mm, Avg speed: 1.13mm/s, Max speed: 38.86mm/s
17: Start: 29.93s, Arc length: 126.31mm, Avg speed: 0.93mm/s, Max speed: 26.35mm/s
18: Start: 114.55s, Arc length: 33.34mm, Avg speed: 4.33mm/s, Max speed: 32.93mm/s
19: Start: 0.00s, Arc length: 55.03mm, Avg speed: 0.50mm/s, Max speed: 56.20mm/s
20: Start: 29.93s, Arc length: 155.83mm, Avg speed: 1.32mm/s, Max speed: 15.72mm/s
21: Start: 0.00s, Arc length: 42.65mm, Avg speed: 0.32mm/s, Max speed: 23.07mm/s
22: Start: 0.00s, Arc length: 42.61mm, Avg speed: 0.57mm/s, Max speed: 26.78mm/s

Figure C.18: Information corresponding to tracks for Blue-OD1-P0-R3. Start time indicates when the track was first registered.

Total speed, Blue-OD1-P0-R3

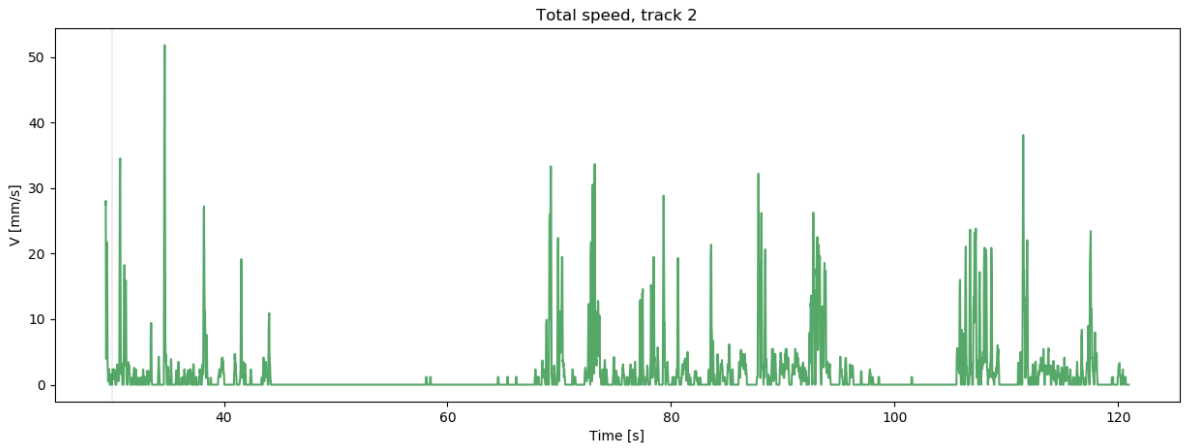

Figure C.19: Speed profile of track 2 in Blue-OD1-P0-R3. The light was turned on after 30 s.

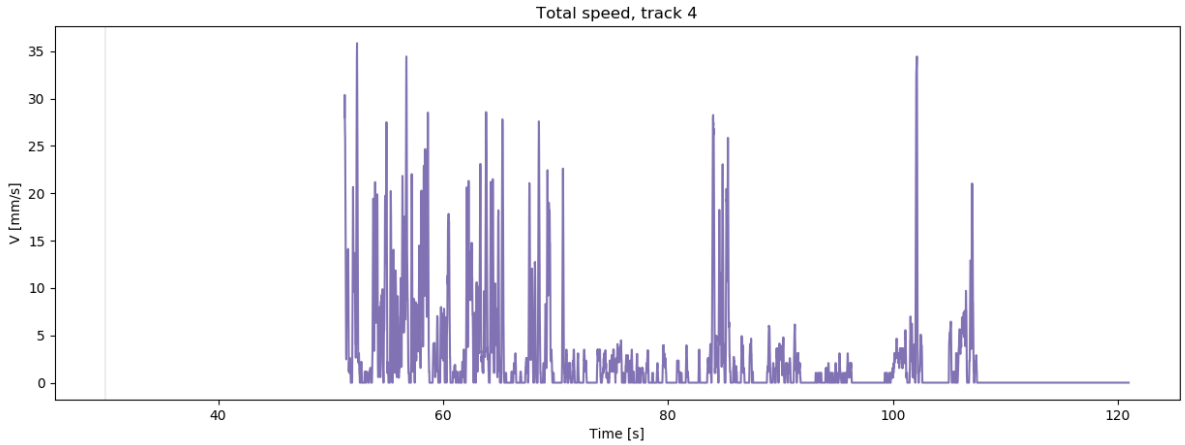

Figure C.20: Speed profile of track 4 in Blue-OD1-P0-R3. The light was turned on after 30 s.

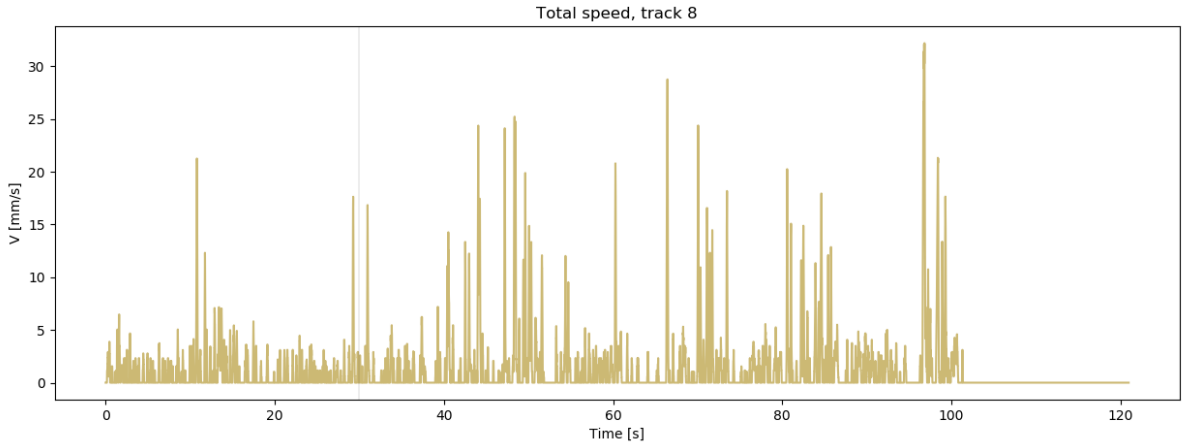

Figure C.21: Speed profile of track 8 in Blue-OD1-P0-R3. The light was turned on after 30 s.

Velocity in x-direction, Blue-OD1-P0-R3

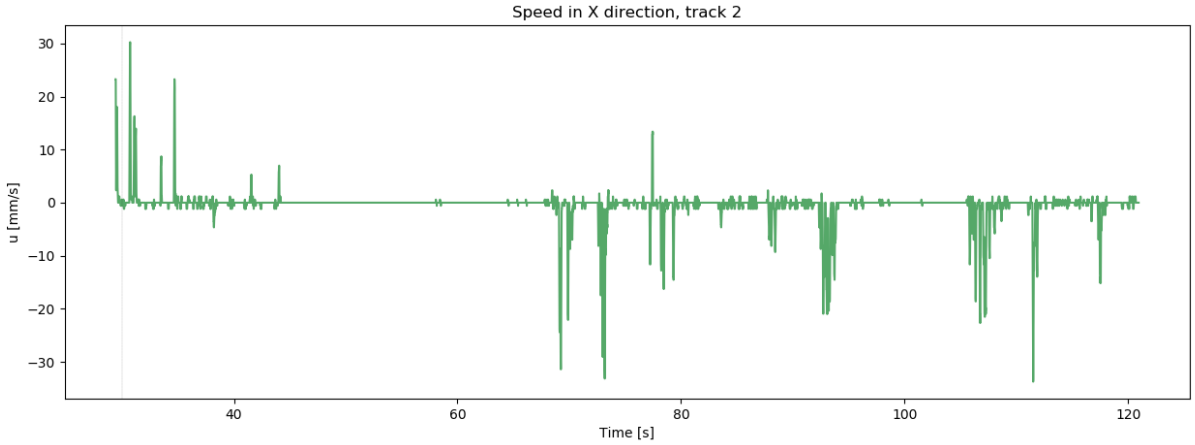

Figure C.22: Velocity profile for track 2 in Blue-OD1-P0-R3. The light was turned on after 30 s.

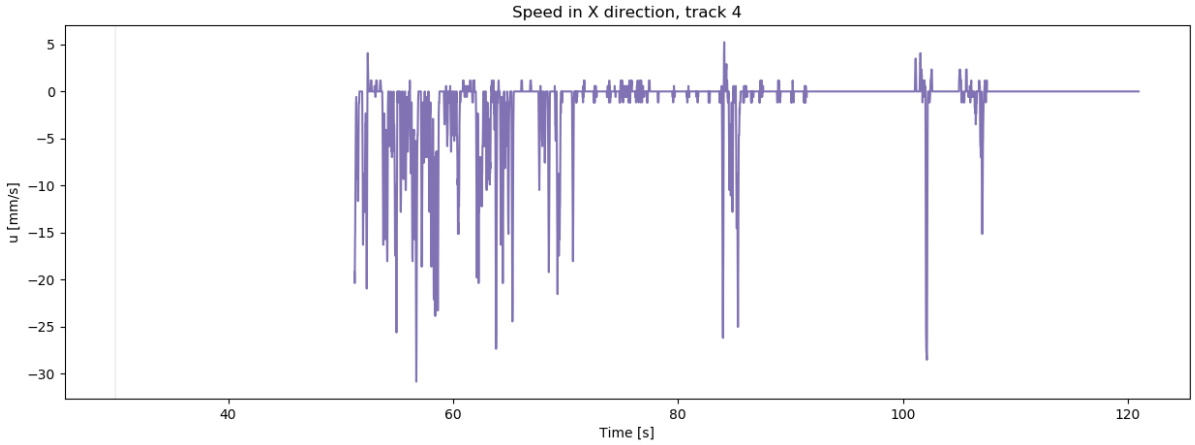

Figure C.23: Velocity profile for track 4 in Blue-OD1-P0-R3. The light was turned on after 30 s.

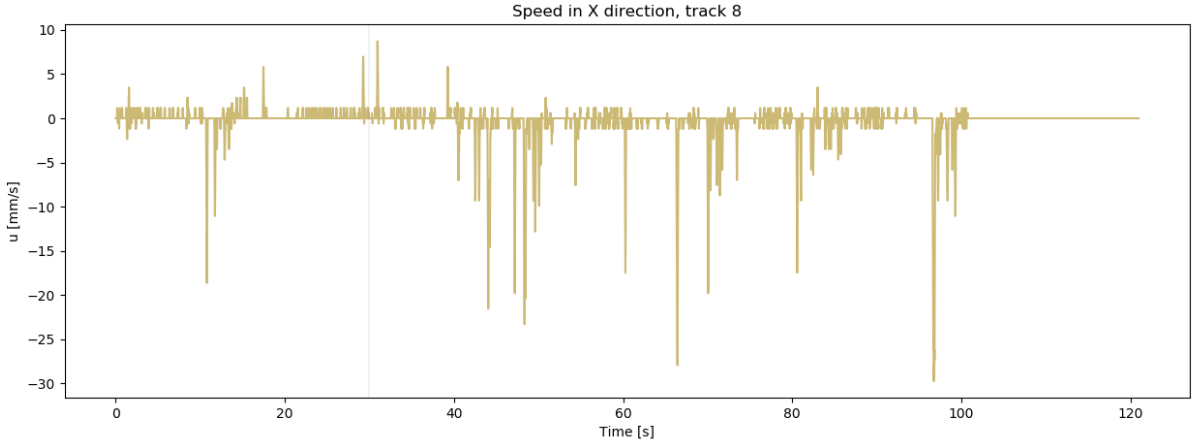

Figure C.24: Velocity profile for track 8 in Blue-OD1-P0-R3. The light was turned on after 30 s.

C.4 Green-OD1-P2-R1

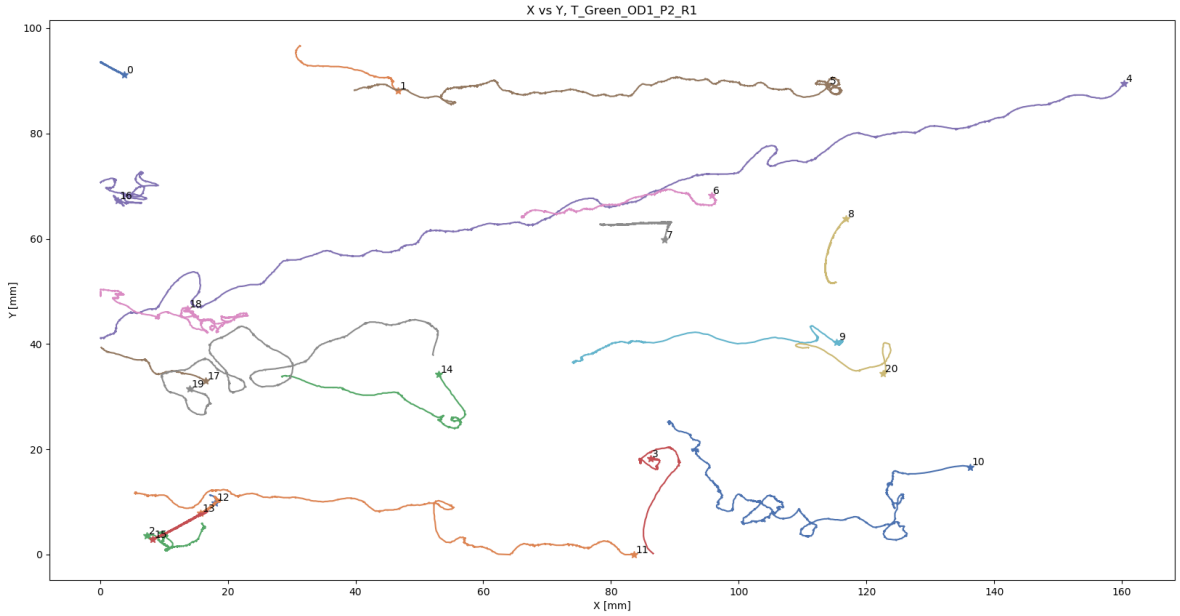

Figure C.25: Tracks found in the two minute long experimental video for Green-OD1-P2-R1. Stars denote the start of each track.

0: Start: 0.00s, Arc length: 49.69mm, Avg speed: 0.44mm/s, Max speed: 6.63mm/s
1: Start: 0.00s, Arc length: 117.76mm, Avg speed: 1.14mm/s, Max speed: 39.81mm/s
2: Start: 0.09s, Arc length: 197.00mm, Avg speed: 1.56mm/s, Max speed: 44.52mm/s
3: Start: 0.00s, Arc length: 91.56mm, Avg speed: 0.84mm/s, Max speed: 79.77mm/s
4: Start: 36.59s, Arc length: 315.08mm, Avg speed: 3.27mm/s, Max speed: 60.92mm/s
5: Start: 0.00s, Arc length: 317.94mm, Avg speed: 1.88mm/s, Max speed: 44.82mm/s
6: Start: 0.00s, Arc length: 272.72mm, Avg speed: 1.61mm/s, Max speed: 22.42mm/s
7: Start: 1.06s, Arc length: 266.92mm, Avg speed: 1.70mm/s, Max speed: 19.47mm/s
8: Start: 13.80s, Arc length: 42.38mm, Avg speed: 0.30mm/s, Max speed: 11.61mm/s
9: Start: 87.75s, Arc length: 90.94mm, Avg speed: 2.17mm/s, Max speed: 99.20mm/s
10: Start: 0.00s, Arc length: 352.62mm, Avg speed: 2.43mm/s, Max speed: 88.83mm/s
11: Start: 56.61s, Arc length: 194.36mm, Avg speed: 2.47mm/s, Max speed: 74.88mm/s
12: Start: 90.40s, Arc length: 85.27mm, Avg speed: 1.89mm/s, Max speed: 11.39mm/s
13: Start: 67.03s, Arc length: 138.37mm, Avg speed: 2.05mm/s, Max speed: 18.51mm/s
14: Start: 37.20s, Arc length: 68.80mm, Avg speed: 1.16mm/s, Max speed: 74.69mm/s
15: Start: 22.84s, Arc length: 216.28mm, Avg speed: 1.75mm/s, Max speed: 23.85mm/s
16: Start: 0.08s, Arc length: 92.69mm, Avg speed: 1.02mm/s, Max speed: 30.05mm/s
17: Start: 51.62s, Arc length: 52.89mm, Avg speed: 0.79mm/s, Max speed: 36.02mm/s
18: Start: 0.00s, Arc length: 157.30mm, Avg speed: 1.34mm/s, Max speed: 27.51mm/s
19: Start: 0.00s, Arc length: 172.77mm, Avg speed: 1.81mm/s, Max speed: 47.74mm/s
20: Start: 0.00s, Arc length: 265.76mm, Avg speed: 0.96mm/s, Max speed: 94.19mm/s

Figure C.26: Information corresponding to tracks for Green-OD1-P2-R1. Start time indicates when the track was first registered.

Total speed, Green-OD1-P2-R1

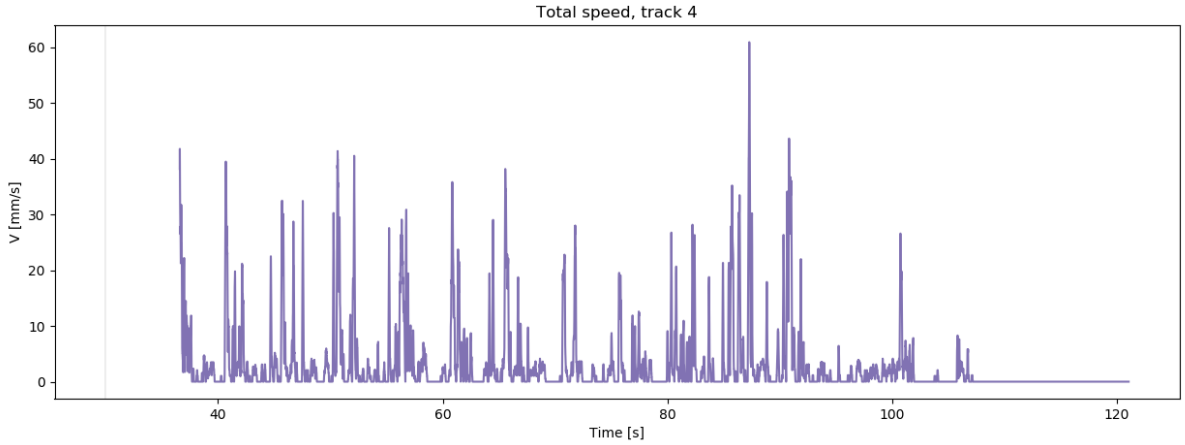

Figure C.27: Speed profile of track 4 in Green-OD1-P2-R1. The light was turned on after 30 s.

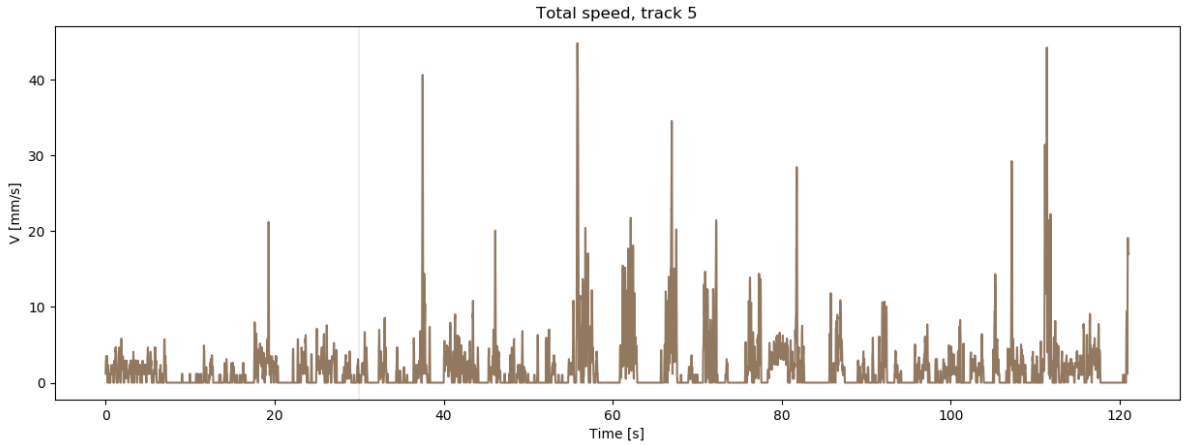

Figure C.28: Speed profile of track 5 in Green-OD1-P2-R1. The light was turned on after 30 s.

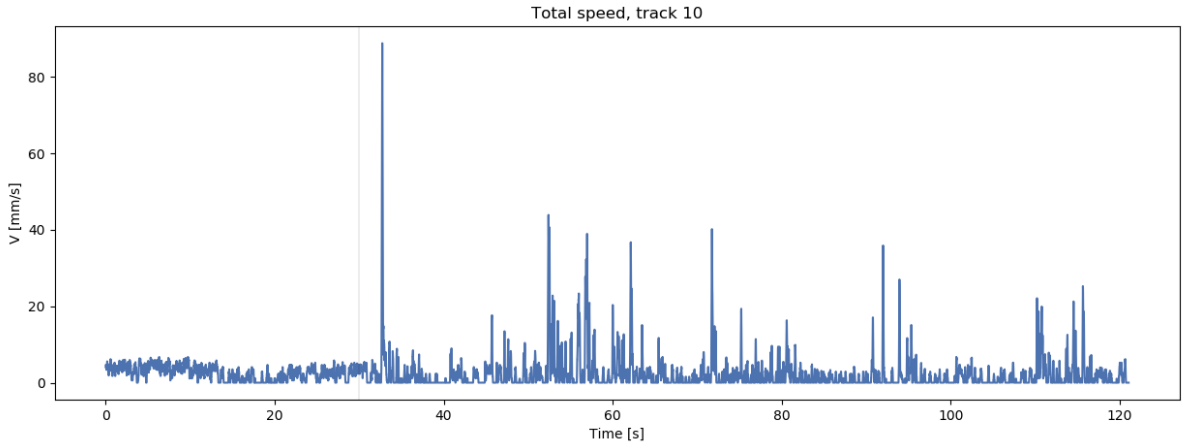

Figure C.29: Speed profile of track 10 in Green-OD1-P2-R1. The light was turned on after 30 s.

Velocity in x-direction, Green-OD1-P2-R1

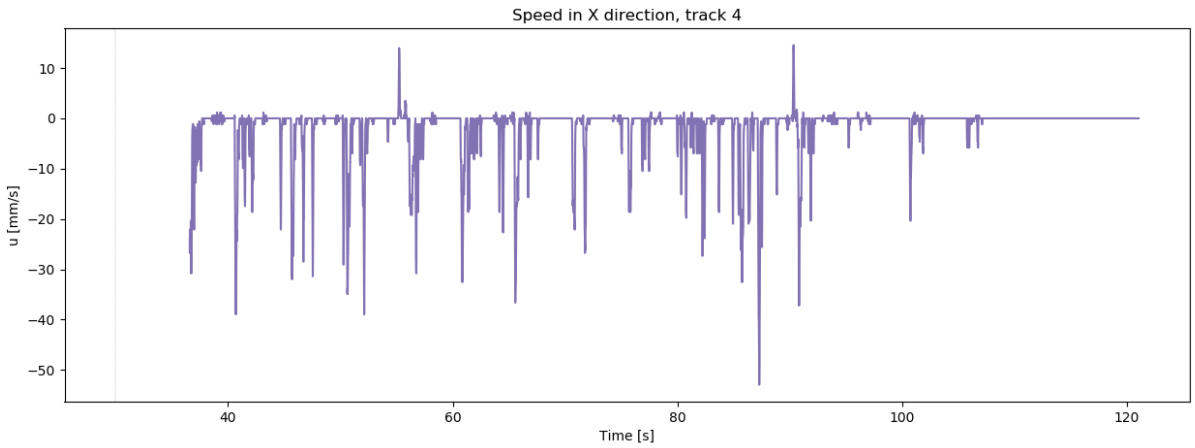

Figure C.30: Velocity profile for track 4 in Green-OD1-P2-R1. The light was turned on after 30 s.

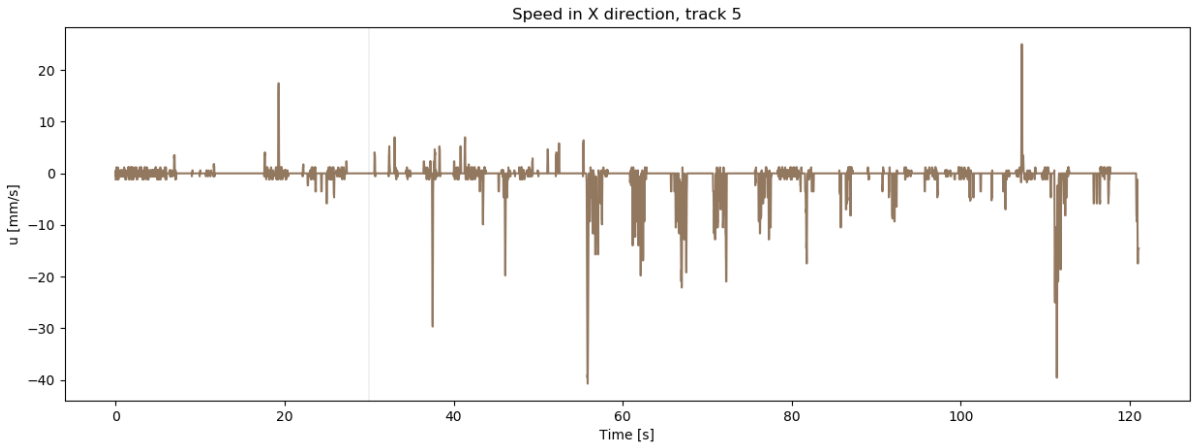

Figure C.31: Velocity profile for track 5 in Green-OD1-P2-R1. The light was turned on after 30 s.

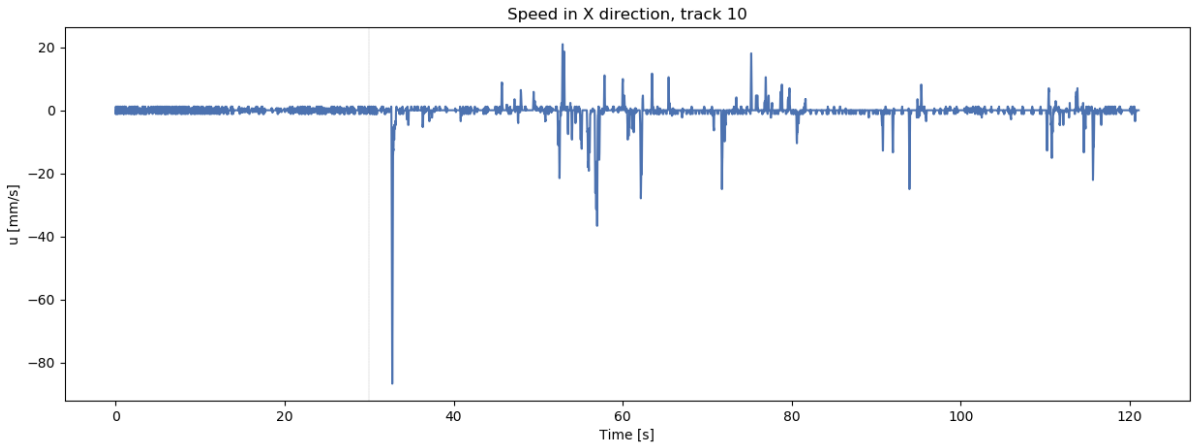

Figure C.32: Velocity profile for track 10 in Green-OD1-P2-R1. The light was turned on after 30 s.

C.5 Green-OD1-P2-R2

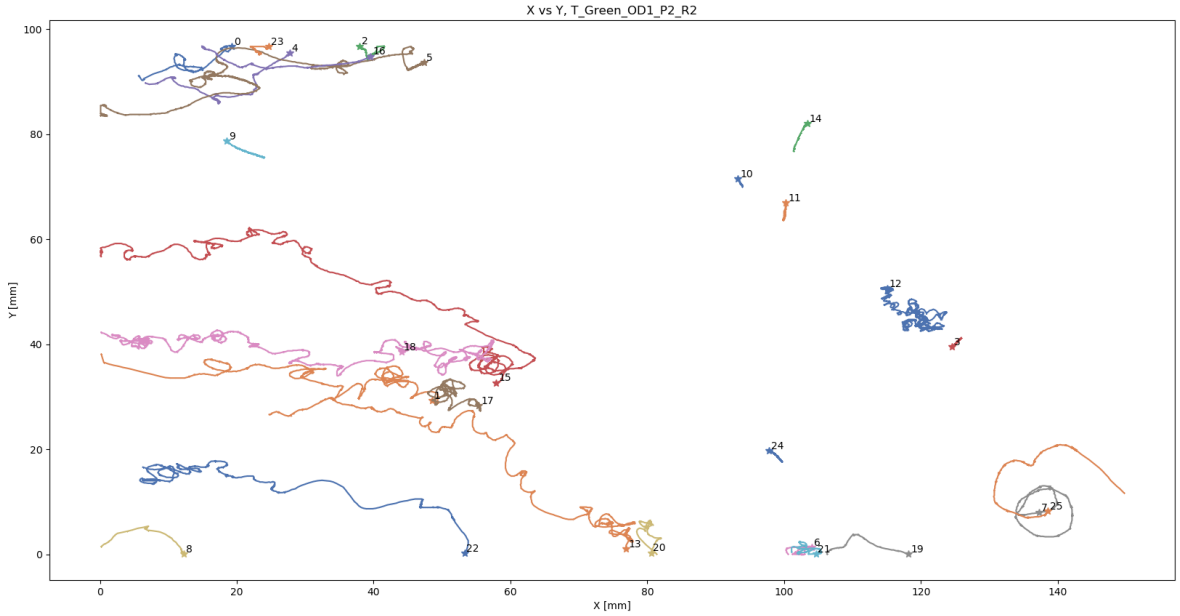

Figure C.33: Tracks found in the two minute long experimental video for Green-OD1-P2-R2. Stars denote the start of each track.

0: Start: 50.65s, Arc length: 47.96mm, Avg speed: 0.96mm/s, Max speed: 48.42mm/s
1: Start: 8.07s, Arc length: 164.57mm, Avg speed: 2.09mm/s, Max speed: 101.80mm/s
2: Start: 48.20s, Arc length: 16.77mm, Avg speed: 0.36mm/s, Max speed: 19.52mm/s
3: Start: 0.05s, Arc length: 11.13mm, Avg speed: 0.09mm/s, Max speed: 4.65mm/s
4: Start: 77.11s, Arc length: 47.42mm, Avg speed: 1.36mm/s, Max speed: 28.89mm/s
5: Start: 0.00s, Arc length: 219.52mm, Avg speed: 1.65mm/s, Max speed: 61.53mm/s
6: Start: 0.00s, Arc length: 58.31mm, Avg speed: 0.59mm/s, Max speed: 37.91mm/s
7: Start: 0.00s, Arc length: 65.24mm, Avg speed: 0.78mm/s, Max speed: 41.32mm/s
8: Start: 64.02s, Arc length: 17.59mm, Avg speed: 0.55mm/s, Max speed: 49.06mm/s
9: Start: 0.81s, Arc length: 67.56mm, Avg speed: 0.37mm/s, Max speed: 5.50mm/s
10: Start: 112.53s, Arc length: 13.59mm, Avg speed: 1.01mm/s, Max speed: 5.05mm/s
11: Start: 104.45s, Arc length: 18.08mm, Avg speed: 1.21mm/s, Max speed: 5.11mm/s
12: Start: 0.00s, Arc length: 295.01mm, Avg speed: 1.78mm/s, Max speed: 46.15mm/s
13: Start: 77.11s, Arc length: 188.40mm, Avg speed: 3.80mm/s, Max speed: 59.03mm/s
14: Start: 7.63s, Arc length: 10.64mm, Avg speed: 0.14mm/s, Max speed: 13.45mm/s
15: Start: 0.44s, Arc length: 253.88mm, Avg speed: 2.32mm/s, Max speed: 64.34mm/s
16: Start: 77.11s, Arc length: 38.80mm, Avg speed: 1.29mm/s, Max speed: 28.86mm/s
17: Start: 0.00s, Arc length: 83.19mm, Avg speed: 1.10mm/s, Max speed: 35.08mm/s
18: Start: 0.00s, Arc length: 304.41mm, Avg speed: 2.45mm/s, Max speed: 37.59mm/s
19: Start: 44.51s, Arc length: 17.73mm, Avg speed: 0.40mm/s, Max speed: 34.94mm/s
20: Start: 68.14s, Arc length: 26.94mm, Avg speed: 0.80mm/s, Max speed: 65.49mm/s
21: Start: 35.01s, Arc length: 48.67mm, Avg speed: 0.80mm/s, Max speed: 55.47mm/s
22: Start: 34.94s, Arc length: 152.29mm, Avg speed: 2.06mm/s, Max speed: 77.61mm/s
23: Start: 43.30s, Arc length: 10.13mm, Avg speed: 0.22mm/s, Max speed: 25.63mm/s
24: Start: 0.00s, Arc length: 76.46mm, Avg speed: 0.54mm/s, Max speed: 5.45mm/s
25: Start: 0.11s, Arc length: 66.07mm, Avg speed: 0.78mm/s, Max speed: 93.53mm/s

Figure C.34: Information corresponding to tracks for Green-OD1-P2-R2. Start time indicates when the track was first registered.

Total speed, Green-OD1-P2-R2

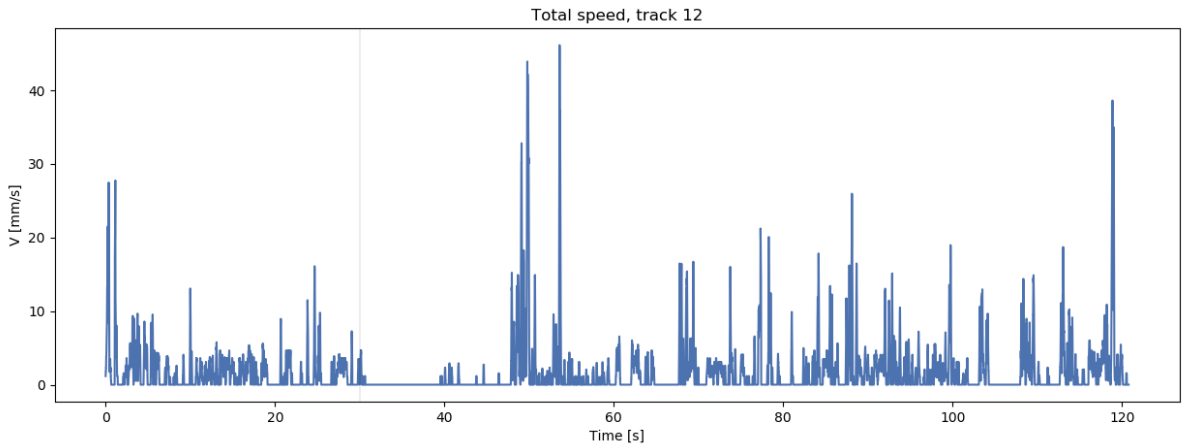

Figure C.35: Speed profile of track 12 in Green-OD1-P2-R2. The light was turned on after 30 s.

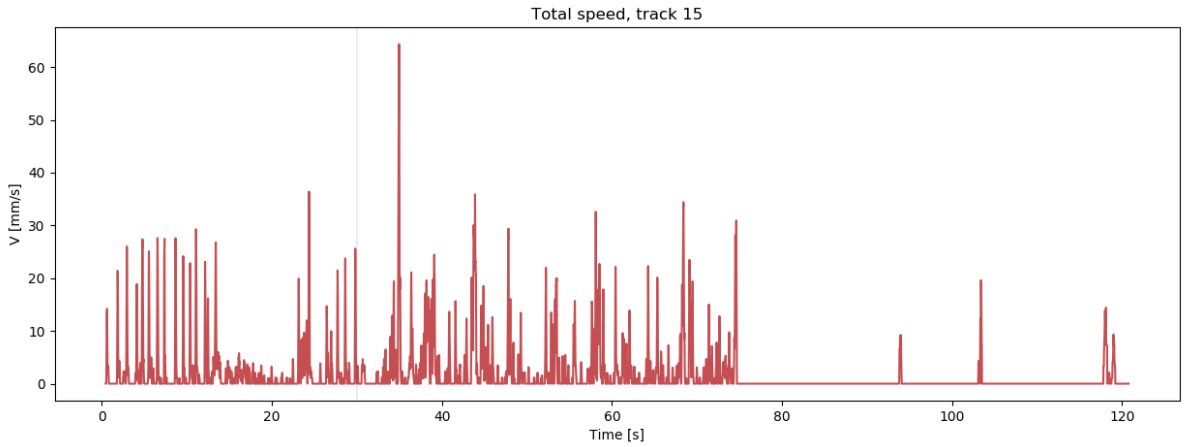

Figure C.36: Speed profile of track 15 in Green-OD1-P2-R2. The light was turned on after 30 s.

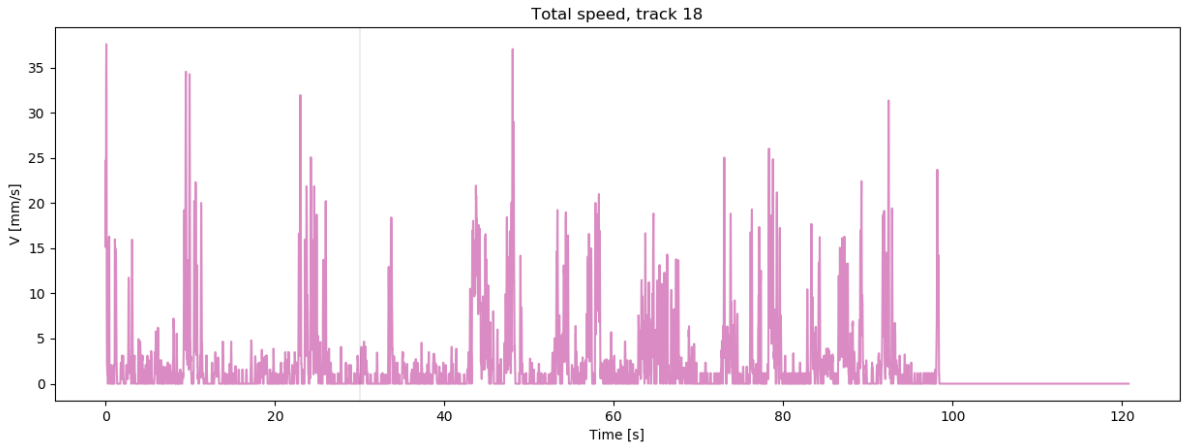

Figure C.37: Speed profile of track 18 in Green-OD1-P2-R2. The light was turned on after 30 s.

Velocity in x-direction. Green-OD1-P2-R2

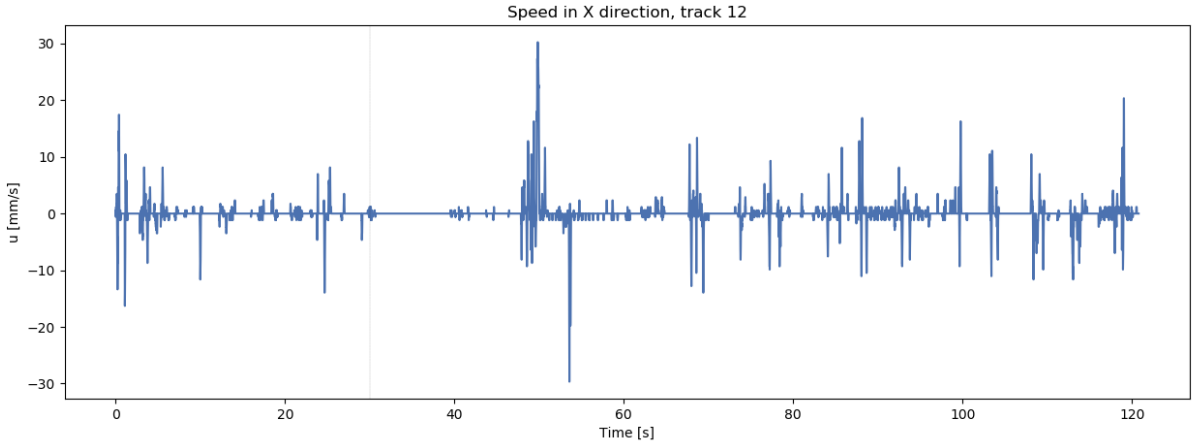

Figure C.38: Velocity profile for track 12 in Green-OD1-P2-R2. The light was turned on after 30 s.

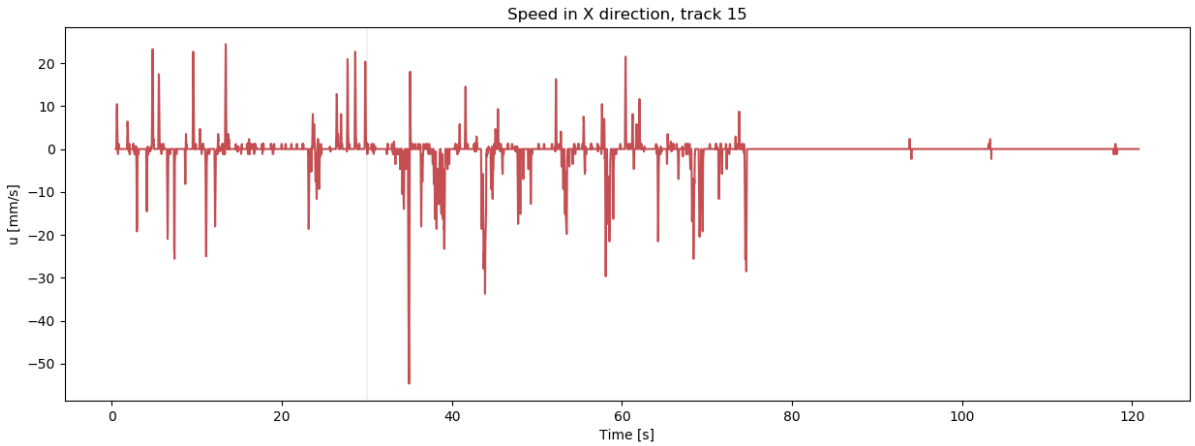

Figure C.39: Velocity profile for track 15 in Green-OD1-P2-R2. The light was turned on after 30 s.

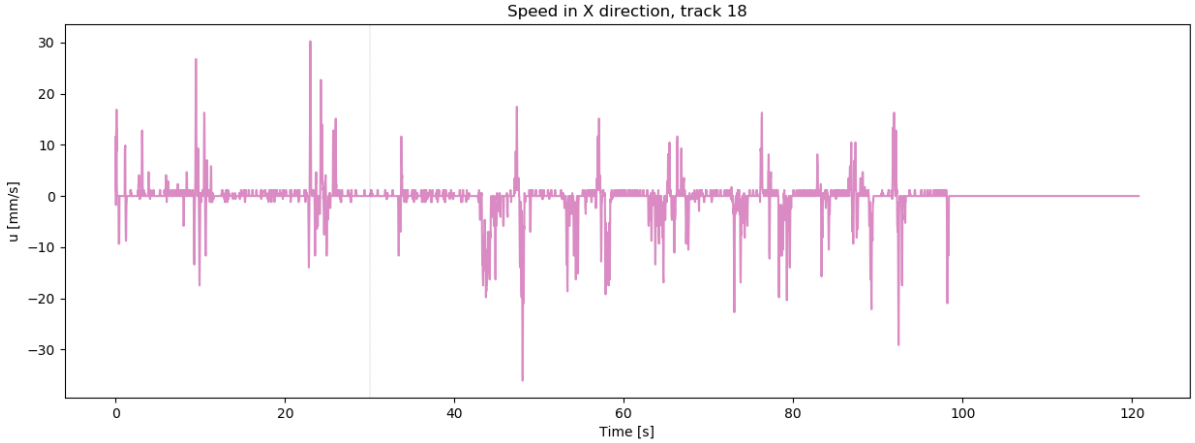

Figure C.40: Velocity profile for track 18 in Green-OD1-P2-R2. The light was turned on after 30 s.

C.6 Green-OD1-P2-R3

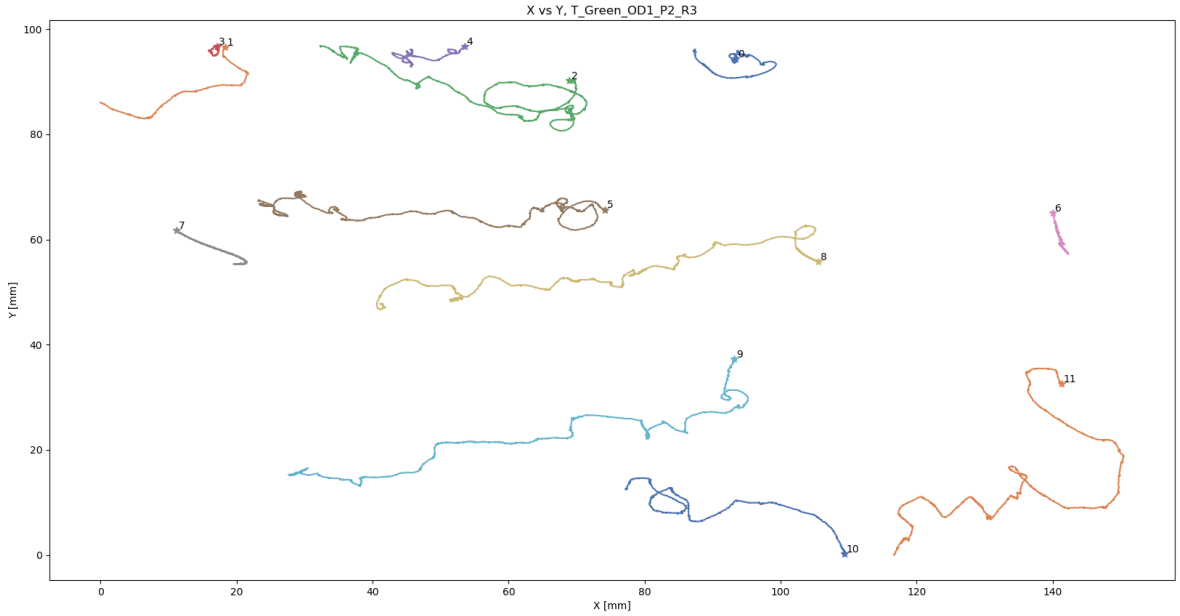

Figure C.41: Tracks found in the two minute long experimental video for Green-OD1-P2-R3. Stars denote the start of each track.

0: Start: 0.00s, Arc length: 98.37mm, Avg speed: 0.83mm/s, Max speed: 62.44mm/s
1: Start: 19.63s, Arc length: 69.04mm, Avg speed: 0.77mm/s, Max speed: 45.06mm/s
2: Start: 0.00s, Arc length: 181.55mm, Avg speed: 1.70mm/s, Max speed: 64.03mm/s
3: Start: 88.17s, Arc length: 13.19mm, Avg speed: 0.50mm/s, Max speed: 9.82mm/s
4: Start: 99.79s, Arc length: 52.85mm, Avg speed: 2.00mm/s, Max speed: 26.38mm/s
5: Start: 0.00s, Arc length: 224.51mm, Avg speed: 1.41mm/s, Max speed: 40.54mm/s
6: Start: 0.46s, Arc length: 156.51mm, Avg speed: 0.95mm/s, Max speed: 12.22mm/s
7: Start: 0.00s, Arc length: 137.97mm, Avg speed: 0.63mm/s, Max speed: 6.23mm/s
8: Start: 0.00s, Arc length: 203.43mm, Avg speed: 1.37mm/s, Max speed: 32.18mm/s
9: Start: 0.00s, Arc length: 259.51mm, Avg speed: 1.71mm/s, Max speed: 60.81mm/s
10: Start: 83.87s, Arc length: 99.95mm, Avg speed: 2.28mm/s, Max speed: 41.95mm/s
11: Start: 0.00s, Arc length: 185.79mm, Avg speed: 1.55mm/s, Max speed: 32.18mm/s

Figure C.42: Information corresponding to tracks for Green-OD1-P2-R3. Start time indicates when the track was first registered.

Total speed, Green-OD1-P2-R3

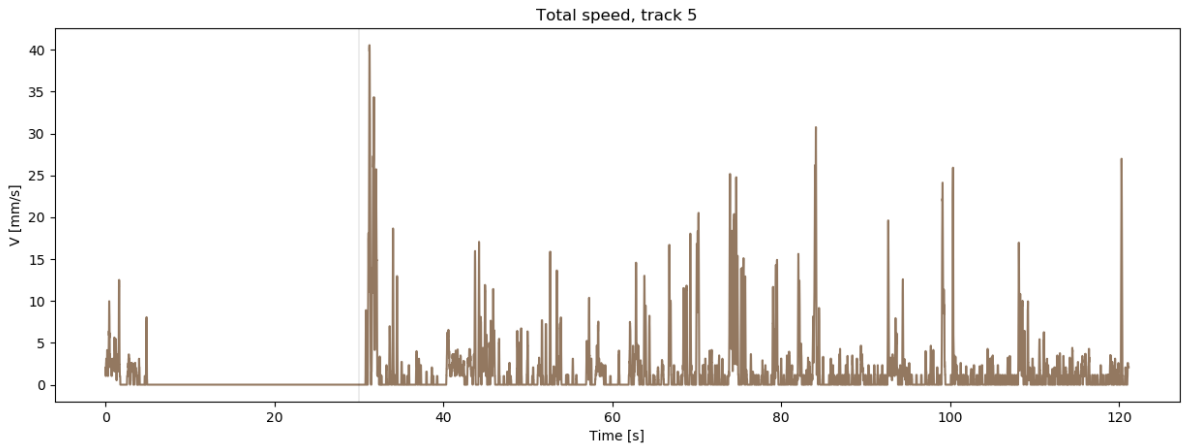

Figure C.43: Speed profile of track 5 in Green-OD1-P2-R3. The light was turned on after 30 s.

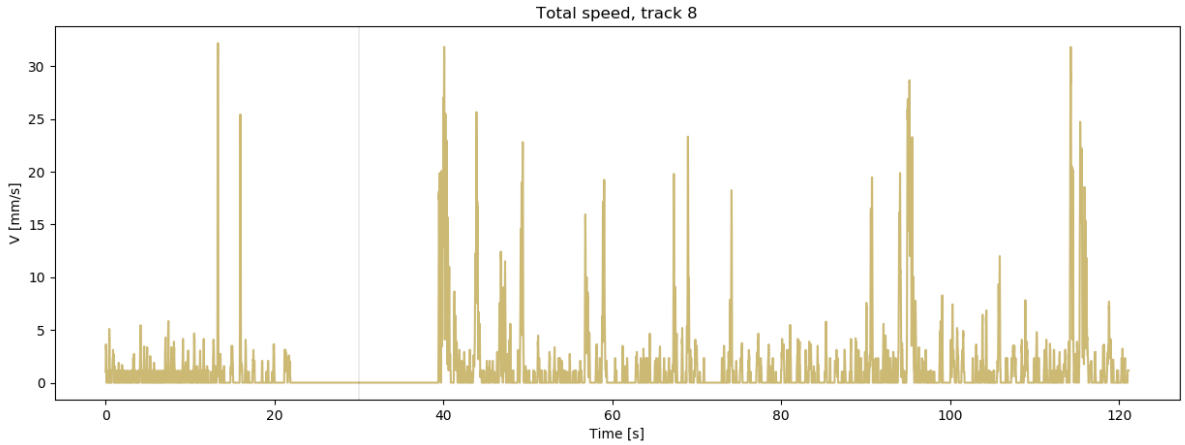

Figure C.44: Speed profile of track 8 in Green-OD1-P2-R3. The light was turned on after 30 s.

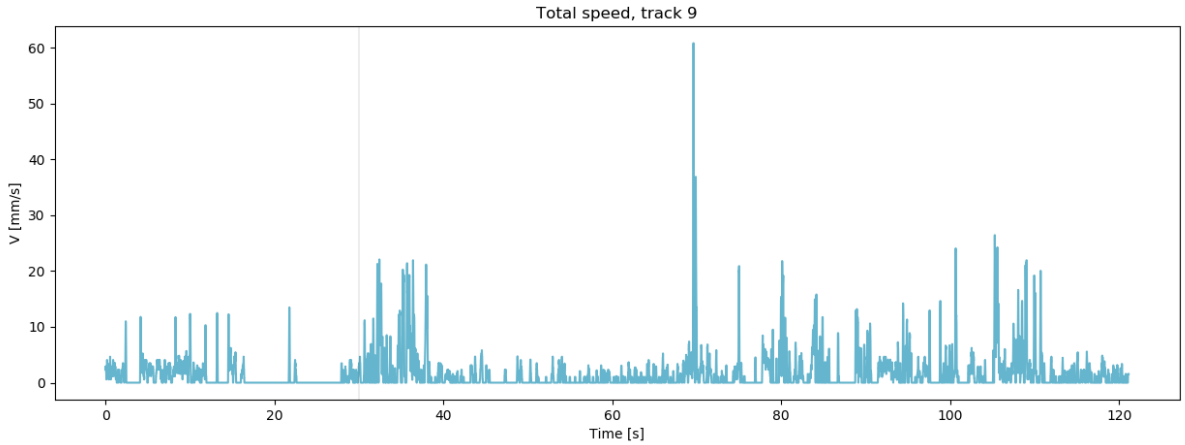

Figure C.45: Speed profile of track 9 in Green-OD1-P2-R3. The light was turned on after 30 s.

Velocity in x-direction, Green-OD1-P2-R3

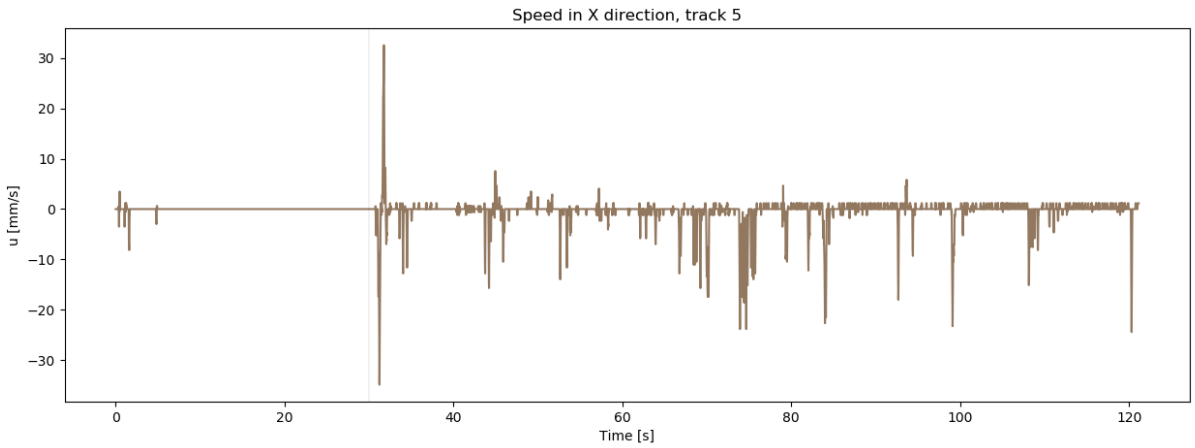

Figure C.46: Velocity profile for track 5 in Green-OD1-P2-R3. The light was turned on after 30 s.

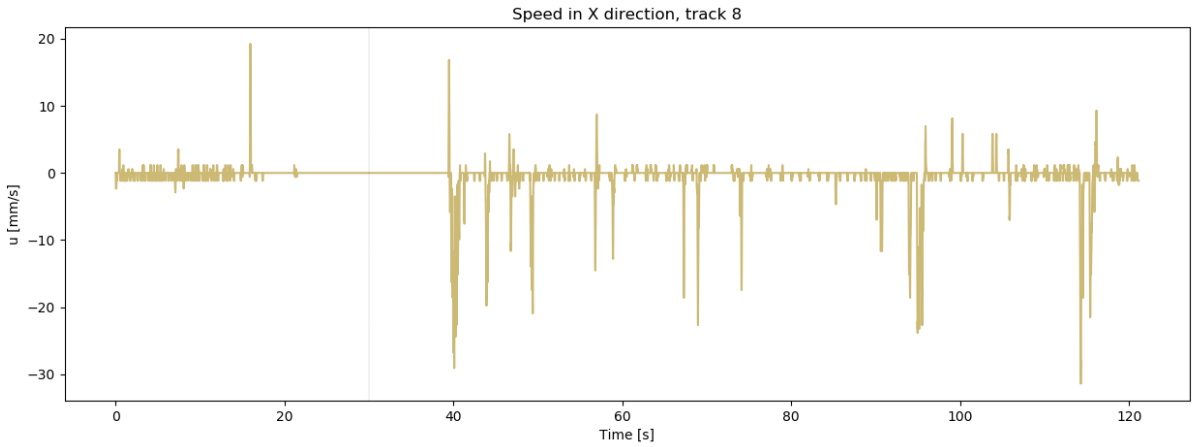

Figure C.47: Velocity profile for track 8 in Green-OD1-P2-R3. The light was turned on after 30 s.

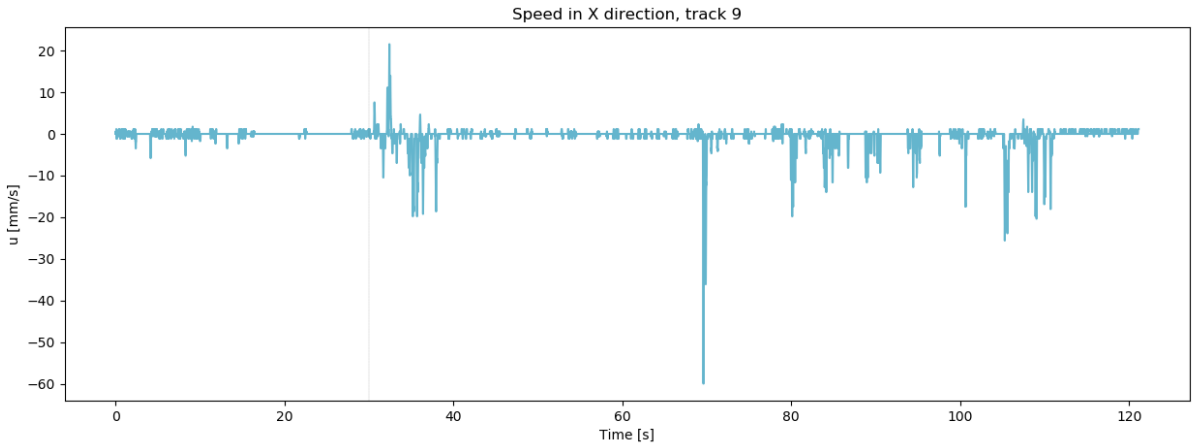

Figure C.48: Velocity profile for track 9 in Green-OD1-P2-R3. The light was turned on after 30 s.

C.7 White-OD1-P3-R1

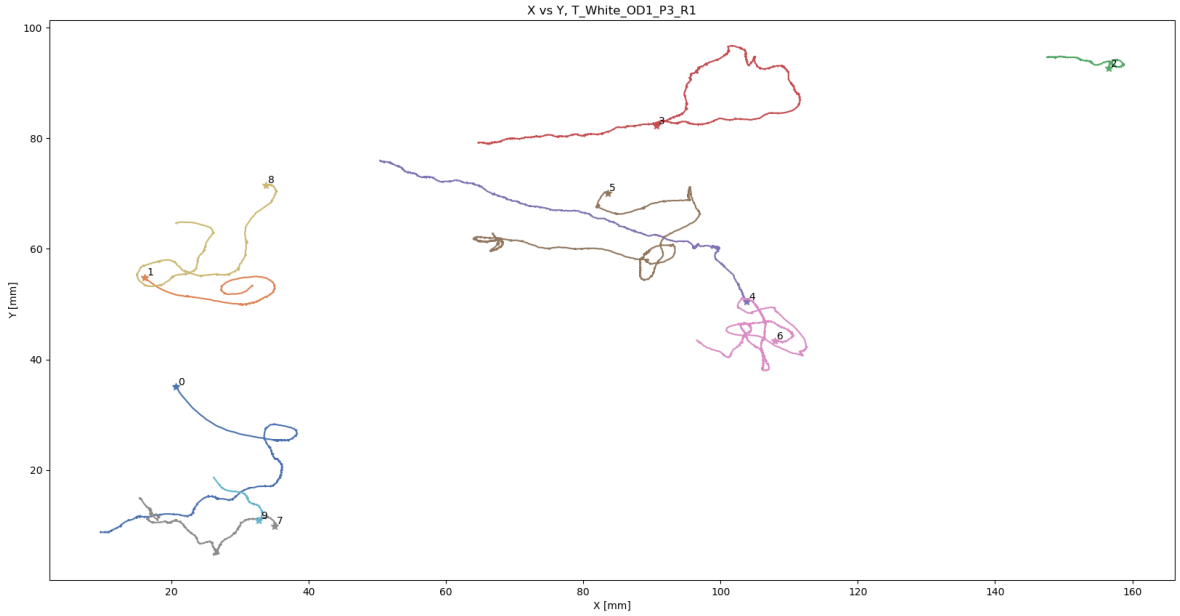

Figure C.49: Tracks found in the two minute long experimental video for White-OD1-P3-R1. Stars denote the start of each track.

0: Start: 35.35s, Arc length: 117.41mm, Avg speed: 1.54mm/s, Max speed: 90.97mm/s
1: Start: 30.28s, Arc length: 42.00mm, Avg speed: 0.75mm/s, Max speed: 80.96mm/s
2: Start: 0.00s, Arc length: 174.83mm, Avg speed: 0.51mm/s, Max speed: 15.33mm/s
3: Start: 0.00s, Arc length: 248.96mm, Avg speed: 1.66mm/s, Max speed: 30.00mm/s
4: Start: 0.00s, Arc length: 244.00mm, Avg speed: 1.26mm/s, Max speed: 43.12mm/s
5: Start: 0.00s, Arc length: 256.44mm, Avg speed: 1.53mm/s, Max speed: 47.27mm/s
6: Start: 0.00s, Arc length: 255.49mm, Avg speed: 1.58mm/s, Max speed: 87.14mm/s
7: Start: 35.05s, Arc length: 161.35mm, Avg speed: 1.17mm/s, Max speed: 21.39mm/s
8: Start: 0.00s, Arc length: 102.87mm, Avg speed: 1.08mm/s, Max speed: 78.41mm/s
9: Start: 0.00s, Arc length: 107.43mm, Avg speed: 0.91mm/s, Max speed: 20.54mm/s

Figure C.50: Information corresponding to tracks for White-OD1-P3-R1. Start time indicates when the track was first registered.

Total speed, White-OD1-P3-R1

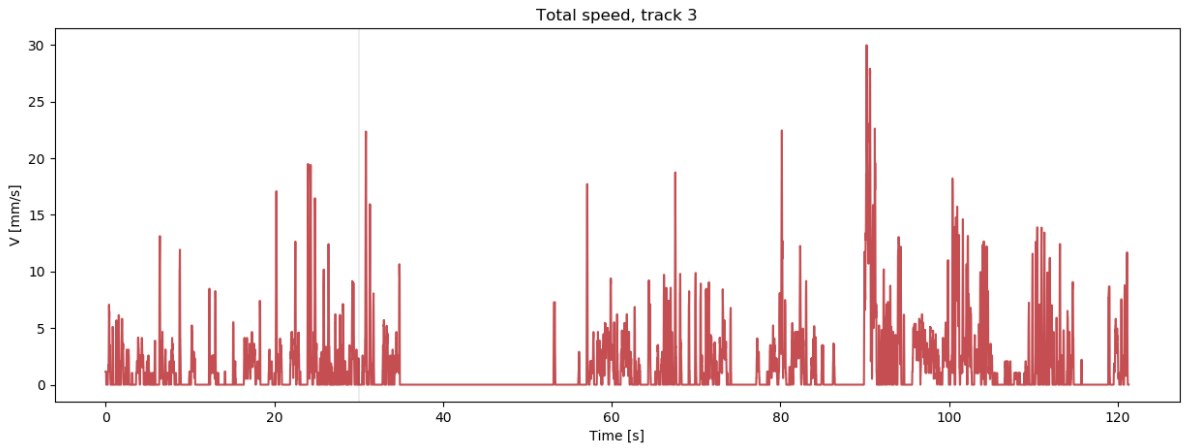

Figure C.51: Speed profile of track 3 in White-OD1-P3-R1. The light was turned on after 30 s.

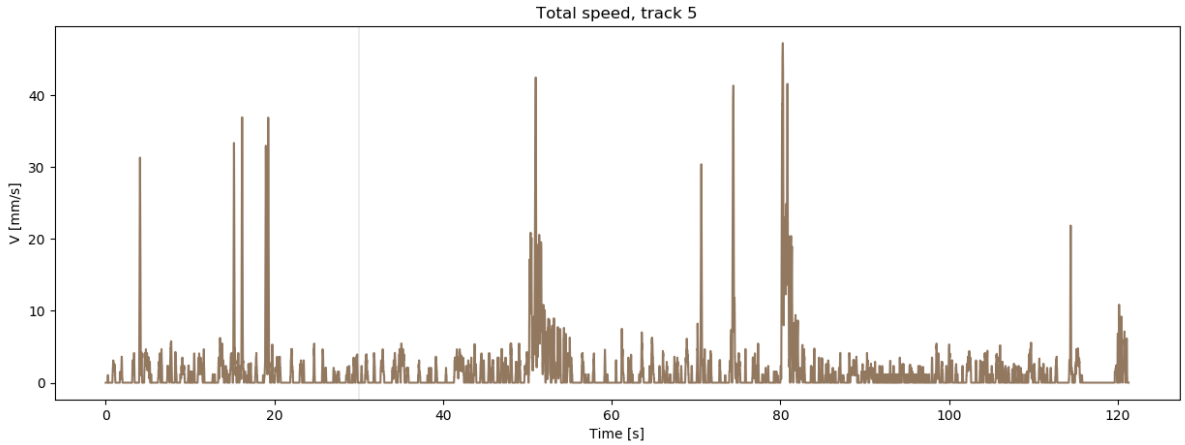

Figure C.52: Speed profile of track 5 in White-OD1-P3-R1. The light was turned on after 30 s.

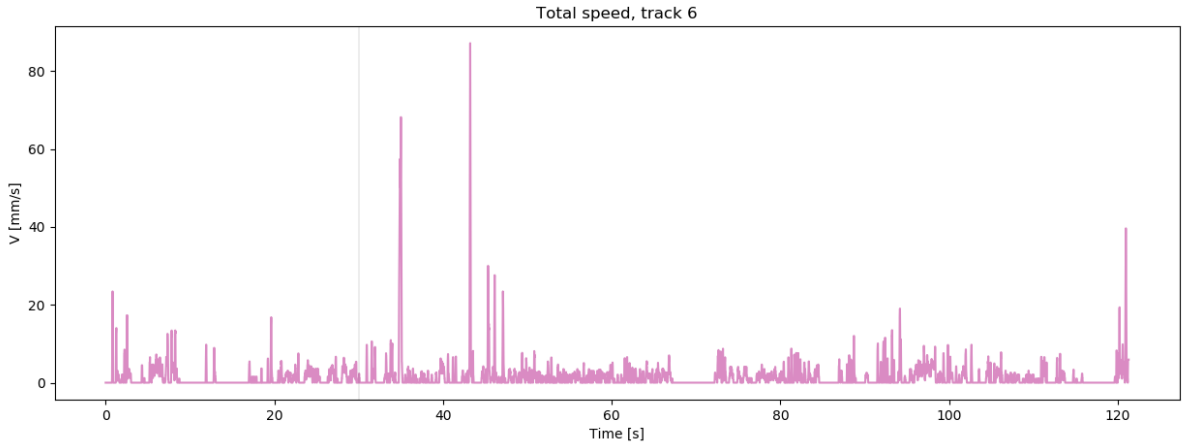

Figure C.53: Speed profile of track 6 in White-OD1-P3-R1. The light was turned on after 30 s.

Velocity in x-direction, White-OD1-P3-R1

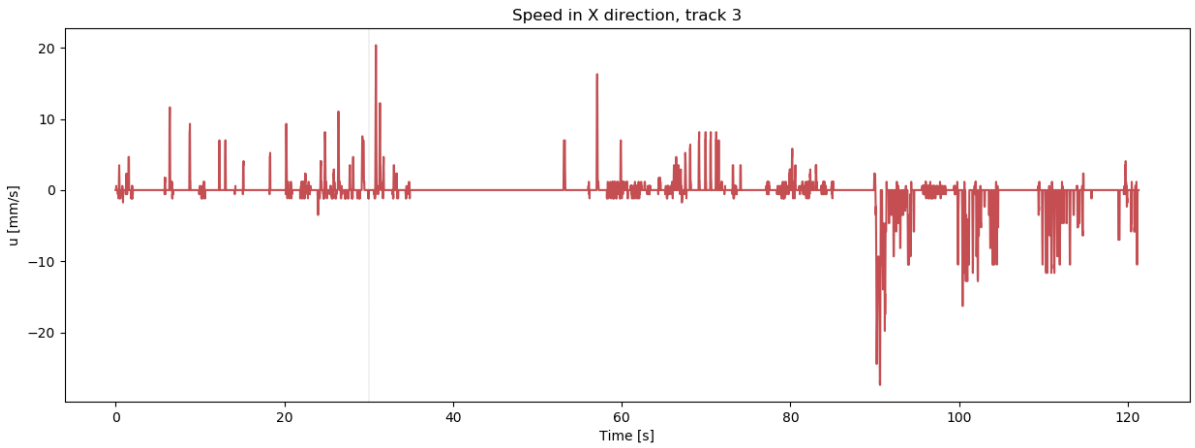

Figure C.54: Velocity profile for track 3 in White-OD1-P3-R1. The light was turned on after 30 s.

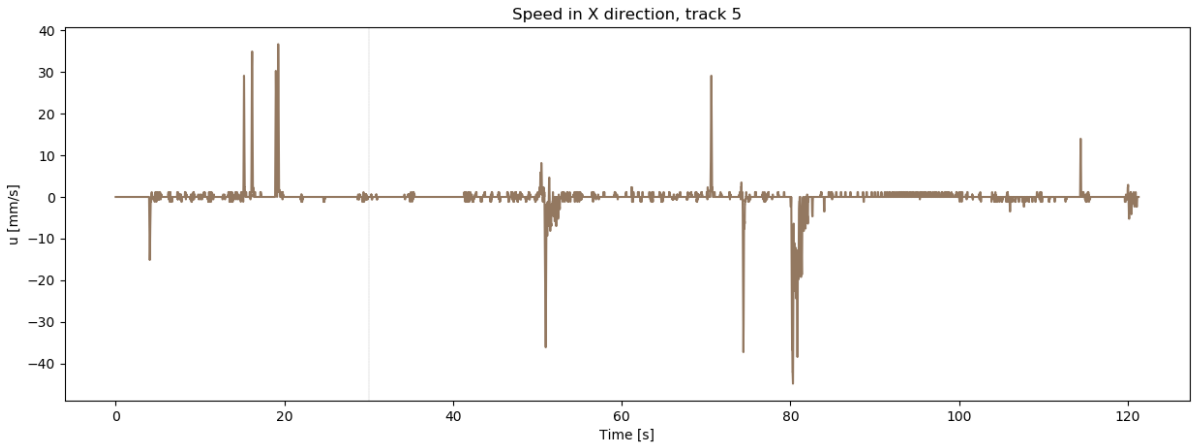

Figure C.55: Velocity profile for track 5 in White-OD1-P3-R1. The light was turned on after 30 s.

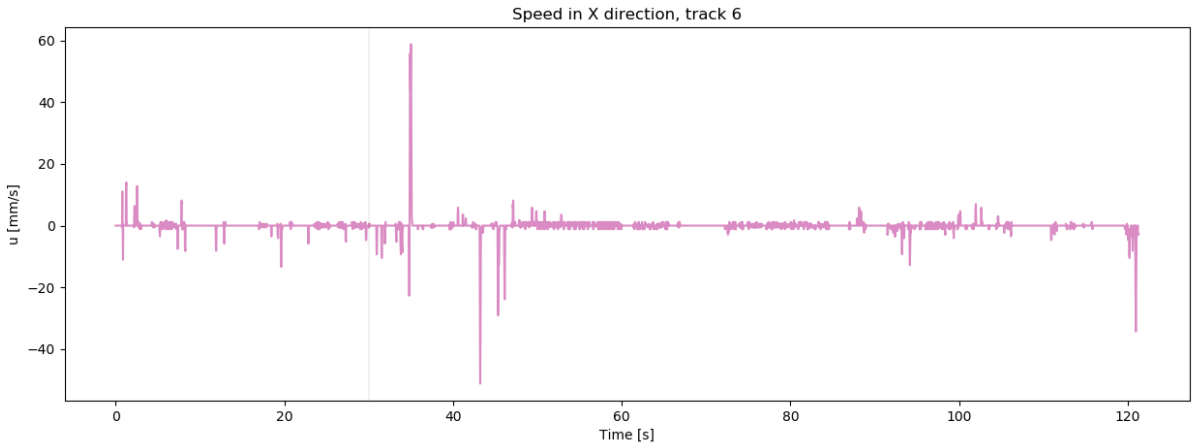

Figure C.56: Velocity profile for track 6 in White-OD1-P3-R1. The light was turned on after 30 s.

C.8 White-OD1-P3-R2

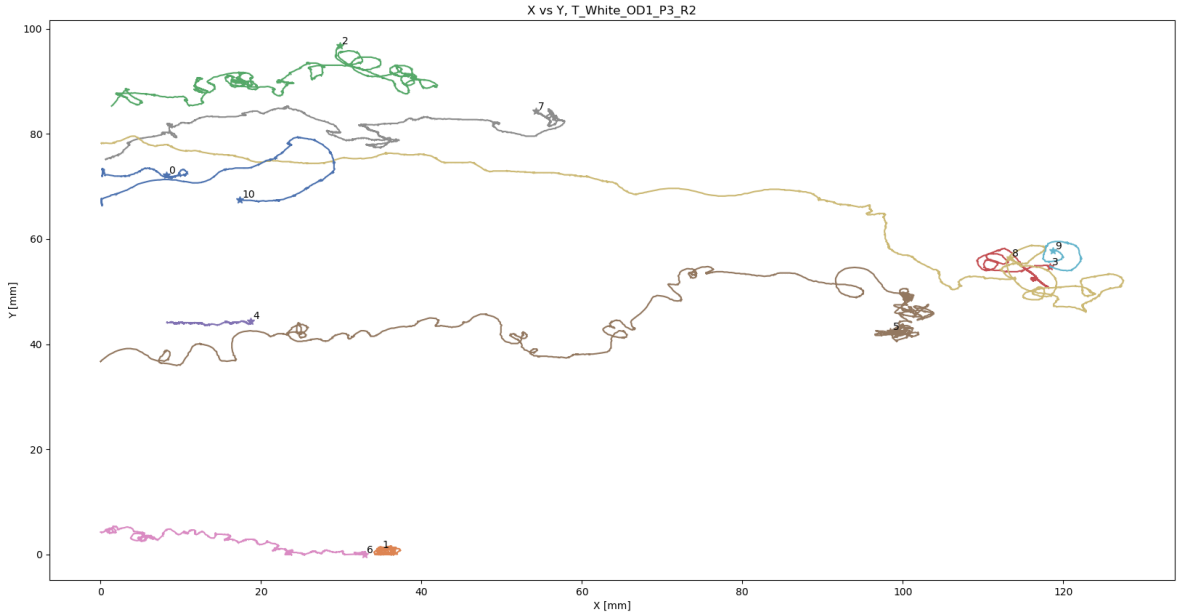

Figure C.57: Tracks found in the two minute long experimental video for White-OD1-P3-R2. Stars denote the start of each track.

0: Start: 0.00s, Arc length: 131.51mm, Avg speed: 1.13mm/s, Max speed: 30.47mm/s
1: Start: 0.00s, Arc length: 84.15mm, Avg speed: 0.82mm/s, Max speed: 24.12mm/s
2: Start: 2.89s, Arc length: 316.51mm, Avg speed: 2.04mm/s, Max speed: 47.53mm/s
3: Start: 6.99s, Arc length: 172.19mm, Avg speed: 1.07mm/s, Max speed: 31.01mm/s
4: Start: 5.89s, Arc length: 98.26mm, Avg speed: 0.82mm/s, Max speed: 15.82mm/s
5: Start: 0.34s, Arc length: 404.69mm, Avg speed: 3.55mm/s, Max speed: 73.06mm/s
6: Start: 34.57s, Arc length: 175.02mm, Avg speed: 1.66mm/s, Max speed: 20.61mm/s
7: Start: 0.00s, Arc length: 228.55mm, Avg speed: 1.50mm/s, Max speed: 35.54mm/s
8: Start: 0.00s, Arc length: 318.82mm, Avg speed: 2.56mm/s, Max speed: 73.17mm/s
9: Start: 0.00s, Arc length: 28.17mm, Avg speed: 0.35mm/s, Max speed: 31.01mm/s
10: Start: 0.05s, Arc length: 102.66mm, Avg speed: 0.90mm/s, Max speed: 53.93mm/s

Figure C.58: Information corresponding to tracks for White-OD1-P3-R2. Start time indicates when the track was first registered.

Total speed, White-OD1-P3-R2

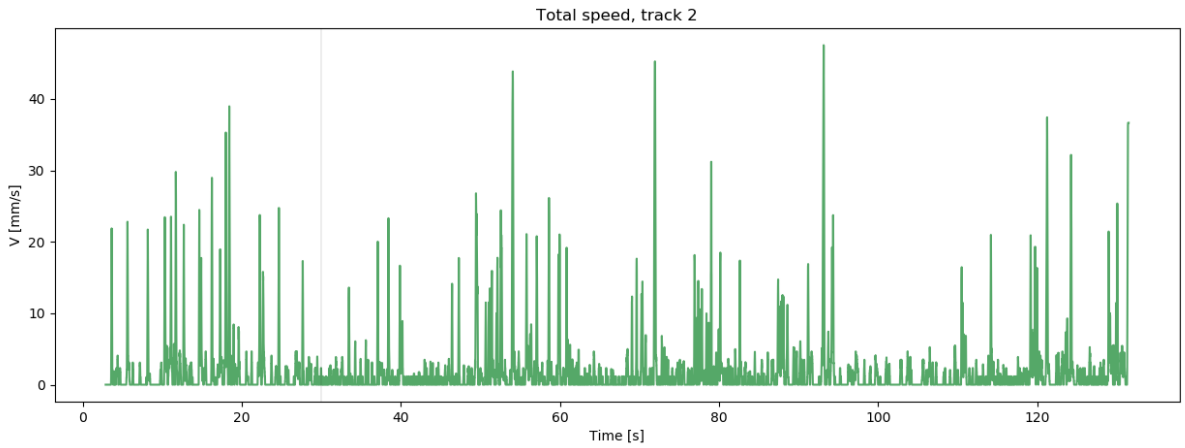

Figure C.59: Speed profile of track 2 in White-OD1-P3-R2. The light was turned on after 30 s.

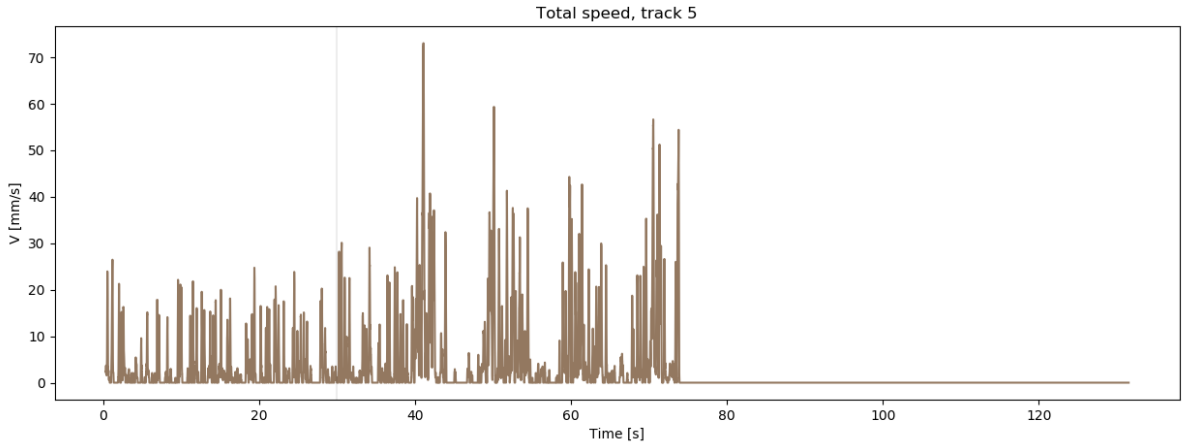

Figure C.60: Speed profile of track 5 in White-OD1-P3-R2. The light was turned on after 30 s.

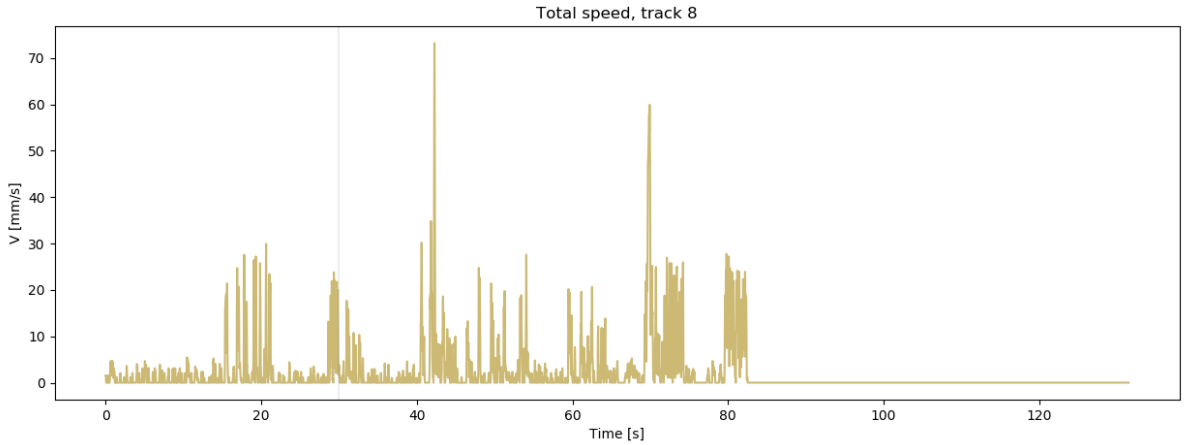

Figure C.61: Speed profile of track 8 in White-OD1-P3-R2. The light was turned on after 30 s.

Velocity in x-direction, White-OD1-P3-R2

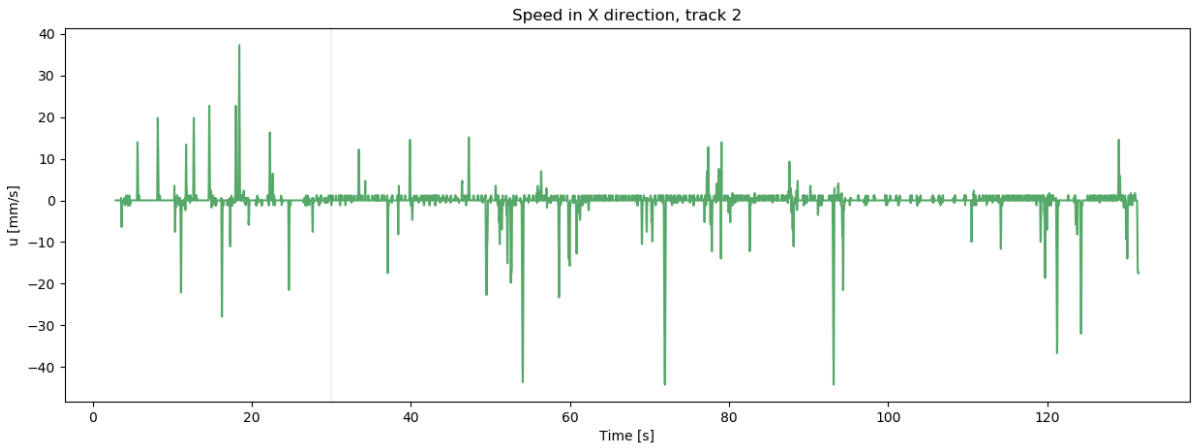

Figure C.62: Velocity profile for track 2 in White-OD1-P3-R2. The light was turned on after 30 s.

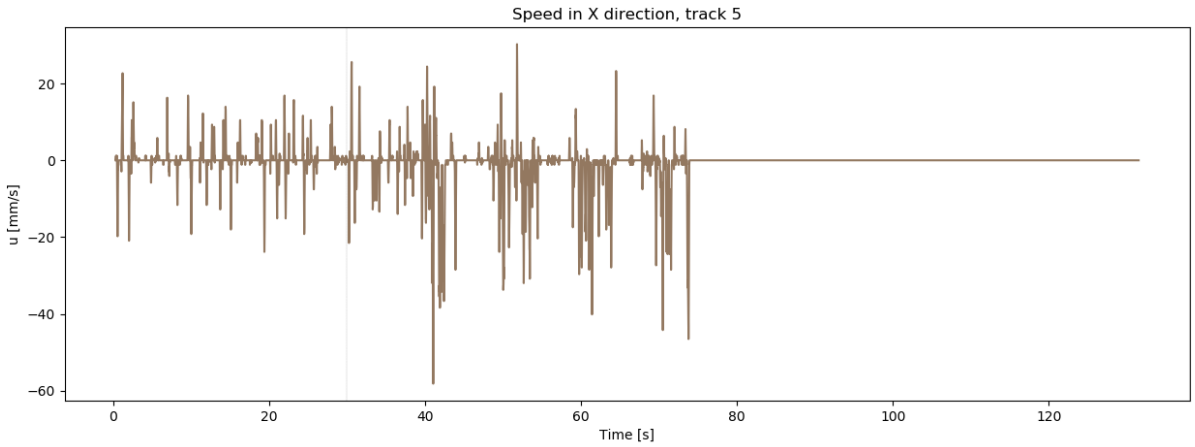

Figure C.63: Velocity profile for track 5 in White-OD1-P3-R2. The light was turned on after 30 s.

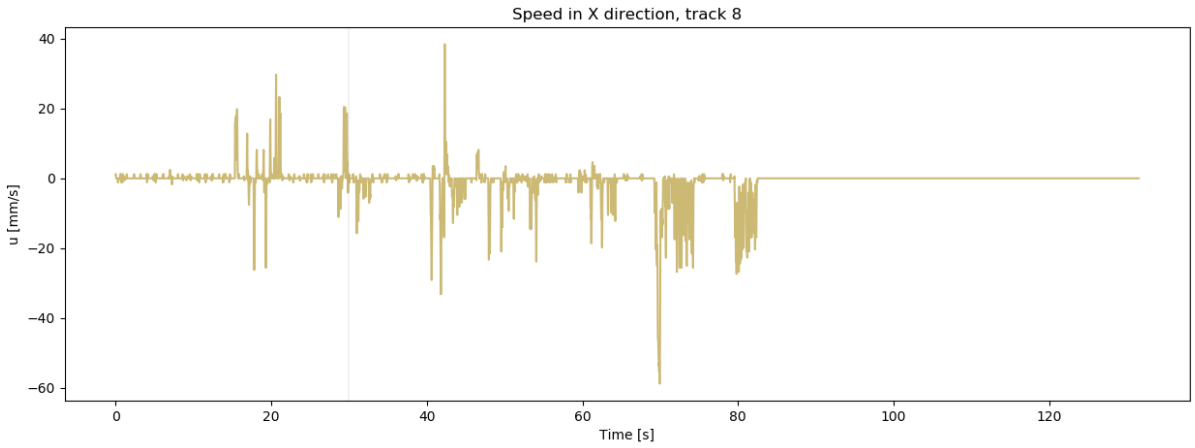

Figure C.64: Velocity profile for track 8 in White-OD1-P3-R2. The light was turned on after 30 s.

C.9 White-OD1-P3-R3

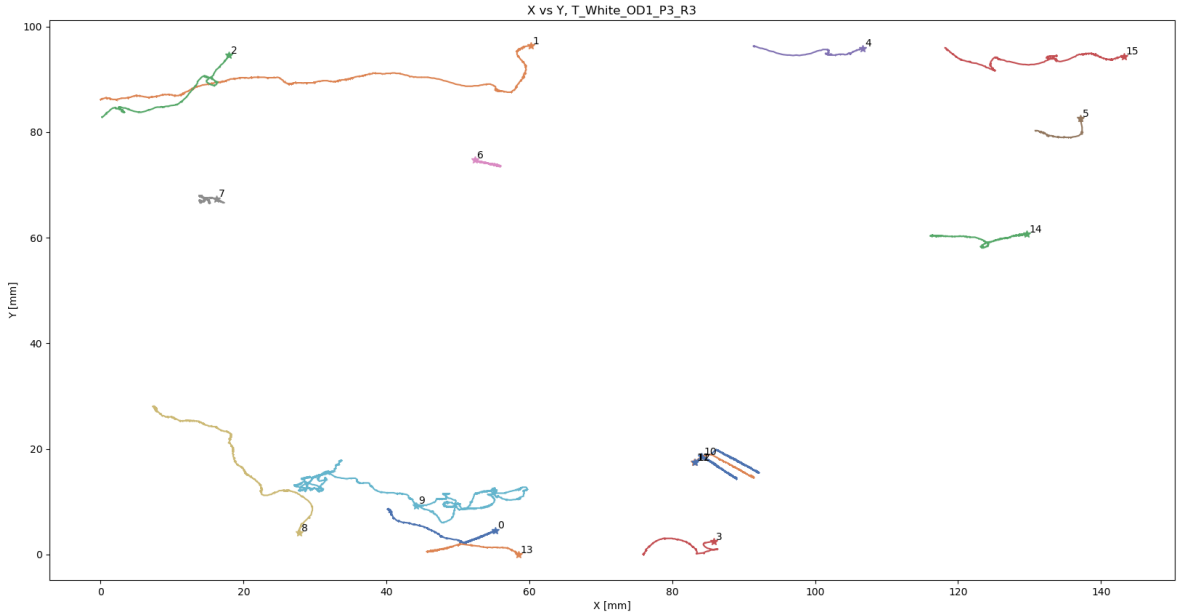

Figure C.65: Tracks found in the two minute long experimental video for White-OD1-P3-R3. Stars denote the start of each track.

0: Start: 68.78s, Arc length: 79.89mm, Avg speed: 1.11mm/s, Max speed: 21.05mm/s
1: Start: 1.18s, Arc length: 184.63mm, Avg speed: 1.18mm/s, Max speed: 44.62mm/s
2: Start: 0.00s, Arc length: 88.63mm, Avg speed: 0.88mm/s, Max speed: 40.01mm/s
3: Start: 0.00s, Arc length: 46.10mm, Avg speed: 0.26mm/s, Max speed: 26.87mm/s
4: Start: 107.83s, Arc length: 32.38mm, Avg speed: 2.19mm/s, Max speed: 52.65mm/s
5: Start: 0.00s, Arc length: 312.45mm, Avg speed: 0.87mm/s, Max speed: 24.98mm/s
6: Start: 0.00s, Arc length: 219.29mm, Avg speed: 1.00mm/s, Max speed: 12.45mm/s
7: Start: 0.00s, Arc length: 215.36mm, Avg speed: 0.81mm/s, Max speed: 11.75mm/s
8: Start: 0.00s, Arc length: 151.62mm, Avg speed: 0.92mm/s, Max speed: 30.12mm/s
9: Start: 0.00s, Arc length: 217.34mm, Avg speed: 1.56mm/s, Max speed: 30.60mm/s
10: Start: 0.00s, Arc length: 199.55mm, Avg speed: 0.89mm/s, Max speed: 32.55mm/s
11: Start: 0.00s, Arc length: 45.82mm, Avg speed: 0.42mm/s, Max speed: 37.50mm/s
12: Start: 0.12s, Arc length: 182.29mm, Avg speed: 0.99mm/s, Max speed: 19.90mm/s
13: Start: 85.94s, Arc length: 35.56mm, Avg speed: 0.99mm/s, Max speed: 20.94mm/s
14: Start: 0.00s, Arc length: 164.56mm, Avg speed: 0.90mm/s, Max speed: 17.55mm/s
15: Start: 0.00s, Arc length: 195.98mm, Avg speed: 1.13mm/s, Max speed: 50.00mm/s

Figure C.66: Information corresponding to tracks for White-OD1-P3-R3. Start time indicates when the track was first registered.

Total speed, White-OD1-P3-R3

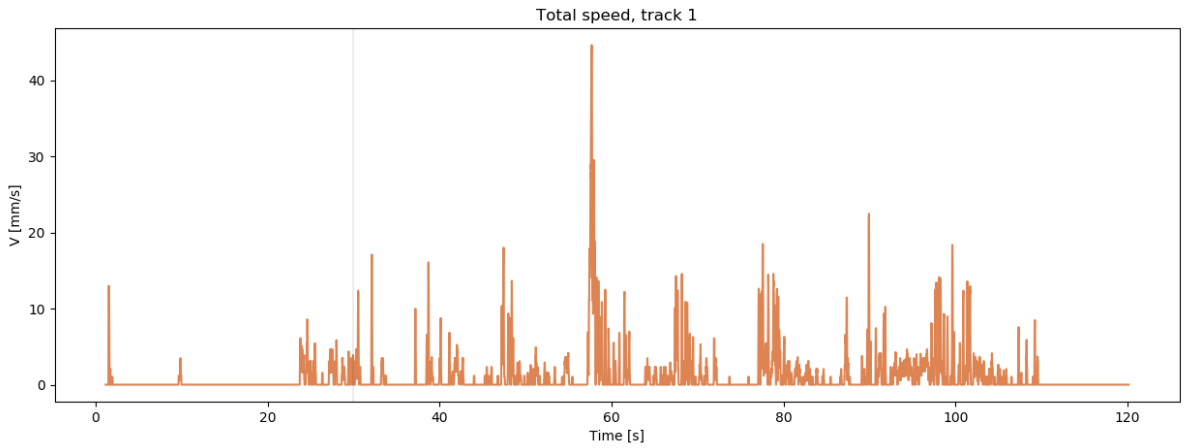

Figure C.67: Speed profile of track 1 in White-OD1-P3-R3. The light was turned on after 30 s.

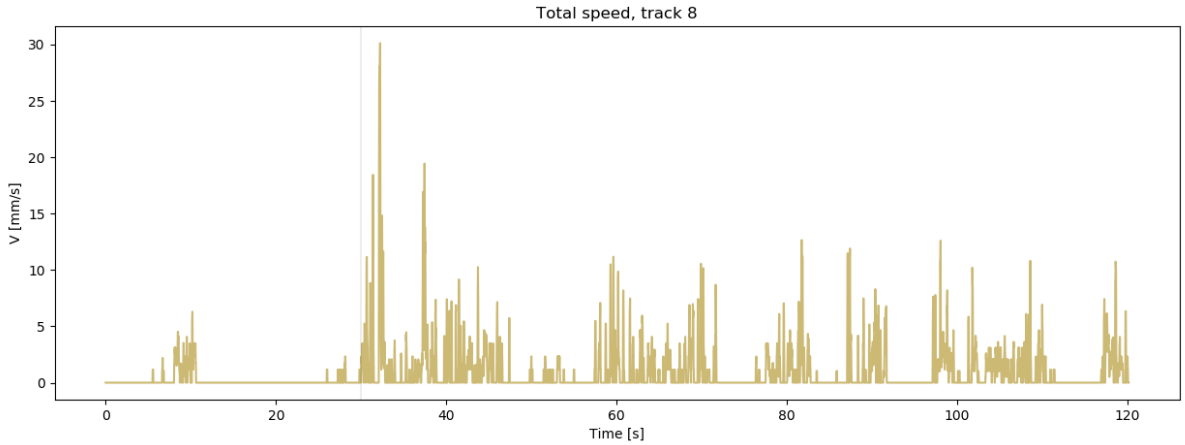

Figure C.68: Speed profile of track 8 in White-OD1-P3-R3. The light was turned on after 30 s.

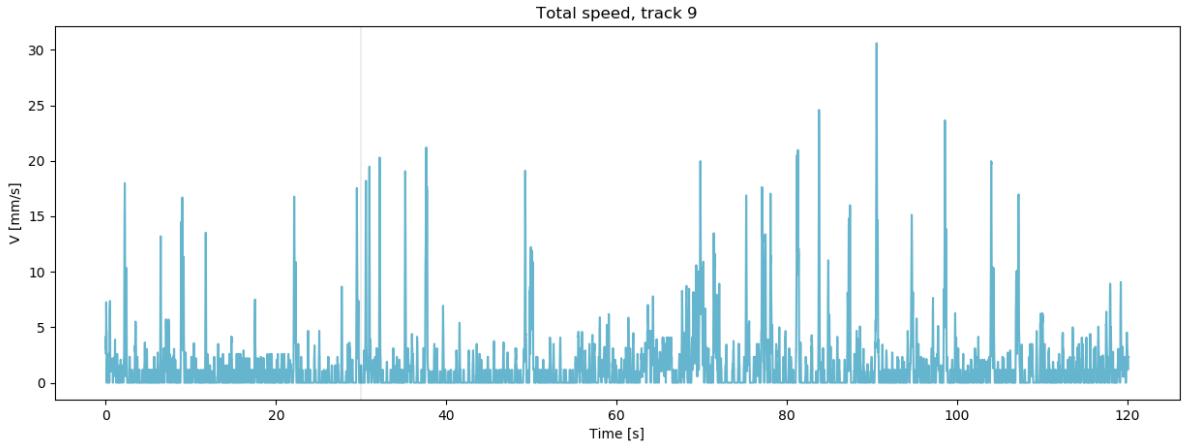

Figure C.69: Speed profile of track 9 in White-OD1-P3-R3. The light was turned on after 30 s.

Velocity in x-direction, White-OD1-P3-R3

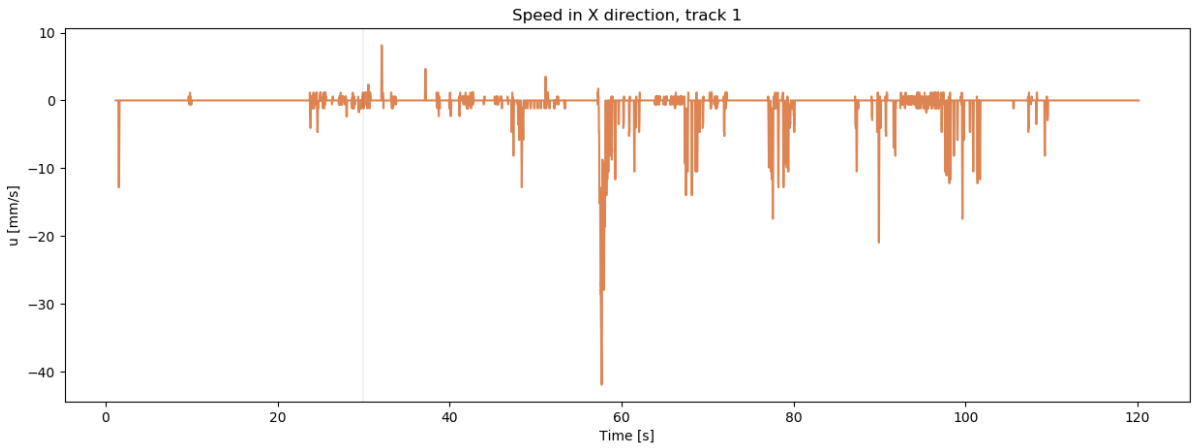

Figure C.70: Velocity profile for track 1 in White-OD1-P3-R3. The light was turned on after 30 s.

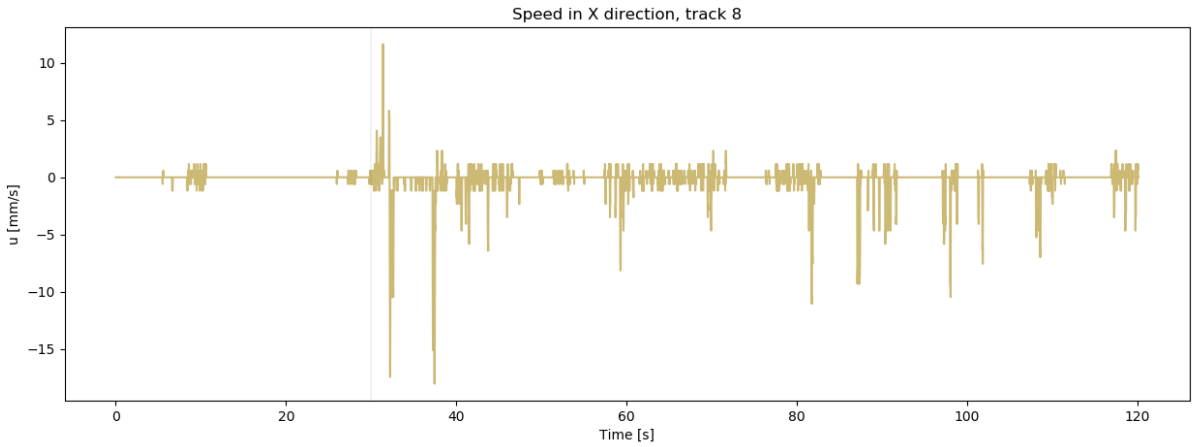

Figure C.71: Velocity profile for track 8 in White-OD1-P3-R3. The light was turned on after 30 s.

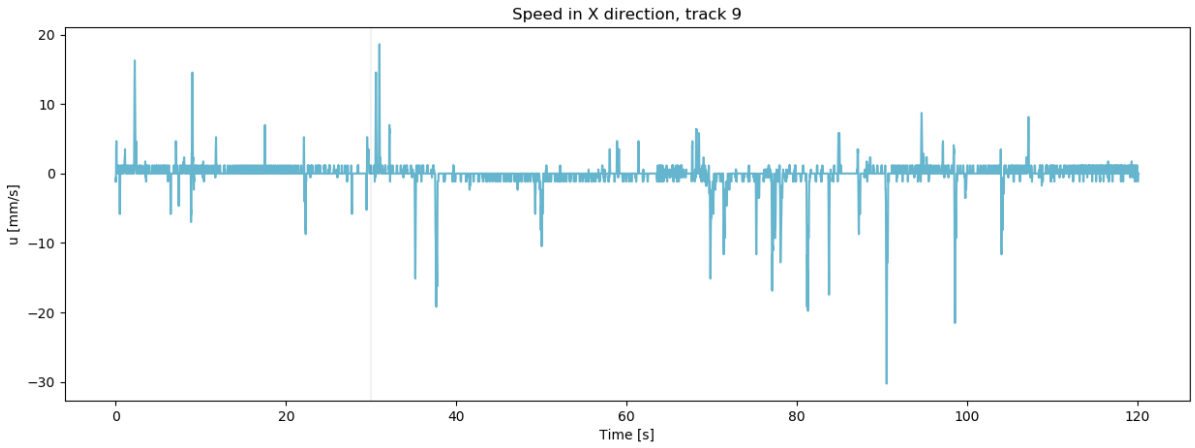

Figure C.72: Velocity profile for track 9 in White-OD1-P3-R3. The light was turned on after 30 s.